Functional Renormalisation Group and Nuclear Matter

A thesis submitted to
The University of Manchester
for the degree of Doctor of Philosophy
in the Faculty of Engineering and Physical Sciences

2015

Benjamín Raziel Jaramillo Ávila

School of Physics and Astronomy

Contents

This thesis contains 46 000 words, 32 figures, and 7 tables.

List of Figures

List of Tables

Abstract

The University of Manchester

Abstract of thesis submitted by **Benjamín Raziel Jaramillo Ávila** for the degree of Doctor of Philosophy and entitled **Functional Renormalisation Group and Nuclear Matter**.

Month and Year of Submission: June, 2015.

This thesis deals with systems of interacting particles with very low energy in the limit where the particle-particle scattering is much larger than the range of the interactions. We use a quantum-field-theory approach which allows us to study both few-body and dense-matter systems in a unified framework. This allows to introduce composite fields of two and three particles (when appropriate). The quantum corrections are calculated nonperturbatively with the Functional Renormalisation Group.

We deal with three types of systems. First we study systems with three and four scalar particles. For three-particle systems our framework describes the Efimov effect. During the FRG flow in the scaling limit, the four-particle system has an infinite sequence of (unphysical) four-particle states on top of each Efimov trimer. This is a case of super Efimov behaviour. Three of these four-particle states survive to the physical limit. Two of these three states have been found in exact quantum-mechanical calculations, and have also been observed in gases of ultracold atoms.

Next, this thesis studies systems of three and four spin-$\frac{1}{2}$ particles. In the scaling limit, we find attractive fixed points for the three- and four-particle systems. Out of the scaling limit, we study atom-molecule scattering and molecule-molecule scattering, in particular their scattering length.

Finally, we study dense-matter systems of spin-$\frac{1}{2}$ particles. This calculation includes all the two-, three-, and four-particle interactions. These systems show spontaneous symmetry breaking: the two-particle field has a finite classical value. We find the value of the atom gap in units of the chemical potential.

Declaration

No portion of the work referred to in this thesis has been submitted in support of an application for another degree or qualification of this or any other university or other institute of learning.

Copyright and ownership of intellectual property rights

1. The author of this thesis (including any appendices and/or schedules to this thesis) owns certain copyright or related rights in it (the "Copyright") and s/he has given The University of Manchester certain rights to use such Copyright, including for administrative purposes.

2. Copies of this thesis, either in full or in extracts and whether in hard or electronic copy, may be made **only** in accordance with the Copyright, Designs and Patents Act 1988 (as amended) and regulations issued under it or, where appropriate, in accordance with licensing agreements which the University has from time to time. This page must form part of any such copies made.

3. The ownership of certain Copyright, patents, designs, trade marks and other intellectual property (the "Intellectual Property") and any reproductions of copyright works in the thesis, for example graphs and tables ("Reproductions"), which may be described in this thesis, may not be owned by the author and may be owned by third parties. Such Intellectual Property and Reproductions cannot and must not be made available for use without the prior written permission of the owner(s) of the relevant Intellectual Property and/or Reproductions.

4. Further information on the conditions under which disclosure, publication and commercialisation of this thesis, the Copyright and any Intellectual Property and/or Reproductions described in it may take place is available in the University IP Policy (see `http://documents.manchester.ac.uk/DocuInfo.aspx?DocID=487`), in any relevant Thesis restriction declarations deposited in the University Library, The University Library's regulations (see `http://www.manchester.ac.uk/library/aboutus/regulations`) and in The University's policy on Presentation of Theses.

Acknowledgements

First of all, I thank my mother for the love and support that she has always given me. My mother is an endless source of patience and wisdom. Uziel, thank you for putting up with me. I am lucky to have you as a brother. I am also very proud of my extended family. Gabriel, Mundo, ...

Erick and René, you can turn any topic into an interesting talk. I thank you for the time you spend with me, and I hope to spend more time with you in the future.

I am also very happy of having worked with Mike Birse. He is both a great physicist and supervisor.

Priscila, meeting you has been a great experience. I thank you for your love and for putting up with me. I hope you keep doing so.

Selim, you are the person that got me interested in physics in the first place. I thank you for that, I guess...

Finally, feelings of gratitude for a government institution are rare—at least for me. However, I am grateful for the support I have received from CONACyT. I hope it will be fruitful.

Chapter 1

Introduction

This introduction discusses two types of physical systems that fit the theoretical framework in this work. First, we talk about systems of ultracold atoms in Section 1.1. Next, we discuss nuclear systems: nuclei and nuclear interactions are treated in Section 1.2, and nuclear matter is introduced in Section 1.3. Finally, we discuss the role of quantum fluctuations in the physical systems mentioned above, in Section 1.4.

1.1 Ultracold gases of atoms

Gases of fermions with near-zero temperature display different types of behaviour. Consider a gas that contains two species of fermions, and where there is an interaction between every pair of fermions that are not in the same species. If the interaction is very weakly attractive, then the gas is in the Bardeen-Cooper-Schrieffer (BCS) regime. There, the ground state of the system contains correlated pairs of fermions with zero centre-of-mass momentum. In this regime, the correlated pairs can be separated by distances much larger than the average interparticle distance. On the other hand, if there is a strong attraction between pairs of fermions, the interaction forms deeply bound bosonic molecules. These molecules form a Bose-Einstein condensate (BEC).

The BCS-BEC crossover is a regime between these two behaviours. This consists of Fermi gases where the interaction is close to creating weakly bound two-particle states. This includes both systems where the interaction creates weak two-particle bound states, and systems where the interaction is slightly weaker and does not create these bound states. Furthermore, the limit where the two-particle interaction creates a zero-energy bound state is known as unitary limit.

The BCS-BEC crossover has conceptual importance for different fields of physics, in particular for nuclear and condensed matter. However, the interest in this regime exploded in the last decade, when experimentalists found a way to produce and

control systems with these characteristics [65, 76]. In carefully prepared ultracold gases of atoms, the atom-atom interaction is controlled by an external magnetic field. This interaction can be set such that it creates weakly bound two-atom states, or it can be manipulated such these bound states are not created. This allows to explore systems very close to the unitary limit.

Experiments with ultracold gases of atoms are often performed with atoms that have a single electron in the outer shell, called alkali metals. The control over the atom-atom interaction is possible because the interaction is close to a Feshbach resonance. We understand the Feshbach resonance in terms of a model where the atom-atom interaction occurs through two different channels. These channels arise from the hyperfine structure of the atoms. In these systems, one of these channels is open and the other is closed.[1] The open channel is a spin-triplet interaction, whereas the closed channel is a spin-singlet interaction.[2] Due to an external magnetic field, the electron spin is polarised, and when two atoms collide, their outer electrons are aligned. In consequence, the interaction must occur through the triplet (open) channel. However, the hyperfine interaction can trade electron and nuclear spin, and the atoms can tunnel into a bound state of the singlet channel. This tunnelling couples the open and closed channels.

The coupling between the two channels can be manipulated because the magnetic moments of the open an closed channels are different. Changing the magnetic field moves the energy of the bound state (closed channel) with respect to the open channel. Now, the magnetic field can be controlled and set close to a value where the energy of the bound state is close to zero. There, the low-energy atom-atom scattering receives a resonant contribution from the coupling to the closed channel. This produces atom-atom scattering lengths much larger than both the range of the interaction and the average interatomic spacing.

Close to the resonance, the details of the two-channel interaction are not important. There, low-energy interactions are fully described by one scattering length. These systems can be described as a gas of fermions with two species and a single channel of interaction. The two species of atoms are often referred to as spin-up and spin-down degrees of freedom.

The independence of the details of the interaction opens the possibility of studying universal behaviour in ultracold gases of atoms. Furthermore, these systems can be used as a testing ground for many-body theoretical techniques that can be tried later in nuclear and condensed matter systems. In this sense, the study of ultracold gases

[1] The interaction through an open channel is close to creating a two-atom bound state, but it is insufficiently attractive. In contrast, the interaction through a closed channel forms two-atom bound states.

[2] When two atoms interact, the spins of their (respective) outer-shell electrons can be in a triplet or in a singlet state.

of atoms connects different fields of physics.

1.2 Nuclei and nuclear interactions

There is an enormous diversity both in the species of atomic nuclei that exist in nature, and in the transitions that these nuclei can suffer. Nuclei can have from a few to a few hundred nucleons. Also, while some nuclei have half-lives of fractions of a second, others have half-lives of millions of years, and others are completely stable. All this diversity stems from an interplay of different interactions.

The interactions in the nucleus originate from the standard model of particle physics, and we separate these interactions in two groups. The first group consists of interactions from the electroweak part of the standard model. These interactions produce electrostatic repulsion between protons and β decays. Both of these phenomena have an effect in the stability of nuclei.

The second group consists of interactions from the quantum chromodynamics (QCD) part of the standard model. QCD interactions strongly bind quarks into states with zero QCD charge. Quarks are degrees of freedom in the standard model, and they correctly describe high-energy collisions of nuclei (above ~ 10 GeV). However, at low energy, the appropriate degrees of freedom are protons and neutrons (below ~ 100 MeV).

Event though nucleons have zero QCD charge, there is a residual QCD interaction between nucleons. This residual interaction is called nuclear force, and it keeps protons and nucleons bound inside the nucleus. This work does not try to explain the origin of nuclear forces. Instead, it tries to explain collective effects in the nucleus. To do this, we use a low-energy effective theory that parametrises nuclear forces.

Experimental data suggest that, for large nuclei, the binding energy of the nucleus receives a constant contribution from each nucleon. This is known as volume contribution,[3] and it is the same for a proton or a neutron. The volume contribution is not the sole contribution to the binding energy of nucleons, but it is the dominant one.[4]

The constant contribution (to the binding energy) from each nucleon leads to an effect called *saturation of nuclear forces*. This effect suggests that nuclear forces have short range, *i.e.* their range is similar to the average separation of nucleons in the nucleus. This is because each nucleon interacts with the nucleons close to it, but not with all the nucleons in the nucleus. If nuclear forces had a range as large as

[3] The volume of the nucleus is roughly proportional to the number of nucleons. In consequence, this contribution is roughly proportional to the volume.

[4] Other effects are considered in the Weizsäcker semiempirical mass formula. This formula includes effects due to the finite size of the nucleus, electrostatic repulsion of protons, effects from a difference in the number of protons and neutrons, and effects from the pairing of particles.

the size of the nucleus, each nucleon would interact with every other nucleon. This would give a contribution roughly proportional to the number of nucleons squared. Instead, we have a contribution proportional to the number of nucleons

This work does not attempt to describe actual nuclei. It focuses on hypothetical systems called nuclear matter. These systems have infinitely many nucleons homogeneously distributed in space. Nuclear matter receives effects from nuclear forces, but it ignores electroweak interactions. Furthermore, the effects due to the finite size of the nucleus are absent in nuclear matter. Nuclear matter disentangles the effect of nuclear forces from electroweak interactions and finite-size effects.

Nuclear matter can help us understand some properties of the nucleus, like the saturation of nuclear forces, in terms of few-nucleon interactions. Before continuing the discussion on nuclear matter, we discuss low-energy interactions between two nucleons.

1.2.1 Nuclear force

Spin and isospin

A proton can be distinguished from a neutron because the quarks inside them have different electroweak charges.[5] However, QCD interactions are independent of these charges. This encourages us to treat protons and neutrons as two species of the same particle, the nucleon.[6] The degree of freedom that chooses between a proton and a neutron is called isospin. Nuclear forces have global isospin symmetry, and therefore conserve isospin.[7]

The mathematical realisation of isospin is analogous to the realisation of spin (hence its name). Fields with spin-$\frac{1}{2}$ have two species, spin-up or spin-down. These fields are accommodated in a doublet,

$$\begin{pmatrix} \psi_\uparrow \\ \psi_\downarrow \end{pmatrix}. \tag{1.1}$$

Likewise, proton and neutron fields are accommodated in a doublet,

$$\psi_N = \begin{pmatrix} \psi_p \\ \psi_n \end{pmatrix}, \tag{1.2}$$

where ψ_p is the proton field, ψ_n is the neutron field, and ψ_N is the nucleon field.

The nucleon field has two independent indices, $\psi_{i,a}$ where i is the isospin index

[5] The electric charge is part of the electroweak charges.

[6] Treating protons and neutrons as two species of the same particle neglects the small difference in their masses. This difference is $\sim 0.1\%$.

[7] Electroweak interactions do not have isospin symmetry, and do not conserve isospin.

spin triplet ($S=1$)	
$m_S = 1$	$\lvert\uparrow,\uparrow\rangle$
$m_S = 0$	$\frac{1}{\sqrt{2}}\big(\lvert\uparrow,\downarrow\rangle + \lvert\downarrow,\uparrow\rangle\big)$
$m_S = -1$	$\lvert\downarrow,\downarrow\rangle$

spin singlet ($S=0$)	
$m_S = 0$	$\frac{1}{\sqrt{2}}\left(\lvert\uparrow,\downarrow\rangle - \lvert\downarrow,\uparrow\rangle\right)$

Table 1.1: Spin decomposition of the two-nucleon state.

($i = p, n$) and a is the spin index ($a = \uparrow, \downarrow$). Accommodating protons and neutrons in a doublet is useful to write isospin-symmetric interactions like the nuclear force.

Two-nucleon interaction

The simplest interaction between nucleons is the nucleon-nucleon interaction. It is convenient to discuss this interaction in terms of the decomposition of two-nucleon systems. These systems can be decomposed into a spatial part, a spin part, and an isospin part.

The spatial part can be written in terms of the position of the centre of mass and the relative position between the two nucleons. The centre of mass behaves as a free particle, hence the dependence (of the two-nucleon system) on the centre-of-mass coordinates is trivial.

We turn to the dependence on the relative position of the nucleons. Low-energy systems are dominated by states with zero-total orbital angular momentum, $L = 0$. In consequence, we focus on nucleon-nucleon systems with $L = 0$. These systems are spherically symmetric with respect to the relative position of the nucleons. Furthermore, the spatial part of two-nucleon states (with $L = 0$) is symmetric under the interchange of nucleons.

The spin and isospin decompositions of two-nucleon systems are very similar. The spin part is decomposed into a symmetric triplet and an antisymmetric singlet. The total spin of the spin triplet is $S = 1$, and the total spin of the spin singlet is $S = 0$. The states for the spin triplet and singlet are displayed in Table 1.1.

The isospin part of two-nucleon systems can also be decomposed into a symmetric triplet and an antisymmetric singlet. The total isospin of the isospin triplet is $I = 1$, and the total isospin of the isospin singlet is $I = 0$. The states for the isospin triplet and singlet appear in Table 1.2.

The spatial part of low-energy two-nucleon systems is symmetric under the interchange of nucleons. In consequence, the product of spin and isospin parts must be antisymmetric. This means that the spin triplet (symmetric) combines itself with the isospin singlet (antisymmetric), and the spin singlet (antisymmetric) combines itself with the isospin triplet (symmetric). In spectroscopic notation the channel

isospin triplet ($I = 1$)	
$m_I = 1$	$\lvert p, p\rangle$
$m_I = 0$	$\frac{1}{\sqrt{2}}\big(\lvert p, n\rangle + \lvert n, p\rangle\big)$
$m_I = -1$	$\lvert n, n\rangle$

isospin singlet ($I = 0$)	
$m_I = 0$	$\frac{1}{\sqrt{2}}\big(\lvert p, n\rangle - \lvert n, p\rangle\big)$

Table 1.2: Isospin decomposition of the two-nucleon state.

with $S = 1$ and $I = 0$ (spin-triplet channel) is denoted by ${}^3\mathcal{S}_1$, and the channel with $S = 0$ and $I = 1$ (spin-singlet channel) is denoted by ${}^1\mathcal{S}_0$.[8]

In the zero-energy limit, nucleon-nucleon interactions occur only through the channels ${}^3\mathcal{S}_1$ and ${}^1\mathcal{S}_0$. These channels are independent between themselves, but they are the low-energy form of QCD interactions. Each of these two channels can be described by a spherically-symmetric potential. However, in the zero-energy limit, the scattering lengths of these channels are sufficient to describe two-nucleon interactions. These scattering lengths are $a_t = 5.42$ fm for ${}^3\mathcal{S}_1$, and $a_s = -23.71$ fm and for ${}^1\mathcal{S}_0$. The interaction through ${}^3\mathcal{S}_1$ creates the only two-nucleon bound state, the deuteron, which has binding energy -2.22 MeV.[9]

In terms of high-energy dynamics, nucleons interact by exchanging virtual particles. The lightest particle that two nucleons can exchange is the pion. Its mass is $m_\pi \simeq 140$ MeV$/c^2$. If nuclear forces are the low-energy form of virtual-pion exchanges, then the range of the nuclear force is about $\hbar/m_\pi\, c \simeq 1.4$ fm. Furthermore, pion exchange is not sufficient to explain all low-energy scattering data [6]. This means that low-energy nuclear forces also receive contributions from interactions with energy scales above $m_\pi\, c^2$. In particular, they receive contributions from QCD interactions with typical energy scales ~ 1 GeV. This means that low-energy nuclear forces also have significant contributions from ranges $\sim \hbar\, c/\text{GeV} \simeq 0.2$ fm.

Nucleon-nucleon scattering lengths are larger than the range of nuclear interactions. This indicates that two-nucleon systems have strong low-energy interactions. Two-nucleon subsystems play an important role in the dynamics of nuclear systems.

1.3 Nuclear and neutron matter

Nuclear matter is an hypothetical system formed by infinitely many nucleons homogeneously distributed in space. This system is a simplification of actual nuclei, and

[8] Spectroscopic notation has the form ${}^{(2S+1)}L_J$, where S is the total spin, L is the total orbital angular momentum, and J is the total angular momentum, $J = L + S$. The total orbital angular momentum is denoted as $\mathcal{S}$ for $L = 0$, $\mathcal{P}$ for $L = 1$, $\mathcal{D}$ for $L = 2$, $\mathcal{F}$ for $L = 3$, ...

[9] The magnetic moment of the deuteron suggests that the deuteron is a mixture of ${}^3\mathcal{S}_1$ and a small contribution from a two-nucleon state with nonzero total orbital angular momentum, ${}^3\mathcal{D}_1$.

we study it to understand the effect of few-particle nuclear forces on large numbers of fermions.[10]

Nuclear matter is free from finite-size effects present in nuclei, and it also ignores electroweak interactions. The latter are well understood, and they are not the main contribution to the binding of nucleons.[11] Furthermore, this discussion of nuclear matter is restricted to zero-temperature systems.

Assume that we turn off all interactions in nuclear matter: we have a homogeneous system with infinitely many noninteracting fermions at zero temperature. The ground state of this system consists of fermions piled on top of each other—identical fermions pile on top of each other because they cannot occupy the same one-particle state. For each species of fermions,[12] the lowest one-particle state is occupied by one fermion. The next available one-particle state is occupied by another fermion. This goes on until we reach the highest occupied one-particle state. The energy of the highest occupied one-particle state is the Fermi energy. In nuclear matter there is a Fermi energy for protons, and one for neutrons.[13]

Proton density and neutron density, ρ_p and ρ_n, are associated with their respective Fermi energies. Integrating over the density of states in momentum space yields,

$$\rho_i = 2 \int_0^{p_i^F} \frac{\mathrm{d}^3 q}{(2\,\pi)^3} = \frac{(p_i^F)^3}{3\,\pi^2}, \tag{1.3}$$

where p_i^F is the three-momentum that corresponds to the Fermi energy, and where $i = p$ corresponds to protons, and $i = n$ to neutrons. The factor of two before the integral comes from the spin-up, spin-down degeneracy.

Fermions can be excited above the level of energy that they occupy, leaving a hole in the sea of particles. This puts the system in a *particle-hole* state. However, fermions cannot be excited into an occupied state: if a fermion is excited above the Fermi energy, the energy of the excitation is larger than the difference between the Fermi energy and the initial energy of the excited fermion. In consequence, excitations with near-zero energy occur around the Fermi surface, not around the lowest one-particle state. Both fermions and holes can propagate, therefore a quantum description of the system needs to account for paths with virtual holes and virtual particles. This dynamics is different from the dynamics of fermion systems with zero density.

[10] Nucleon-nucleon interactions are the main few-particle nuclear force, but three-nucleon interactions also play a role in the binding of nucleons [64, 39].

[11] In reality, nuclear matter with a finite density of protons is impossible because the electrostatic repulsion would dominate over the binding of nuclear forces and break the system apart.

[12] Nuclear matter has four species for fermions, which correspond to the four possible combinations of indices for the nucleon field, $\psi_{i,a}$ with $i = p, n$ and $a = \uparrow, \downarrow$.

[13] We assume that the Fermi energy is the same for spin-up and spin-down nucleons. Different Fermi energies for spin-up and spin-down particles would produce an anisotropic system, and this work is restricted to isotropic systems.

We return to the interacting system. Interactions change the ground state, which is now a combination of the ground state of the noninteracting system and fluctuations with particle-hole states. However, the system should still have a finite density of fermions.

Interactions can also create a degenerate set of ground states, a phenomenon called spontaneous symmetry breaking. For example, if a two-fermion interaction is attractive enough, two-fermion fields can have a nonzero classical value. This is known as superfluidity.

1.3.1 Nucleon matter

So far we have discussed nuclear matter without specifying the relative densities of protons and neutrons. If proton and neutrons densities are equal, the system is called symmetric nuclear matter. As discussed above, infinitely large, homogeneous systems with a finite density of protons cannot exist because of the Coulomb repulsion.

Large systems formed by neutrons do exist. Neutron stars are astronomical objects formed by the gravitational collapse of a star's core.[14] Neutron stars are extremely massive objects, and gravity plays an important role by producing extremely dense systems. Studying neutron matter can produce an equation of state which can be compared with observational data from neutron stars. In particular, the mass and radius of these stars provides data which can be compared with the equation of state.

1.4 Quantum fluctuations

Above we discussed ultracold gases of atoms close to the Feshbach resonance and nuclear matter. These systems share important characteristics. **a)** First, they have a strong quantum behaviour, hence they should be described in a quantum framework. **b)** Second, in these systems, the interaction between two particles is close to the resonance.[15] There, the interactions are strong in the sense that they create strongly correlated pairs of particles. This work uses a path-integral formalism to describe these systems. This formalism and some issues with strongly-interacting systems are discussed below.

The path-integral formalism gives a framework to study the dynamics of quantum systems: to calculate the probability that a system goes from one state to another, we must consider all the possible ways in which this can occur. We refer to each of

[14] The gravitational collapse forces electrons and protons together, creating neutrons. This collapse also releases enormous amounts of energy, creating a supernova explosion.

[15] The resonance occurs when the two-particle interaction is just strong enough to create a zero-energy two-particle bound state.

these possible ways as a *path*, and the dynamics (that describes the system) gives an amplitude for each path. Adding (or integrating) all of these paths gives the total amplitude for the transition. The total amplitude is a complex number, and the probability that the transition occurs, $P_{A\to B}$, is the square of the amplitude's modulus. A transition amplitude can receive contributions from a classical path. This is a path that takes the system from state A to state B in a classical description of the system. The contributions from other paths, which cannot occur classically, are known as *quantum fluctuations*.

This work uses a quantum-field-theory framework, where particles can be created and annihilated. There, an initial state formed by a collection of particles can transition to a final state, formed by other particles. The transition is caused by interactions between the particles. Again, the transition amplitude is given by adding all possible paths. Furthermore, a transition can occur through a path that creates (and annihilates) particles that do not appear in the final state. These particles are known as virtual. Transitions often have paths with an arbitrarily-high number of virtual particles.

The paths for a process can be organised and visualised with Feynman diagrams. In these diagrams, particles propagating in time are represented by lines. In one side of the diagram, the initial particles start, and these particles meet each other in vertices that represent the interactions (prescribed by the dynamics). These vertices may create or annihilate particles, or transfer four-momenta between the particles. After the interactions create the final particles, the diagram ends.

If a diagram has virtual particles, these particles may form loops. Each loop in a diagram has an undetermined four-momentum. Adding all the possible paths for a transition means adding all possible diagrams, and integrating over the undetermined four-momentum in each loop. This seems like a very complicated task, but there are schemes to organise the paths and calculate transition probabilities.

The perturbative expansion is one of these schemes. It organises the sum of amplitudes (corresponding to a transition) in a series expansion. The n-th order in the expansion contains all diagrams with exactly n loops. Perturbative schemes work when the couplings that describe each vertex are very small numbers. Higher orders in the expansion have more loops, which requires more vertices. In consequence, higher orders in the expansion have higher powers of the couplings. Since the couplings are small, higher orders in the expansion have neglectable contributions.

Since its development, the perturbative expansion has been crucial in high-energy physics and condensed matter. This work, however, does not rely on organising quantum fluctuations in terms of loops. Instead, we use a nonperturbative technique which organises the integration of quantum fluctuations in a different way. It gradually integrates fluctuations with lower and lower momenta, but it does not in-

volve expansions in the number of loops. It is called the Functional Renormalisation Group.

There is one remaining issue with quantum fluctuations. Particles in the systems under study are low-energy degrees of freedom, and they only describe systems with energy below some ultraviolet (UV) scale. In consequence, we integrate quantum fluctuations with four-momentum between zero and the UV scale. Quantum fluctuations above the UV scale are already included in the framework that uses ultracold atoms or nucleons as degrees of freedom.

1.5 Contents

- Chapter 2 of this thesis discusses the methods that will be used in subsequent chapters of this thesis. This chapter is divided in two sections. Section 2.1 deals with the Functional Renormalisation Group (FRG) in general, and Section 2.2 deals with methods that combined with the FRG are used in the following chapters.

- Next, Chapter 3 studies the FRG flow of systems formed by few scalar particles. This chapter deals with the Efimov effect, and with four-body states.

- Chapter 4 treats systems with few spin-$\frac{1}{2}$ particles. This chapter discusses the unitary limit and universality in systems with two, three, and four particles. Out of the unitary limit, this chapter discusses scattering between a particle and a two-particle state, and scattering between two two-particle states.

- Chapter 5 deals with systems formed by infinitely many spin-$\frac{1}{2}$ particles.

- Finally, Chapter 6 contains closing remarks.

Chapter 2

Functional Renormalisation Group and nonrelativistic systems

> The way fluctuations are summed over in perturbation theory is not appropriate since fluctuations of all wavelengths are treated on the same footing in Feynman diagrams. This is what produces integrals: at a given order of the perturbation expansion all fluctuations are summed over.
>
> Wilson's idea is to organize the summation over fluctuations in a better way.
>
> **Bertrand Delamotte on nonperturbative renormalisation, pages 52 and 53 of [68]**

This chapter introduces the techniques that, in subsequent chapters, are used to deal with systems of nonrelativistic particles.[1] There is an interaction between each pair of particles in these systems. Furthermore, the strength of this interaction is close to the minimum strength that creates a two-particle bound state.

We treat both few-particle and dense-matter systems. Few-particle systems are formed by a finite (and small) number of particles. In contrast, dense-matter systems are formed by an infinite number of particles homogeneously distributed in space.

To deal with these two types of systems, we use a quantum-field-theory (QFT) approach. In QFT, the complete dynamical information is contained in the effective action, and to calculate the latter, it is necessary to integrate over all quantum fluctuations. We perform this integration using the Functional Renormalisation Group (FRG).

Alternatively, the systems in question can be studied using the Schrödinger equation. In consequence, a QFT approach might seem unnecessarily complicated compared with Schrödinger-equation approaches. Nonetheless, a renormalisation-group

[1] A nonrelativistic approach is sufficient because we work with particles where the kinetic energy is much smaller than their mass times c^2.

approach also has advantages. Firstly, it can provide insight on the universal behaviour of these systems with more ease than the Schrödinger equation. Secondly, a renormalisation-group approach also allows to work without specifying an explicit form for the particle-particle potential. Thirdly, a FRG approach allows a unified description of few- and dense-matter systems with large (particle-particle) scattering length, which is a desirable feature in this work.

We deal with particles that are indistinguishable, and treat two cases, spin-0 (or scalar) particles and spin-$\frac{1}{2}$ particles. Scalar particles are bosons, and several identical bosons can combine to form a state. This state, however, must be totally symmetric under the interchange of particles. In contrast, spin-$\frac{1}{2}$ particles are fermions, and Pauli's exclusion principle forbids two fermions from occupying the same state. The fermion or boson character of particles has an impact on the dynamics of the systems that we study.

This chapter is divided in two parts. The first part, Section 2.1, discusses the FRG in general. The second part, Section 2.2, deals with techniques that, together with the FRG, are used to study nonrelativistic systems.

2.1 Functional Renormalisation Group

We use a version of the Functional Renormalisation Group (FRG) that was devised by Christof Wetterich building on ideas by Kenneth G. Wilson [72, 73]. For reviews see [7, 57, 4, 66, 63, 68]. The FRG is a technique to integrate low-momentum quantum fluctuations into the effective action. The latter acts as the generating function for all one-particle irreducible transition amplitudes. The FRG is a nonperturbative technique because it does not rely on power-series expansions to calculate the effective action, and therefore it is suitable to study systems where couplings are not small enough to produce converging power series.

In perturbation theory, each order in the series contains quantum fluctuations with all possible values of momenta. These fluctuations are added by four-momentum integrals in the loops, and each loop integrates all values of momenta simultaneously. There, all quantum fluctuations are included when the perturbative series converges. In contrast, nonperturbative renormalisation techniques reorganise the integration of quantum fluctuations.[2] The FRG integrates the momentum in the fluctuations gradually, but each value of momentum that is integrated includes fluctuations with any number of loops.

The FRG introduces a momentum scale k, and modifies the dynamics by suppressing quantum fluctuations with momentum below k. This suppression is achieved by adding artificial, k-dependent mass terms to the action. This produces a new ac-

[2] Bertrand Delamotte discusses these ideas in Chapter 2 of [68].

tion for the modified dynamics. Next, an auxiliary object is introduced, the running action. The latter is closely related to the effective action, but it changes with the scale k. We assume that the dynamics with quantum fluctuations (with momentum) above some ultraviolet (UV) scale is known. This scale is denoted as K_0. The FRG provides a flow equation that interpolates the running action from $k = K_0$ to the limit $k \to 0$. In the latter limit, the running action matches the effective action, which includes all quantum fluctuations.

The FRG sits on the framework of quantum field theory, therefore this chapter starts with a brief reminder on the latter. This helps to set the notation and conventions.

2.1.1 Effective action

In QFT, particle interactions are represented by fields, and there is one field for each species of particles. The information on the interaction and propagation of particles—*i.e.* the dynamics—is prescribed by the action

$$S[\mathbf{\Phi}]\,, \tag{2.1}$$

which is a functional of fields, where $\mathbf{\Phi}$ is an array with all the fields in the action. Any field in $\mathbf{\Phi}$ is selected by an index, say Φ_a. This index runs over fields and their conjugates, treating them as different components in $\mathbf{\Phi}$. This index also runs over spin numbers, treating them as different components as well. Fields and their sources are commuting or anticommuting objects, depending on whether they correspond to bosons or fermions. In this section, we express each field or source as a function of a four-momentum, $\mathbf{q} = (q^0, \vec{q})$. The space-dependent object (field or source) can be retrieved by taking the Fourier transform of the momentum-dependent object.

The *quantum action functional* or *partition function* of a quantum field theory is

$$Z[\mathbf{J}] = \int D\mathbf{\Phi} \left(\mathrm{e}^{\mathrm{i}\, S[\mathbf{\Phi}] + \mathrm{i}\, \mathbf{J}\cdot\mathbf{\Phi}}\right), \tag{2.2}$$

where $\int D\mathbf{\Phi}$ denotes a path integral. All possible configurations of the fields are considered in it. The exponent $\exp\{\mathrm{i}\, S[\mathbf{\Phi}]\}$ works as a weight function in this integration. The partition function $Z[\mathbf{J}]$ is a functional of the sources $\mathbf{J}$, where there is one source for each field,[3] and each source depends on $\mathbf{q}$. To avoid cluttering equations, the four-momentum dependence is kept implicit when there is no ambiguity. The dot product in the partition function is independent of four-momenta, and is

[3] Like in the array of fields, each source in $\mathbf{J}$ can be selected with an index.

defined as

$$\mathbf{J}\cdot\mathbf{\Phi} = \sum_b \int_{\mathbf{q}'} \; J_b(-\mathbf{q}') \;\; \Phi_b(\mathbf{q}'), \tag{2.3}$$

where b runs over fields and sources and $\int_{\mathbf{q}}$ represents $\int \frac{\mathrm{d}^4 q}{(2\,\pi)^4}$. The fields $\mathbf{\Phi}$ and the sources $\mathbf{J}$ are conjugate variables.

The object $W[\mathbf{J}]$ is defined as

$$W[\mathbf{J}] = -\mathfrak{i}\,\log\left(Z[\mathbf{J}]\right), \tag{2.4}$$

and is also a functional of the sources. It is a useful auxiliary object in the theory.

The expectation value of a field, also known as classical field, is calculated with a path integral,

$$\Phi_a^{\mathrm{clss}}(\mathbf{q}) = \langle\Phi_a(\mathbf{q})\rangle = \frac{1}{Z[\mathbf{J}]_{\mathbf{J}=0}} \int D\mathbf{\Phi} \;\; \left(\Phi_a(\mathbf{q}) \;\; \mathrm{e}^{\mathfrak{i}\,S[\mathbf{\Phi}]}\right), \tag{2.5}$$

and can also be written as a functional derivative[4] of $W[\mathbf{J}]$,

$$\Phi_a^{\mathrm{clss}}(\mathbf{q}) = \left.\frac{\delta W[\mathbf{J}]}{\delta J_a(-\mathbf{q})}\right|_{\mathbf{J}=0}. \tag{2.6}$$

The effective action is defined as a Legendre transform of the functional $W[\mathbf{J}]$

$$\Gamma[\mathbf{\Phi}^{\mathrm{clss}}] = W[\mathbf{J}] - \mathbf{J}\cdot\mathbf{\Phi}^{\mathrm{clss}}, \tag{2.7}$$

or more explicitly

$$\Gamma[\mathbf{\Phi}^{\mathrm{clss}}] = W[\mathbf{J}] - \sum_b \int_{\mathbf{q}'} \; J_b(-\mathbf{q}') \;\; \Phi_b^{\mathrm{clss}}(\mathbf{q}'). \tag{2.8}$$

By construction, the effective action is a functional of the classical fields, and it does not depend on the sources $\mathbf{J}$. This is verified by taking the functional derivative of Γ with respect to a source,

$$\left.\frac{\delta\,\Gamma[\mathbf{\Phi}^{\mathrm{clss}}]}{\delta J_a(-\mathbf{q})}\right|_{\mathbf{J}=0} = \left.\frac{\delta\,W[\mathbf{J}]}{\delta J_a(-\mathbf{q})}\right|_{\mathbf{J}=0} - \Phi_a^{\mathrm{clss}}(\mathbf{q}) = \Phi_a^{\mathrm{clss}}(\mathbf{q}) - \Phi_a^{\mathrm{clss}}(\mathbf{q}) = 0, \tag{2.9}$$

where Eq. (2.7) and (2.6) are used.

The effective action is the generator of all one-particle irreducible diagrams (1PI), and all quantum fluctuations are included in it. If we use the effective action Γ

[4] The functional derivative of the functional $F\,[f]$ with respect to the object $f(\mathbf{q})$ is

$$\frac{\delta}{\delta f(\mathbf{q})}\left(\int_{\mathbf{q}'}\left(F\,[f(\mathbf{q}')]\right)\right) = \int_{\mathbf{q}'}\left((2\pi)^4 \;\; \delta^4(\mathbf{q}-\mathbf{q}') \;\; \frac{\delta F\,[f(\mathbf{q}')]}{\delta f(\mathbf{q}')}\right).$$

(instead of the action S) to build the Feynman diagrams for a process, then tree-level calculations yield exact results.

2.1.2 Mass terms and modified dynamics

The FRG introduces a momentum scale k, and modifies the dynamics by suppressing quantum fluctuations with momentum below k. This suppression is achieved by adding artificial, k-dependent mass terms to the action.

We deal with actions that have the general form $T - V$, where T are the kinetic terms and V is the potential. Mass terms appear as $-\mu^2\ \Phi_a^\dagger\,\Phi_a$ in the action. The artificial mass terms that modify the dynamics in the FRG have the form

$$\Delta S[\mathbf{\Phi}] = -\frac{1}{2}\ \sum_{a,b}\int_{\mathbf{q}_1',\,\mathbf{q}_2'}\Big(\Phi_a(\mathbf{q}_1')\ \hat{R}^{ab}(\mathbf{q}_1',\mathbf{q}_2')\ \Phi_b(\mathbf{q}_2')\Big)\,, \tag{2.10}$$

where $\hat{R}^{ab}(\mathbf{q}_1',\mathbf{q}_2')$ are k-dependent bilinear coefficients. The regulators $\hat{R}^{ab}(\mathbf{q}_1',\mathbf{q}_2')$ have two indices running over the fields in the action, and hence can be arranged in a matrix.[5] This matrix could have nonzero coefficients for every pair of fields and nontrivial dependence on both $\mathbf{q}_1'$ and $\mathbf{q}_2'$. Nonetheless we are only interested in artificial mass terms with the form $-\alpha(\mathbf{q},k)\ \Phi_a^\dagger(\mathbf{q})\,\Phi_a(\mathbf{q})$ because these are the terms that could suppress low-momentum modes in the dynamics.[6]

For each dynamic field and its conjugate, there is a kinetic term in the action

$$\Phi_a^\dagger(\mathbf{q})\ \mathcal{T}_a(\mathbf{q})\ \Phi_a(\mathbf{q}), \tag{2.11}$$

where $\mathcal{T}_a(\mathbf{q})$ is the inverse propagator for Φ_a.[7] Quantum fluctuations are generated by virtual Φ_a's with all possible values of energy and three-momentum. Each inverse propagator has a part that depends on three-momentum, or $\|\vec{q}\|$. This part dictates the kinetic energy in the propagation of Φ_a. If we add (to the inverse propagator) a three-momentum term evaluated at k (instead of $\|\vec{q}\|$), then for $\|\vec{q}\| \ll k$, the $\|\vec{q}\|$ dependence in the new propagator is neglectable. This replaces the contribution of virtual Φ_a's with momentum $\|\vec{q}\| \ll k$ by unphysical modes with momentum $\sim k$. This is what the regulators do in the FRG: they suppress essential $\|\vec{q}\|$ dependence in low-momentum virtual modes. In the limit $k \to 0$, there should be no mode suppression and the regulators must vanish. This feature is essential to recover the effective action corresponding to $S[\mathbf{\Phi}]$.

[5] There is no unique way to order the fields in an index, but once an order is chosen, it must be used consistently.

[6] In practical examples we use matrices with momentum dependence $\hat{R}^{ab}(\mathbf{q}_1',\mathbf{q}_2') = \alpha(\mathbf{q}_1')\ \delta^4\,(\mathbf{q}_1' - \mathbf{q}_2')$, and where all the nonzero elements connect a field and its conjugate.

[7] There is no implicit sum over the index a in Eq. (2.11).

The action of the modified dynamics is

$$S_{\text{MOD}}[\mathbf{\Phi}] = S[\mathbf{\Phi}] + \Delta S[\mathbf{\Phi}]\,, \tag{2.12}$$

where $S_{\text{MOD}}[\mathbf{\Phi}]$ and $\Delta S[\mathbf{\Phi}]$ are k-dependent.

The modified dynamics has a partition function, W-functional, and effective action. These are

$$Z_{\text{MOD}}[\mathbf{J}] = \int D\mathbf{\Phi}\, \left(\mathrm{e}^{\mathrm{i}\, S_{\text{MOD}}[\mathbf{\Phi}] + \mathrm{i}\, \mathbf{J}\cdot\mathbf{\Phi}}\right) \tag{2.13a}$$

$$W_{\text{MOD}}[\mathbf{J}] = -\mathrm{i} \log\left(Z_{\text{MOD}}[\mathbf{J}]\right) \tag{2.13b}$$

$$\Gamma_{\text{MOD}}[\mathbf{\Phi}^{\text{clss}}] = W_{\text{MOD}}[\mathbf{J}] - \mathbf{J}\cdot\mathbf{\Phi}^{\text{clss}}. \tag{2.13c}$$

They are analogous to the ones in Eq. (2.2), (2.4), and (2.7), but with S_{MOD} replacing S. The classical fields in the modified effective action are expectation values with respect to the modified dynamics, not the original one.

Next, the FRG introduces the running action, or Γ_k. It is related to the effective action of the modified dynamics by

$$\Gamma_k[\mathbf{\Phi}^{\text{clss}}] = \Gamma_{\text{MOD}}[\mathbf{\Phi}^{\text{clss}}] - \Delta S[\mathbf{\Phi}^{\text{clss}}]\,. \tag{2.14}$$

The label MOD is used on the functionals of the modified dynamics, *e.g.* S_{MOD}, W_{MOD}, and Γ_{MOD}. Even though Γ_k does not contain the label MOD, it corresponds to the modified dynamics as well. Furthermore, we must distinguish between Γ (the effective action of the original dynamics), Γ_{MOD} (the effective action of the modified dynamics), and Γ_k (the running action of the modified dynamics).

The FRG flow equation gives $\partial_k \Gamma_k$. This equation can be used to find the running action in the limit $k \to 0$, or $\Gamma_{k\to 0}$. The latter matches the effective action of the unmodified dynamics, and contains all quantum fluctuations. We proceed with the derivation of the FRG flow equation.

2.1.3 Flow equation: derivation

To obtain the FRG flow equation we begin by differentiating the modified effective action with respect to k,

$$\begin{aligned}\frac{\mathrm{d}}{\mathrm{d}k}\Big(\Gamma_{\text{MOD}}\left[\Phi^{\text{clss}}\right]\Big) &= \partial_k\left(W_{\text{MOD}}[\mathbf{J}]\right) + \sum_b \int_{\mathbf{q}'}\left(\partial_k J_b(-\mathbf{q}')\ \frac{\delta W_{\text{MOD}}}{\delta J_b(-\mathbf{q}')}\right) \\ &\quad - \sum_b \int_{\mathbf{q}'}\Big(\partial_k J_b(-\mathbf{q}')\ \Phi_b^{\text{clss}}(\mathbf{q}')\Big) \\ &= \partial_k\left(W_{\text{MOD}}[\mathbf{J}]\right), \end{aligned} \tag{2.15}$$

where the second term on the right-hand side comes from the implicit k-dependence of the modified effective action, which appears through the sources $\mathbf{J}$. The factor $\frac{\delta W_{\text{MOD}}}{\delta J_b(\mathbf{q}')}$ on the second term on the right-hand side is the classical field $\Phi_b^{\text{clss}}(\mathbf{q}')$, hence the second and third terms on the right-hand side cancel. The only terms that contribute to $\frac{\mathrm{d}\Gamma_{\text{MOD}}}{\mathrm{d}k}$ are the ones that have explicit k-dependence,

$$\frac{\mathrm{d}}{\mathrm{d}k}\Big(\Gamma_{\text{MOD}}\left[\Phi^{\text{clss}}\right]\Big) = \frac{\partial}{\partial k}\Big(\Gamma_{\text{MOD}}\left[\Phi^{\text{clss}}\right]\Big). \tag{2.16}$$

Continuing with Eq. (2.15) and differentiating the explicit k-dependence in W_{MOD} yields

$$\begin{aligned}\partial_k\Gamma_{\text{MOD}}\left[\Phi^{\text{clss}}\right] &= \partial_k\left(W_{\text{MOD}}[\mathbf{J}]\right)\\ &= \partial_k\left(-\mathfrak{i}\log\left(Z_{\text{MOD}}\right)\right)\\ &= -\frac{1}{2}\sum_{a,b}\int_{\mathbf{q}_1',\,\mathbf{q}_2'}\Big\{\partial_k\left(\hat{R}^{ab}(\mathbf{q}_1',\mathbf{q}_2')\right)\,\langle\Phi_a(\mathbf{q}_1')\,\Phi_b(\mathbf{q}_2')\rangle\Big\},\end{aligned} \tag{2.17}$$

where it was assumed that the fields are k-independent and hence ∂_k acts only on $\hat{R}^{ab}(\mathbf{q}_1',\mathbf{q}_2')$.

Next, we focus on the term $\langle\Phi_a(\mathbf{q}_1')\,\Phi_b(\mathbf{q}_2')\rangle$, which is the two-point Green function for the fields $\Phi_a(\mathbf{q}_1')$ and $\Phi_b(\mathbf{q}_2')$. There, the fields can be (anti)commuted, giving

$$\langle\Phi_a(\mathbf{q}_1')\,\Phi_b(\mathbf{q}_2')\rangle = s_{ab}\,\langle\Phi_b(\mathbf{q}_2')\,\Phi_a(\mathbf{q}_1')\rangle \tag{2.18}$$

where s_{ab} is -1 if both a and b correspond to fermion fields. If either a or b correspond to a scalar field, then s_{ab} is $+1$.[8]

We return to the k-derivative of the effective action (of the modified dynamics) in Eq. (2.17). There, we perform two steps. First we (anti)commute the fields in the two-point Green function [using Eq. (2.18)], and next we apply the identity in Appendix A [Eq. (A.1)]. This yields

$$\begin{aligned}\partial_k\Gamma_{\text{MOD}} = -\frac{1}{2}\sum_{a,b}\int_{\mathbf{q}_1',\,\mathbf{q}_2'}\Bigg\{\partial_k\Big(\hat{R}^{ab}(\mathbf{q}_1',\mathbf{q}_2')\Big)\;s_{ab}\Bigg(\mathfrak{i}\Bigg(\Bigg(\frac{\delta}{\delta\Phi_b^{\text{clss}}(\mathbf{q}_2')}\left(\Gamma_{\text{MOD}}\right)\Bigg)\frac{\overleftarrow{\delta}}{\delta\Phi_a^{\text{clss}}(\mathbf{q}_1')}\Bigg)^{-1}\\ + s_{ab}\,\Phi_a^{\text{clss}}(\mathbf{q}_1')\,\Phi_b^{\text{clss}}(\mathbf{q}_2')\Bigg)\Bigg\},\end{aligned} \tag{2.19}$$

where $\left((\bullet)\frac{\overleftarrow{\delta}}{\delta f}\right)$ is a functional derivative acting from the right. The last term in

[8] The terms in ΔS should have the form of mass terms. This means that the bilinear coefficients $\hat{R}^{ab}$ should only be nonzero when Φ_b is the conjugate field of Φ_a. Bilinear coefficients $\hat{R}^{ab}$ that do not fulfil this condition are not relevant to the FRG.

Eq. (2.19) is a term ΔS evaluated at the classical fields, $\mathbf{\Phi}_{\text{clss}}$. In consequence,

$$\partial_k \Gamma_{\text{MOD}} = -\frac{\mathrm{i}}{2} \sum_{a,b} \int_{\mathbf{q}_1', \mathbf{q}_2'} \left\{ \partial_k \left(\hat{R}^{ab}(\mathbf{q}_1', \mathbf{q}_2') \right) \, s_{ab} \left(\left(\left(\frac{\delta}{\delta \Phi_b^{\text{clss}}(\mathbf{q}_2')} \left(\Gamma_{\text{MOD}} \right) \right) \frac{\overleftarrow{\delta}}{\delta \Phi_a^{\text{clss}}(\mathbf{q}_1')} \right)^{-1} \right) \right\} + \partial_k \left(\Delta S \left[\mathbf{\Phi}_{\text{clss}} \right] \right). \tag{2.20}$$

Using the second term on the right-hand side together with the the partial derivative of the effective action, we recover the running action [see Eq. (2.14)]

$$\partial_k \Gamma_k = -\frac{\mathrm{i}}{2} \sum_{a,b} \int_{\mathbf{q}_1', \mathbf{q}_2'} \left\{ \partial_k \left(\hat{R}^{ab}(\mathbf{q}_1', \mathbf{q}_2') \right) \, s_{ab} \left(\left(\left(\frac{\delta}{\delta \Phi_b^{\text{clss}}(\mathbf{q}_2')} \left(\Gamma_{\text{MOD}} \right) \right) \frac{\overleftarrow{\delta}}{\delta \Phi_a^{\text{clss}}(\mathbf{q}_1')} \right)^{-1} \right) \right\}. \tag{2.21}$$

This equation contains a matrix of second functional derivatives, which is transformed using Eq. (2.10) and (2.14),

$$\begin{aligned} \left(\frac{\delta}{\delta \Phi_b^{\text{clss}}(\mathbf{q}_2')} \left(\Gamma_{\text{MOD}} \right) \right) \frac{\overleftarrow{\delta}}{\delta \Phi_a^{\text{clss}}(\mathbf{q}_1')} &= \left(\frac{\delta}{\delta \Phi_b^{\text{clss}}(\mathbf{q}_2')} \left(\Gamma_k + \Delta S \right) \right) \frac{\overleftarrow{\delta}}{\delta \Phi_a^{\text{clss}}(\mathbf{q}_1')} \\ &= \left(\frac{\delta}{\delta \Phi_b^{\text{clss}}(\mathbf{q}_2')} \left(\Gamma_k \right) \right) \frac{\overleftarrow{\delta}}{\delta \Phi_a^{\text{clss}}(\mathbf{q}_1')} \\ &\quad - \frac{1}{2} \left(\hat{R}^{ba}(\mathbf{q}_2', \mathbf{q}_1') + s_{ab} \, \hat{R}^{ab}(\mathbf{q}_1', \mathbf{q}_2') \right) \\ &= \left(\Gamma_k^{(2)} \right)_{ba} (\mathbf{q}_2', \mathbf{q}_1') - \hat{R}^{ba}(\mathbf{q}_2', \mathbf{q}_1'), \end{aligned} \tag{2.22}$$

where the matrix $\Gamma_k^{(2)}$ is defined as

$$\left(\Gamma_k^{(2)} \right)_{ba} (\mathbf{q}_2', \mathbf{q}_1') = \left(\frac{\delta}{\delta \Phi_b^{\text{clss}}(\mathbf{q}_2')} \left(\Gamma_k \right) \right) \frac{\overleftarrow{\delta}}{\delta \Phi_a^{\text{clss}}(\mathbf{q}_1')} \tag{2.23}$$

and it was assumed that

$$\hat{R}^{ba}(\mathbf{q}_2', \mathbf{q}_1') = \frac{1}{2} \left(\hat{R}^{ba}(\mathbf{q}_2', \mathbf{q}_1') + s_{ab} \, \hat{R}^{ab}(\mathbf{q}_1', \mathbf{q}_2') \right). \tag{2.24}$$

This assumption is valid if $\hat{R}^{ba}(\mathbf{q}_2', \mathbf{q}_1')$ is symmetric when a and b correspond to boson fields; antisymmetric when a and b correspond to fermion fields; and zero when one index corresponds to a fermion and the other to a boson. Regulators necessary to suppress low-momentum modes are discussed in Subsection 2.1.2, and they fulfil the conditions above.

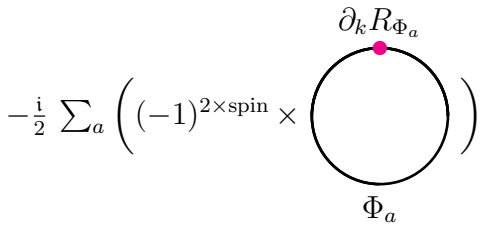

Figure 2.1: One-loop structure in the FRG flow equation.

Reinserting the definition of $\Gamma_k^{(2)}$ in $\partial_k\Gamma_k$ in Eq. (2.21) yields

$$\partial_k\Gamma_k = -\frac{\mathrm{i}}{2}\sum_{a,b}\int_{\mathbf{q}_1',\mathbf{q}_2'}\left\{s_{ab}\,\partial_k\hat{R}^{ab}(\mathbf{q}_1',\mathbf{q}_2')\,\left(\left(\Gamma_k^{(2)}-\hat{R}\right)_{ba}(\mathbf{q}_2',\mathbf{q}_1')\right)^{-1}\right\}, \tag{2.25}$$

and with a little cosmetic rearrangements gives the flow equation in its usual form,

$$\partial_k\Gamma_k = -\frac{\mathrm{i}}{2}\,\mathrm{STr}\left(\partial_k\mathbf{R}\,\left(\Gamma_k^{(2)}-\mathbf{R}\right)^{-1}\right), \tag{2.26}$$

where symbol STr means supertrace operation, which sums over field indices while giving a -1 sign to fermion entries. The supertrace operation also integrates the four-momenta in $\mathbf{R}$ and in $\Gamma_k^{(2)}$.

The matrices $\Gamma_k^{(2)}$ and $\mathbf{R}$ in the flow equation have indices running over the fields. $\Gamma_k^{(2)}$ is a matrix with all the second-order field derivatives of the running action, and $\mathbf{R}$ is the matrix of regulators. The latter has a regulator for each pair of fields with the form $\Phi_a^\dagger$, Φ_a. The indices in $\mathbf{R}$ are symmetric when they correspond to boson fields, and antisymmetric when they correspond to fermions fields. Furthermore, any entry that does not correspond to a pair of fields with the form $\Phi_a^\dagger$, Φ_a is zero.

The integration over four-momentum in the flow equation gives a one-loop structure to the flow. There is a one-loop contribution from each field in the action, and each loop has an insertion of $\partial_k R_{\Phi_a}$, corresponding to the regulator of the field in the loop. Additionally, each contribution has a factor $(-1)^{2\times\mathrm{spin}}$, which gives a -1 for fermion fields and a $+1$ for boson fields. This structure is displayed in Fig. 2.1.

2.1.4 Flow equation: discussion

The FRG flow equation, Eq. (2.26), can be used to continuously evolve from one value of k to another. To integrate quantum fluctuations, we assume that the dynamics (including quantum fluctuations) with momenta above some UV scale is known. We call this scale K_0. From this information we build the running action at this scale, $\Gamma_{k=K_0}$. Once $\Gamma_{k=K_0}$ is known, we use the FRG flow equation to evolve from $\Gamma_{k=K_0}$ to $\Gamma_{k\to 0}$. The limit $k\to 0$ is known as physical limit. There, the regulators vanish and there is no suppression of low-momentum modes. In the physical limit the modified

dynamics matches the original dynamics, and the running action is equal to the effective action of the unmodified dynamics,

$$\Gamma_{k\to 0} = \Gamma_{\text{MOD}}|_{k=0} = \Gamma. \tag{2.27}$$

If we find $\Gamma_{k\to 0}$, then we have integrated the low-momentum quantum fluctuations into the effective action (of the unmodified dynamics), Γ.

The FRG flow equation contains a partial derivative in k, but it also contains second-order field derivatives (in $\Gamma_k^{(2)}$): it is a second-order functional differential equation. An exact solution of this equation would yield an exact effective action in a nonperturbative way (as long as $\Gamma_{k=K_0}$ is known).

Calculating exact effective actions is usually an extremely difficult task, and the FRG is not an exception: solving the FRG flow equation exactly may seem impossible. Nonetheless, the FRG provides a nonperturbative framework where approximation schemes can be introduced to calculate the effective action.

One scheme to introduce approximations into the FRG is to use an ansatz for the running action. Then, (at least in some cases) the flow equation transforms into a system of ordinary differential equations for k-dependent functions on the ansatz. In this case, the effective-action approximation is only as good as the running-action ansatz. A good approximation has an ansatz that contains terms that are most relevant to the dynamics.

2.1.5 Flow equation with scale-dependent fields

In some FRG analysis, the fields in the running action are composite fields, formed by more than one particle. These fields are often introduced by a Hubbard-Stratonovich transformation at the UV scale, $k = K_0$. This transformation eliminates some terms in the action, but the eliminated terms might be regenerated by the flow. It is necessary to consider the regenerated terms, and there is more than one alternative to do so.

- The first is to treat the eliminated terms as zero at the UV scale, but nonzero for other scales. This alternative is inelegant because the terms eliminated at the UV still appear at lower scales, defeating the purpose of the Hubbard-Stratonovich transformation.

- A second is to prescribe scale-dependence in the fields such that this scale-dependence keeps the eliminated terms at zero. This alternative gives terms beyond the one-loop structure of the flow equation, but (at least sometimes) allows to keep the eliminated terms at zero. Furthermore, the field scale-dependence can be used to freeze other terms that are not eliminated by

Hubbard-Stratonovich transformations. This alternative is used in Chapter 3, and in other approaches [38, 67].

- A third was devised by S. Floerchinger and C. Wetterich. They derived an exact flow equation for composite scale-dependent fields in [36].

The flow equation used so far, Eq. (2.26), does not consider scale-dependent fields. To consider scale-dependent fields, the flow equation is extended to

$$\partial_k \Gamma_k = -\frac{\mathrm{i}}{2}\ \mathrm{STr}\left(\partial_k \mathbf{R}\ \left(\Gamma_k^{(2)} - \mathbf{R}\right)^{-1}\right) + \sum_b \int_{\mathbf{q}'} \left(\partial_k \Phi_b(\mathbf{q}')\ \frac{\delta \Gamma_k}{\delta \Phi_b(\mathbf{q}')}\right). \qquad (2.28)$$

The difference between this equation and the flow equation for scale-independent fields, Eq. (2.26), is the second term on the right-hand side (of the former equation).

2.2 Techniques for nonrelativistic systems

2.2.1 Atoms and interactions

This work deals with systems of interacting nonrelativistic particles. We focus on particle-particle interactions that have a scattering length, a, much larger (in absolute value) than its range, $\mathcal{R}$. This framework is independent on the details of the interaction, and this independence allows this framework to describe different types of systems, *e.g.* systems of nucleons, or gases of ultracold atoms.

A large scattering length indicates that the particle-particle interaction is close to forming zero-energy two-particle bound states. There are different possibilities: **a)** When the scattering length is infinite, the interaction strength is at the threshold for the formation of these states. **b)** When the scattering length is negative but large (in absolute value), the interaction is too weak to create two-particle bound states. Nonetheless, two-particle virtual states still play an important role in the dynamics. **c)** Finally, when the scattering length is positive and large, the interaction creates two-particle bound states with energy $-\frac{1}{m\,a^2}$.

For low-energy interactions, a two-particle interaction can be characterised by the effective-range expansion. The leading quantity in this expansion is the scattering length, followed by the range. If the energy is low enough and the scattering length is longer than the range of the interaction, the range may be neglected. In this work, we assume that this is the case; the particle-particle interaction is solely characterised by its scattering length. This is called zero-range approach.

We use the word *atom* to refer to the fundamental particles in this framework even though these particles might not necessarily represent physical atoms. These two uses of the word *atom* should not be confused. We deal with two cases: spin-0

atoms (or scalar atoms) and spin-$\frac{1}{2}$ atoms. In the former case atoms are represented by commuting fields, ψ. In the latter case atoms are represented by anticommuting fields where there are two species of atoms, spin up and spin down, or ψ_1 and ψ_2.

For scalar atoms, the interaction occurs between identical particles. There, atom-atom scattering is simply $\psi\,\psi \to \psi\,\psi$. In contrast, for spin-$\frac{1}{2}$ atoms, the interaction occurs between atoms with opposite spin, as the interaction between identical fermionic atoms is forbidden. In such case, atom-atom scattering is $\psi_1\,\psi_2 \to \psi_1\,\psi_2$, and two-atom states contain a ψ_1 and a ψ_2.

In this work the dynamics is described by the FRG running action. Depending on the system under study, we use different ansätze[9] for the running action. These ansätze are represented by nonrelativistic local Lagrange densities which are written in terms of space-dependent fields.[10] In those Lagrange densities the kinetic terms for atom fields have the form

$$\mathcal{L}_{\text{kin}} = \psi^\dagger(x)\left(\mathrm{i}\,\partial_0 + \frac{\nabla^2}{2\,m}\right)\psi(x) \qquad \text{(scalar atoms)}, \tag{2.29a}$$

$$\mathcal{L}_{\text{kin}} = \sum_{i=1,2}\left(\psi_i^\dagger(x)\left(\mathrm{i}\,\partial_0 + \frac{\nabla^2}{2\,m}\right)\psi_i(x)\right) \qquad \text{(spin-1/2 atoms)}, \tag{2.29b}$$

where the first line corresponds to scalar atoms, and the second line to spin-$\frac{1}{2}$ atoms. These kinetic terms describe the propagation of an atom with nonrelativistic energy.

Local Lagrange densities describe zero-range interactions, or contact interactions. A contact term in a Lagrange density consists of a vertex where all the fields meet at the same point in space and time, and where the coupling associated with the vertex is momentum-independent.[11] For example, a zero-range interaction of two scalar atoms is described by a term

$$-\mathfrak{g}\;\;\psi^\dagger(x)\;\psi^\dagger(x)\;\psi(x)\;\psi(x), \tag{2.30}$$

where each of the two $\psi^\dagger$ fields represents an initial atom, and each of the ψ fields represents a final atom. The strength of this interaction is quantified by the momentum-independent coupling g. The left diagram in Fig. 2.3 represents this contact interaction.

Interactions with momentum close or above $1/\mathcal{R}$ may reveal a more complicated interaction. The latter may be described by a potential, or by Feynman diagrams mediated by other particles. Nonetheless, interactions with low-enough momentum are independent of such details, and a contact interaction is sufficient to describe them.

[9] The word *ansätze* is the plural of *ansatz*.

[10] A local Lagrange density is a polynomial of fields and field derivatives, where all of these are evaluated at the same point in space and time, $x = (ct, \vec{x})$.

[11] This momentum independence refers to the momenta in the initial and final particles in the process.

Figure 2.2: The details of the high-energy interaction (left) are unimportant when the energy is low enough. In the latter case the interaction can be described by a contact term (right).

Fig. 2.2 shows an interaction mediated by some unknown particle (left diagram), and a contact interaction (right diagram) which can describe the low-momentum limit.

This work considers many interaction terms where the initial and final particles are atoms, or even fields composed of two or three atoms. All the interaction terms between these atoms and the composite fields have contact interactions with momentum-independent couplings. The following subsection discusses how some of the composite fields are introduced.

2.2.2 Hubbard-Stratonovich transformations

A Hubbard-Stratonovich transformation is a QFT technique that acts on a Lagrange density with quartic terms [70, 48]. The transformation introduces an auxiliary field, and replaces these quartic terms by interaction terms with the auxiliary field. After the transformation, the path integral of the auxiliary fields has Gaussian form, and hence, these fields can be integrated out to recover the original Lagrange density. This integration can be performed because the auxiliary fields are not dynamical, *i.e.* they do not have kinetic terms. At this stage, a Hubbard-Stratonovich transformation is an identity and has no effect on the dynamics.

This work uses Hubbard-Stratonovich transformations to introduce fields composed of two atoms. This is both for scalar and spin-$\frac{1}{2}$ atoms. The composite fields, $\phi(x)$, are called dimers. For scalar atoms, the dimer is formed by two identical atoms, $\phi(x) \sim \psi(x)\,\psi(x)$. For spin-$\frac{1}{2}$ atoms, the dimer is formed by a spin-up and a spin-down atom, $\phi(x) \sim \psi_1(x)\,\psi_2(x)/2$.

Before the Hubbard-Stratonovich transformation, the Lagrange density has nonrelativistic kinetic terms for atom fields, and a four-atom contact interaction. Explicitly,

$$\mathcal{L} = \psi^\dagger(x)\left(\mathfrak{i}\,\partial_0 + \frac{\nabla^2}{2m}\right)\psi(x) - \mathfrak{g}\;\psi^\dagger(x)\,\psi^\dagger(x)\,\psi(x)\,\psi(x) \qquad \text{(scalar atoms)}, \tag{2.31a}$$

$$\mathcal{L} = \sum_{i=1,2}\left(\psi_i^\dagger(x)\left(\mathfrak{i}\,\partial_0 + \frac{\nabla^2}{2\,m}\right)\psi_i(x)\right) - \mathfrak{g}\;\psi_2^\dagger(x)\,\psi_1^\dagger(x)\,\psi_1(x)\,\psi_2(x) \quad \text{(spin-1/2 atoms)}, \tag{2.31b}$$

where the first line corresponds to scalar atoms, and the second one corresponds to spin-$\frac{1}{2}$ atoms. All the fields in these equations are evaluated at the same point in space-time and the sum over i (in the second line) runs over the spin indices.

With these Lagrange densities, atom-atom scattering is given by the four-atom interaction. One tree-level diagram contributes to this process. It is the diagram in the left in Fig. 2.3.

After the Hubbard-Stratonovich transformation, the Lagrange density for scalar atoms is

$$\begin{aligned}\mathcal{L} = \psi^\dagger(x)\left(\mathrm{i}\,\partial_0 + \frac{\nabla^2}{2m}\right)\psi(x) - \frac{g}{2}\left(\phi^\dagger(x)\,\psi(x)\,\psi(x) + \psi^\dagger(x)\,\psi^\dagger(x)\,\phi(x)\right) \\ - u_d\,\phi^\dagger(x)\,\phi(x),\end{aligned} \tag{2.32a}$$

and the Lagrange density for spin-$\frac{1}{2}$ atoms is

$$\begin{aligned}\mathcal{L} = \sum_{i=1,2}\left(\psi_i^\dagger(x)\left(\mathrm{i}\,\partial_0 + \frac{\nabla^2}{2\,m}\right)\psi_i(x)\right) - g\left(\phi^\dagger(x)\,\psi_1(x)\,\psi_2(x) + \psi_2^\dagger(x)\,\psi_1^\dagger(x)\,\phi(x)\right) \\ - u_d\,\phi^\dagger(x)\,\phi(x),\end{aligned} \tag{2.32b}$$

where all the fields (atoms and dimers) are a function of the same space-time coordinate.

The couplings in the four-atom interactions $\mathfrak{g}$, and the couplings after the Hubbard-Stratonovich transformation g, are related by

$$\mathfrak{g} = -\frac{g^2}{4\,u_d} \qquad \text{(scalar atoms)}, \tag{2.33a}$$

$$\mathfrak{g} = -\frac{g^2}{u_d} \qquad \text{(spin-1/2 atoms)}. \tag{2.33b}$$

With the transformed Lagrange densities, atom-atom scattering is mediated by the dimer field. One tree-level diagram contributes to this process. It is the diagram in the right in Fig. 2.3.

The Hubbard-Stratonovich transformation is performed at the UV scale, and there, the dimer field is not dynamical. However, as the FRG evolves, the quantum fluctuations generate dynamics for the dimer. In consequence, the ansätze (that we use) for the running action contain kinetic terms for the dimer fields.

In some cases the dimer field corresponds to physical particles. This is when two atoms form a bound state. In other cases, two atoms do not form a bound state, and the dimer fields do not represent physical particles. In both cases the dynamics of the dimer plays an important role, as it is a tool to integrate over the quantum fluctuations of two-atom subsystems, while keeping some of their energy dependence.

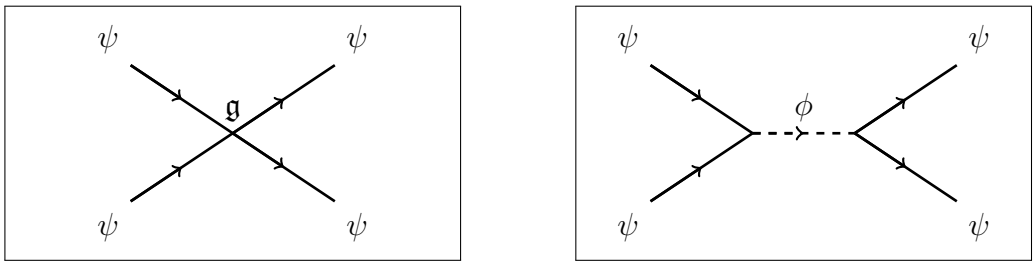

Figure 2.3: Tree-level diagrams for the scattering of two atoms before (left) and after (right) the Hubbard-Stratonovich transformation.

2.2.3 Atom-atom scattering

This subsection introduces a simple ansatz for nonrelativistic atoms with spin $\frac{1}{2}$. This ansatz is used to describe atom-atom scattering, $\psi_1\,\psi_2 \to \psi_1\,\psi_2$. This is the simplest process in this framework. It uses the $\psi_1\,\psi_2 \to \phi$ interaction introduced via a Hubbard-Stratonovich transformation in Subsection 2.2.2. An analogous ansatz for scalar atoms is displayed in Appendix B.

The running action is

$$\Gamma_k = \int \mathrm{d}^4x \left\{ \sum_{i=1,2} \left(\psi_i^\dagger(x) \left(\mathfrak{i}\,\partial_0 + \frac{\nabla^2}{2\,m} \right) \psi_i(x) \right) + Z_d\ \phi^\dagger(x) \left(\mathfrak{i}\,\partial_0 + \frac{\nabla^2}{4\,m} - \frac{u_d}{Z_d} \right) \phi(x) \right.$$
$$\left. - g\ \left(\phi^\dagger(x)\ \psi_1(x)\,\psi_2(x)\ +\ \psi_2^\dagger(x)\,\psi_1^\dagger(x)\ \phi(x) \right) \right\}, \tag{2.34}$$

where all the fields are evaluated at the same space-time coordinate, $x = (c\,t, \vec{x})$. The first term in this ansatz is the atom kinetic term, the second term is the dimer kinetic term, and the third term is the $\psi_1\,\psi_2 \to \phi$ interaction. There are two k-dependent functions in this action: the dimer renormalisation, $Z_d(k)$, and the dimer bilinear, $u_d(k)$. The k-dependent functions in a running action are known collectively as running functions.

In few-body systems, atom-number conservation implies that conjugate fields do not propagate. This makes diagrams with propagating conjugate fields vanish. In consequence g, an atom renormalisation, and an atom bilinear remain constant throughout the FRG evolution.[12]

The amplitude for low-momentum atom-atom scattering is

$$T_{\psi_1\psi_2}(p) = -\frac{2\pi}{\mu_{\psi_1\psi_2}} \left(\frac{1}{-\mathfrak{i}p - 1/a_{\psi_1\psi_2} + \ldots} \right) \to \frac{4\pi}{m} a_{\psi_1\psi_2}, \tag{2.35}$$

where $\mu_{\psi_1\psi_2} = m/2$ is the reduced mass of the two-atom system.

[12] Neither the atom renormalisation nor the atom bilinear are displayed in this ansatz. Their respective UV values are 1 and 0.

In the physical limit, the running action matches the effective action. The dynamics in the latter describes atom-atom scattering with the diagram in the right in Fig. 2.3.[13] The amplitude for this diagram is

$$T_{\psi_1\psi_2} = \frac{g^2}{\Pi_\phi(k \to 0)} = \frac{g^2}{-u_d(k \to 0)}. \tag{2.36}$$

To express the atom-atom interaction in terms of its scattering length, then these two amplitudes must match. This places a boundary condition on u_d in the physical limit,

$$u_d(k \to 0) = -\frac{g^2\, m}{4\,\pi\, a_{\psi_1\psi_2}}. \tag{2.37}$$

2.2.4 Interaction terms with more atoms

The running action in Subsection 2.2.3 contains an interaction term that connects two atoms with a dimer. This interaction has coupling g. Both a two-atom state and a dimer state are composed by two atoms. In that sense, the g-interaction is a two-atom interaction: it connects two initial constituent atoms with two final constituent atoms.

This work includes two-, three-, and four-atom interactions. These interactions (respectively) connect two, three, and four initial constituent atoms with the same number of final constituent atoms. Each of these interactions is described by a term in the running action, where this term contains a product of fields meeting at the same point in space-time. The interaction terms in each running action depend on which fields are present, and on whether the atoms are fermions or bosons. For example, Chapter 3 deals with systems of a few scalar atoms. There, the running action contains atom, dimer, and trimer fields, where these fields (respectively) describe one-, two-, and three-atom subsystems. In consequence, the interaction terms in the running action connect possible combinations of these fields, but with the restriction that the interaction must conserve the number of constituent atoms.

As an example, we consider one of the possible three-atom interaction terms in the case of spin-$\frac{1}{2}$ atoms. This interaction connects an initial spin-up atom and an initial dimer with a final spin-up atom and a final dimer, or $\psi_1\,\phi \to \psi_1\,\phi$.[14] We say that this interaction connects the channel $\psi_1\,\phi$ (initial fields) with itself (final $\psi_1\,\phi$ fields). Both the initial and final channels are formed by three-atoms. The

[13] For the effective action, tree-level diagrams are sufficient to describe a physical process. In this case, the diagram in the right in Fig. 2.3 is the only one that contributes to atom-atom scattering.

[14] We deal with running actions which also contain an analogous term with spin-down atoms, $\psi_2\,\phi \to \psi_2\,\phi$. The couplings for these two terms must be equal, otherwise the dynamics is anisotropic.

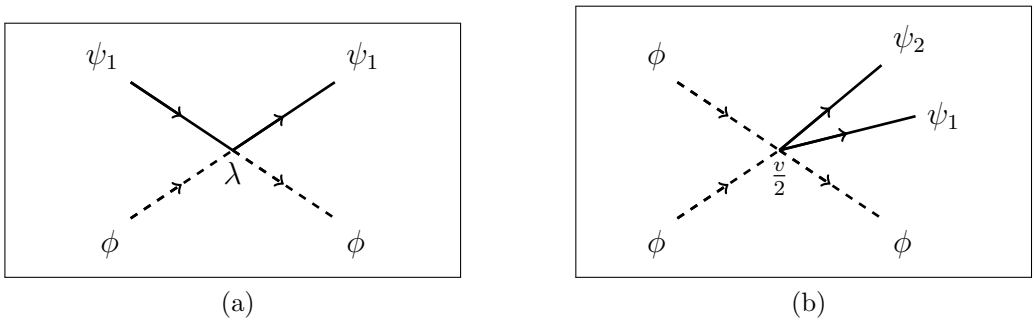

Figure 2.4: A three- and a four-atom interaction, respectively the left and right diagrams.

interaction term (in the running action) for this process is

$$-\lambda \;\; \phi^\dagger(x)\, \psi_1^\dagger(x)\, \psi_1(x)\, \phi(x),$$

where λ is the coupling for this interaction. The vertex corresponding to this interaction term is represented in the left diagram in Fig. 2.4.

As a further example, the four-atom interaction which connects the channels $\phi\,\phi$ and $\psi_1\,\psi_2\,\phi$ has an interaction term

$$-\frac{v}{2} \;\; \phi^\dagger(x)\, \phi^\dagger(x)\, \psi_1(x)\, \psi_2(x)\, \phi(x),$$

where $\frac{v}{2}$ is the coupling for the interaction. The vertex of this interaction is the diagram in the right of Fig. 2.4.

2.2.5 Equations for running functions

This subsection describes a method to calculate flow equations for k-dependent functions, or running functions, in the running action. This method requires a specific form for the running action, usually given by an ansatz. We use this method throughout this work, where the running action has kinetic terms and contact interaction terms.

This method is presented for a particular type of running actions, those with spin-$\frac{1}{2}$ atoms.[15] However, the treatment of scalar atoms is very similar.[16]

[15] These actions are introduced in Subsections 2.2.3 and 2.2.4.

[16] The case of spin-$\frac{1}{2}$ atoms is not identical to the case of scalar atoms. Some signs and factors in some quantities are different. The sign difference originates from the anticommutation of fermions and the commutation of scalars. Furthermore, for scalar atoms there is only one species of atoms, not two.

Matrices in the flow equation

We begin by setting the notation and giving the explicit form of some ingredients in the running action. In particular the matrix of field derivatives $\Gamma_k^{(2)}$, and the matrix of regulators $\mathbf{R}$. First, we chose an order for the fields,

$$(\psi_1^\dagger, \psi_2^\dagger, \psi_1, \psi_2, \phi^\dagger, \phi), \tag{2.38}$$

and use it to write $\Gamma_k^{(2)}$. This matrix has one entry for each pair of fields, where these fields differentiate Γ_k. The rows in $\Gamma_k^{(2)}$ correspond to the first functional derivative and the columns to the second functional derivative. Then, the entry in the a-th row and b-th column of $\Gamma_k^{(2)}$ is

$$\left[\Gamma_k^{(2)}\right]_{ab} = \left(\frac{\delta}{\delta\Phi_a(x)}\left(\Gamma_k\right)\right)\frac{\overleftarrow{\delta}}{\delta\Phi_b(x')}, \tag{2.39}$$

where $\Phi_a, \Phi_b = \psi_1^\dagger, \psi_2^\dagger, \psi_1, \psi_2, \phi^\dagger, \phi$.[17]

The matrix of regulators, $\mathbf{R}$, is also an important ingredient of the FRG flow equation. For the fields under study, it has the form

$$\mathbf{R} = \begin{pmatrix} 0 & 0 & R_a & 0 & 0 & 0 \\ 0 & 0 & 0 & R_a & 0 & 0 \\ -R_a & 0 & 0 & 0 & 0 & 0 \\ 0 & -R_a & 0 & 0 & 0 & 0 \\ 0 & 0 & 0 & 0 & 0 & R_d \\ 0 & 0 & 0 & 0 & R_d & 0 \end{pmatrix}, \tag{2.40}$$

where R_a and R_d are coefficients in the artificial mass terms for atom and dimer fields. This matrix is symmetric under the interchange of indices corresponding to boson fields, but antisymmetric for indices corresponding to fermion fields.

It is easier to calculate the FRG flow using momentum coordinates compared with space-time coordinates. A reason for this is that in momentum coordinates regulators and inverse propagators act as products instead of differential operators (as would be the case in space-time coordinates). However, the running action ansätze in this work are written in terms of space-time coordinates. To use the formulation of the FRG described in this chapter it is necessary to transform the running actions to momentum coordinates. Throughout Subsection 2.2.5, we assume that the latter transformation has already been performed.

If the running action is determined by an ansatz, then $\Gamma_k^{(2)}$ is obtained by field-differentiation. Both the running-action ansatz and $\Gamma_k^{(2)}$ depend on the classical fields,

[17] Field derivatives acting from the right, $\frac{\overleftarrow{\delta}}{\delta f}$, are introduced in Subsection 2.1.3.

but at this point we do not specify any particular value for these fields. However, the flow equation involves $\left(\Gamma_k^{(2)} - \mathbf{R}\right)^{-1}$, not $\Gamma_k^{(2)} - \mathbf{R}$. The latter can be calculated with relative ease, but inverting it (with arbitrary field-dependence) is an extremely difficult task. However, if the fields are evaluated at their classical values, then $\left(\Gamma_k^{(2)} - \mathbf{R}\right)_{\text{clss}}$ takes a simpler form: for all the running-action ansätze in this work, it can be inverted.[18] Furthermore, as we discuss below, the explicit form of $\left(\Gamma_k^{(2)} - \mathbf{R}\right)^{-1}$ (with arbitrary fields) is not necessary to find flow equations for the running functions. The explicit form of $\left(\Gamma_k^{(2)} - \mathbf{R}\right)^{-1}_{\text{clss}}$ is sufficient.

In some systems all the classical fields are zero, but in other systems some classical fields are finite. This work deals with both types of systems. If the classical fields $\psi^\dagger_{1\,\text{clss}}, \psi^\dagger_{2\,\text{clss}}, \psi_{1\,\text{clss}}, \psi_{2\,\text{clss}}, \phi^\dagger_{\text{clss}}, \phi_{\text{clss}}$ are zero, then

$$\left(\Gamma_k^{(2)} - \mathbf{R}\right)^{-1}_{\text{clss}} = \begin{pmatrix} 0 & 0 & 1/\Pi_{\psi^\dagger} & 0 & 0 & 0 \\ 0 & 0 & 0 & 1/\Pi_{\psi^\dagger} & 0 & 0 \\ 1/\Pi_{\psi} & 0 & 0 & 0 & 0 & 0 \\ 0 & 1/\Pi_{\psi} & 0 & 0 & 0 & 0 \\ 0 & 0 & 0 & 0 & 0 & 1/\Pi_{\phi^\dagger} \\ 0 & 0 & 0 & 0 & 1/\Pi_{\phi} & 0 \end{pmatrix}, \tag{2.41}$$

where Π_X is the inverse propagator for the field $X = \psi, \psi^\dagger, \phi, \phi^\dagger$.[19] The inverse propagators have the form

$$\Pi_{\psi} = Z_a \ \left(q^0 - E_a^R\right) \tag{2.42a}$$

$$\Pi_{\psi^\dagger} = Z_a \ \left(q^0 + E_a^R\right) \tag{2.42b}$$

$$\Pi_{\phi} = Z_d \ \left(q^0 - E_d^R\right) \tag{2.42c}$$

$$\Pi_{\psi^\dagger} = -Z_d \ \left(q^0 + E_d^R\right), \tag{2.42d}$$

where E_a^R and E_d^R are the atom and dimer regulated energies.[20]

Chapter 5 deals with systems of fermions in matter, and there the classical fields $\phi_{\text{clss}}, \phi^\dagger_{\text{clss}}$ are not zero. In such case, the form of $\left(\Gamma_k^{(2)} - \mathbf{R}\right)^{-1}_{\text{clss}}$ is more complicated than the one above [in Eq. (2.41)]. However, for the running action discussed there, $\left(\Gamma_k^{(2)} - \mathbf{R}\right)^{-1}_{\text{clss}}$ can be inverted. Now that the matrices $\mathbf{R}$ and $\left(\Gamma_k^{(2)} - \mathbf{R}\right)^{-1}$ are discussed, we turn to a method to obtain flow equations for the running functions.

[18] The label *clss* denotes expressions that are evaluated at the classical fields.

[19] The propagators of ψ_1 and ψ_2 are identical. The same applies to $\psi_1^\dagger$ and $\psi_2^\dagger$.

[20] The form of the propagator for conjugate fields is different for fermion and boson fields. When dealing with scalar atoms the inverse propagator in Eq. (2.42b) changes to $\Pi_{\psi^\dagger} = -Z_a \ \left(q^0 + E_a^R\right)$.

Flow equation for a running function

The flow equation for a generic running function in this work, say $c(k)$, can be obtained from the FRG flow equation. The procedure begins by applying ∂_k on the running-action ansatz. This generates a term $\partial_k\, c(k)$ which can be isolated by taking the appropriate field derivatives of $\partial_k\Gamma_k$ and evaluating at the classical fields. Applying the same procedure to the right-hand side of the flow equation gives an expression for $\partial_k\, c(k)$. The latter expression depends on the running functions and on nonzero classical fields. This expression is called driving term for $c(k)$. The flow equations for all the running functions form a system of first-order, coupled, ordinary differential equations. Solving this system gives the flow of the running functions. This procedure works for all the running functions in this work, except for renormalisations. For the latter, this procedure needs a small modification, which is described at the end of this subsection.

As an example on how to apply the field derivatives to the right-hand side of the flow equation, consider $u_d(k)$ in the running action in Eq. (2.34). The k-derivative of the ansatz yields

$$\partial_k\Gamma_k = \int_{\mathbf{q}} \Big\{ -\partial_k u_d\; \phi^\dagger(\mathbf{q})\, \phi(-\mathbf{q}) \Big\}. \tag{2.43}$$

Next, applying the field derivatives $\phi^\dagger$, ϕ on $\partial_k\Gamma_k$, and evaluating the fields at their classical values yields

$$\big(\delta_\phi\; \delta_{\phi^\dagger}\; (\partial_k\Gamma_k)\big)_{\text{clss}} = -\partial_k u_d(k). \tag{2.44}$$

Therefore, the $\phi^\dagger$- and ϕ-field derivatives isolate $\partial_k u_d$. Applying these field derivatives to the flow equation, and evaluating the fields at their classical values yields

$$\big(\delta_\phi\; \delta_{\phi^\dagger}\; (\partial_k\Gamma_k)\big)_{\text{clss}} = \delta_\phi\; \delta_{\phi^\dagger}\; \left\{ -\frac{\mathrm{i}}{2}\; \mathrm{STr}\Big(\partial_k \mathbf{R}\;\; \Big(\Gamma_k^{(2)} - \mathbf{R}\Big)^{-1} \Big) \right\}_{\text{clss}}. \tag{2.45}$$

A crucial step to obtain the flow equation for u_d is to evaluate this right-hand side. For other running functions, it is crucial to evaluate analogous right-hand sides.

There are two alternatives to evaluate the right-hand side of Eq. (2.45). The first alternative consists on directly applying the field derivatives, which only act on the matrix $\big(\Gamma_k^{(2)} - \mathbf{R}\big)^{-1}$. This yields

$$\begin{aligned} \delta_\phi\; \delta_{\phi^\dagger}\; \big(\mathbf{A}^{-1}\big) = &+ \mathbf{A}^{-1}\cdot(\delta_\phi \mathbf{A})\cdot\mathbf{A}^{-1}\big(\delta_{\phi^\dagger}\mathbf{A}\big)\cdot\mathbf{A}^{-1} + \mathbf{A}^{-1}\cdot\big(\delta_{\phi^\dagger}\mathbf{A}\big)\cdot\mathbf{A}^{-1}(\delta_\phi\mathbf{A})\cdot\mathbf{A}^{-1} \\ &- \mathbf{A}^{-1}\cdot\big(\delta_\phi\,\delta_{\phi^\dagger}\mathbf{A}\big)\cdot\mathbf{A}^{-1}, \end{aligned} \tag{2.46}$$

where $\mathbf{A} = \big(\Gamma_k^{(2)} - \mathbf{R}\big)$ is used as auxiliary notation.

The field derivatives of $\mathbf{A}$ can be calculated, and $(\mathbf{A})^{-1}_{\text{clss}}$ is known. In consequence, if Eq. (2.46) is evaluated at the classical fields, the right-hand side can be explicitly evaluated in terms of the running functions, the classical fields,[21] and the regulators. This yields

$$\partial_k u_d(k) = \int_{\mathbf{q}} \left(\frac{\mathrm{i}\, g^2\, \partial_k R_a}{\Pi^2_{\psi^\dagger}\, \Pi_\psi} - \frac{\mathrm{i}\, g^2\, \partial_k R_a}{\Pi_{\psi^\dagger}\, \Pi^2_\psi} \right), \tag{2.47}$$

where the driving term of $\partial_k u_d(k)$ is given by a four-momentum integral.

The second alternative to evaluate the right-hand side of Eq. (2.45) requires the explicit evaluation of

$$Y = -\frac{\mathrm{i}}{2}\ \mathrm{STr}\Big(\partial_k \mathbf{R}\ \Big((\mathbf{A})^{-1}_{\text{clss}} \cdot \mathbf{B} \cdot (\mathbf{A})^{-1}_{\text{clss}} \cdot \mathbf{B} \cdot (\mathbf{A})^{-1}_{\text{clss}}\ -\ (\mathbf{A})^{-1}_{\text{clss}} \cdot \mathbf{B} \cdot (\mathbf{A})^{-1}_{\text{clss}} \Big)\Big), \tag{2.48}$$

where $\mathbf{B} = (\mathbf{A} - \mathbf{A}_{\text{clss}})$ has arbitrary field-dependence, but $(\mathbf{A})^{-1}_{\text{clss}}$ does not. Y is not a matrix, it is a sum of terms with fields, propagators, and running functions. Once Y is evaluated, the field derivatives $\phi^\dagger$ and ϕ can be applied on it, and the result evaluated at the classical fields. Then we have

$$\big(\delta_\phi\ \delta_{\phi^\dagger}\ (\partial_k \Gamma_k)\big)_{\text{clss}} = \big(\delta_\phi\ \delta_{\phi^\dagger}\ (Y)\big)_{\text{clss}}\,. \tag{2.49}$$

This equation holds because the field differentiation on Y (evaluated at the classical fields) gives the structure in Eq. (2.46).[22] The evaluation of this equation completes the second alternative, which yields the same result as the first one, in Eq. (2.47).

In general the object Y is defined as

$$Y = -\frac{\mathrm{i}}{2}\ \mathrm{STr}\left\{ \partial_k \mathbf{R}\ \cdot\ (\mathbf{A})^{-1}_{\text{clss}}\ \cdot\ \left(\sum_{j=1}^{n} (-1)^j\ (\mathbf{B} \cdot (\mathbf{A})^{-1}_{\text{clss}})^j \right) \right\}, \tag{2.50}$$

where n is the number of fields that will differentiate the flow equation. For a generic running function, $c(k)$, the two ways to calculate the field derivatives of the flow equation yield the same result.

Any running function in this work can be obtained with this method or with the small modification at the end of this subsection. However, the amount of field derivatives that need to be calculated is large, and we use the software *Mathematica* with package *NCAlgebra* to perform these computations.[23] Extra care is necessary

[21] In this example all the classical fields are zero, but in Chapter 5 the running action has a nonzero dimer classical field. There, the flow equations depend on the nonzero classical field.

[22] The field differentiation on Y produces more terms that the ones in Eq. (2.46), but those terms vanish when they are evaluated at the classical fields.

[23] The package NCAlgebra was developed in the Department of Mathematics at the University

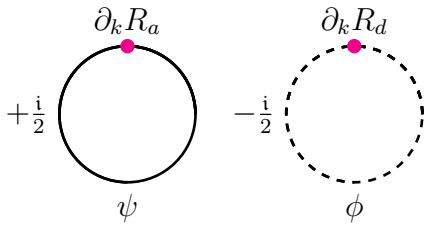

Figure 2.5: Diagram representation of the flow equation for fermionic atoms.

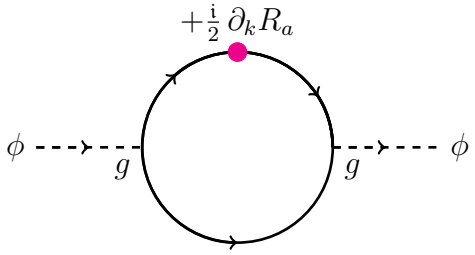

Figure 2.6: Diagram for the flow of $u_d(k)$.

when the field-differentiation contains fermion fields. This is because the field derivatives of two fermion fields anticommute. Furthermore, fermion-field derivatives do not commute with $\Gamma_k^{(2)} - \mathbf{R}$: some entries commute, while others anticommute.[24]

Diagram representation

There is a diagrammatic representation for the driving terms of the running function. This representation stems from the loop representation of the flow equation, Fig. 2.1. For the systems of spin-$\frac{1}{2}$ atoms under study, the one-loop diagrammatic representation of the flow equation is displayed in Fig. 2.5.

The field-differentiation (on $\partial_k \Gamma_k$) to isolate the flow of a running function, $\partial_k c(k)$, creates external legs on the loops in Fig. 2.5. In the example above, to obtain $\partial_k u_d(k)$, the field derivatives $\delta_{\phi^\dagger}$ and δ_ϕ of $\partial_k \Gamma_k$ create an external leg with a ϕ and an external leg with a $\phi^\dagger$. These external legs can only be attached through a g-vertex, hence the dimer loop does not contribute. The driving terms of $\partial_k u_d(k)$ are proportional to the diagram in Fig. 2.6.

The structure of Y, defined in Eq. (2.50), is closely related with the coupling of external legs with the loop in the flow equation. If n is the number of field derivatives

of California San Diego. It is described in `http://math.ucsd.edu/~ncalg/`.

[24] This anticommutation does not come from Γ_k, which is a scalar. It comes from the fermion derivatives that where applied on the running action. The entries in $\Gamma_k^{(2)} - \mathbf{R}$ generated by differentiating (with respect to) two boson or two scalar fields commute with fermion fields (or fermion derivatives). In contrast, entries in $\Gamma_k^{(2)} - \mathbf{R}$ generated by differentiating (with respect to) a boson and a scalar field anticommute with fermion fields (or fermion derivatives). For $\left(\Gamma_k^{(2)}\right)_{a,b}$ in Eq. (2.39), the entries that commute are the ones with $(1 \leq a \leq 4, 1 \leq b \leq 4)$ and the ones with $(5 \leq a \leq 6, 5 \leq b \leq 6)$, while the entries that anticommutation are the ones with $(1 \leq a \leq 4, 5 \leq b \leq 6)$ and the ones with $(5 \leq a \leq 6, 1 \leq b \leq 4)$.

that (will be applied) on $\partial_k \Gamma_k$, then Y has the structure of all the possible one-loop diagrams that have $1, 2, \ldots, n$ possible insertions. After the field derivatives are applied on Y and evaluated at the classical fields, the result corresponds to the diagrams with n external fields that correctly couple to the virtual particles in the Y loops.

The diagrammatic representation could be used to calculate the driving terms for running functions. This work, however, uses the algebraic approach of calculating field derivatives, described above. Nonetheless, the diagrammatic representation is useful to visualise the contributions to particular running functions.

Driving terms for renormalisations

The method (to find driving terms for running functions) described so far, works for all running functions (in this work), except for renormalisations, *e.g.* $Z_d(k)$ in the running action in Eq. (2.34). Let $Z(k)$ be a renormalisation in the running action, then $\partial_k Z(k)$ cannot be isolated solely by taking field derivatives of $\partial_k \Gamma_k$. However, it can be isolated with a small modification in the kinetic terms in the running action. This modification adds artificial terms to q^0 in the kinetic term. These terms have no effect in the dynamics because they are always evaluated at zero. For the running action in Eq. (2.34) this modification consists on

$$\begin{aligned} \left(q^0 - \frac{\vec{q}^{\,2}}{2m}\right) &\to \left((q^0 + P_a) - \frac{\vec{q}^{\,2}}{2m}\right) \\ Z_d \left(q^0 - \frac{\vec{q}^{\,2}}{4m} - \frac{u_d}{Z_d}\right) &\to Z_d \left((q^0 + P_d) - \frac{\vec{q}^{\,2}}{4m} - \frac{u_d}{Z_d}\right). \end{aligned} \tag{2.51}$$

In this case $\partial_k Z_d(k)$ can be isolated by taking $\delta_{\phi^\dagger}$, δ_ϕ, ∂_{P_d}, and evaluating at the classical fields. After ∂_{P_d} is applied, the artificial energies, P_a and P_d, are evaluated at zero. Since the dimer field is formed by two atoms we use the restriction $P_d = 2P_a$.

An analogous procedure can be used to find flow equations for all the renormalisations in this work.

2.2.6 Energy integration and poles

The driving terms for the running functions have a four-momentum integral, *e.g.* the driving term for $u_d(k)$ in Eq. (2.47). This subsection deals with the integration of the q^0-coordinate in the driving terms. This integration uses Cauchy's integral formula because the integrands have poles on q^0.

Cauchy's integral formula states that if $f(z)$ is an holomorphic function of z,[25]

[25] An holomorphic function is complex differentiable in every point of its domain.

and the contour $\mathcal{C}$ encloses z_0 only once in counterclockwise direction, then

$$f(z_0) = \frac{1}{2\,\pi\,\mathrm{i}} \oint_{\mathcal{C}} \frac{f(z)\ \mathrm{d}z}{z - z_0}. \tag{2.52}$$

This formula extends to

$$f^{(r)}(z) = \frac{r!}{2\,\pi\,\mathrm{i}} \oint_{\mathcal{C}} \frac{f(z)\ \mathrm{d}z}{(z - z_0)^{r+1}}, \tag{2.53}$$

where r is a positive integer.

For simplicity, this subsection describes the q^0-integration for running actions with spin-$\frac{1}{2}$ atoms, and where the classical fields are zero. The q^0-integration for scalar atoms is very similar, but the inverse propagator for conjugate atom fields is slightly different. The q^0-integration for nonzero classical dimer field is slightly more complicated, but the ideas behind the integration are the same.

The driving terms for any running function with vanishing classical fields, say $c(k)$, have the form

$$\partial_k c(k) = \int_{\mathbf{q}} \left\{ \sum_{\alpha} \left(\frac{f_\alpha(k)}{(\Pi_\psi)^{a_\alpha} \left(\Pi_{\psi^\dagger}\right)^{b_\alpha} (\Pi_\phi)^{c_\alpha} \left(\Pi_{\phi^\dagger}\right)^{d_\alpha}} \right) \right\}, \tag{2.54}$$

where $f_\alpha(k)$ depends on the regulators and the running functions, but it does not depend on q^0. Additionally, each of the exponents a_α, b_α, c_α, d_α is either zero or a positive integer. In consequence, if we can integrate

$$I_{a,b,c,d} = \int_{-\infty}^{\infty} \frac{\mathrm{d}q^0}{(q^0 - E_a^R)^a\,(q^0 + E_a^R)^b\,(q^0 - E_d^R)^c\,(q^0 + E_d^R)^d}, \tag{2.55}$$

where a, b, c, d are arbitrary positive integers or zero, then we can perform all the q^0-integrals on the driving terms (with classical fields at zero). This integral is useful for the driving terms of both scalar and spin-$\frac{1}{2}$ atoms.

First, the q^0-integral from $-\infty$ to ∞ is equal to the integral on the closed contour $\mathcal{C}_u$ and on $\mathcal{C}_d$. These contours are semicircles in the complex plane for q^0, and they are displayed in Fig. 2.7. In the limit where the radius of the semicircles is infinite, the integrals on the arcs of the semicircles vanish [because the integrand in Eq. (2.55) is zero on those arcs]. In consequence, the integrals on $\mathcal{C}_{u,l}$ reduce to the integral over the real axis,

$$\int_{-\infty}^{\infty} \mathrm{d}q^0 \left\{\text{integrand}\right\} = \oint_{\mathcal{C}_u} \mathrm{d}q^0 \left\{\text{integrand}\right\} = -\oint_{\mathcal{C}_d} \mathrm{d}q^0 \left\{\text{integrand}\right\}, \tag{2.56}$$

where the -1 sign on the third integral comes from the difference in the direction of integration between the first and third integrals.

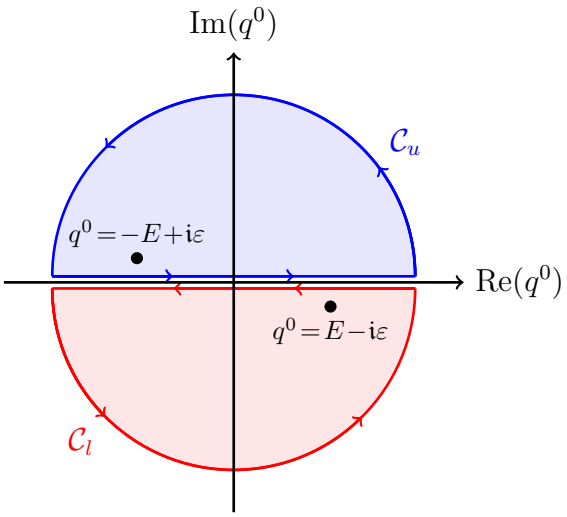

Figure 2.7: Contours of integration $\mathcal{C}_u$ (upper, blue semicircle) and $\mathcal{C}_l$ (lower, red semicircle) in the complex q^0 plane. The points in the fourth and second quadrants are the poles of the functions $1/\left(q^0 - (E - \mathrm{i}\varepsilon)\right)$ and $1/\left(q^0 + (E - \mathrm{i}\varepsilon)\right)$, both of these with $E > 0$.

Instead integrating over the real axis, we use Cauchy's integral formula to evaluate the integrals on the closed contours $\mathcal{C}_{u,l}$. This evaluation uses the poles of the integrand that are enclosed by the contour (on which we are integrating). The integration over $\mathcal{C}_u$ and $\mathcal{C}_l$ should yield the same results.

The integrand in Eq. (2.55) can have poles when q^0 is $\pm E_a^R$ or $\pm E_d^R$. The poles in this integrand sit exactly on the real axis of q^0. Before using Cauchy's integral formula, we apply the prescription

$$\begin{aligned} E_a^R &\to E_a^R - \mathrm{i}\,\varepsilon\, s \\ E_d^R &\to E_d^R - \mathrm{i}\,\varepsilon, \end{aligned} \tag{2.57}$$

where $\varepsilon > 0$. After the q^0-integration, we take the limit $\varepsilon \to 0$. This prescription shifts the poles (in q^0-complex plane) to give the correct character to the propagation of fields. The symbol s represents a ± 1 sign, and we distinguish two possibilities: **a)** Systems of scalar atoms and systems of few spin-$\frac{1}{2}$ atoms always have $s = +1$. This is because in these systems there is no propagation of $\psi^\dagger$ and $\phi^\dagger$. **b)** Systems with a finite density of spin-$\frac{1}{2}$ atoms (dense matter) have $s = \mathrm{sgn}\big(E_a^R\big)$. These systems have a Fermi surface and propagation above the Fermi surface ($E_a^R > 0$) corresponds to propagation of ψ fields. Propagation below the Fermi surface ($E_a^R < 0$) corresponds to propagation of $\psi^\dagger$ fields.

Once the poles are shifted, the integral $I_{a,b,c,d}$ can be calculated with Cauchy's integral formula. The integral on $\mathcal{C}_u$ receives contributions from the poles in the upper-half of the complex q^0 plane, but not from the ones in the lower-half. In contrast, the integral on $\mathcal{C}_l$ receives contributions from the poles in the lower-half,

but not from the upper-half. The explicit form of the integrals on $\mathcal{C}_u$ and on $\mathcal{C}_l$ appears in Appendix C.

Some of the integrands in the driving terms have all their poles either in the upper or on the lower half-planes. These integrals are zero. If the integration is performed on $\mathcal{C}_l$ (for the former) and on $\mathcal{C}_u$ (for the latter), there are no poles enclosed on the integration path, and the integral vanishes.[26]

As an example, the flow of $u_d(k)$ for the running action for spin-$\frac{1}{2}$ atoms in Eq. (2.34) is

$$\begin{aligned}\partial_k u_d(k) &= \int_{\mathbf{q}} \left(\frac{\mathfrak{i}\, g^2\, \partial_k R_a}{\Pi^2_{\psi^\dagger}\, \Pi_\psi} - \frac{\mathfrak{i}\, g^2\, \partial_k R_a}{\Pi_{\psi^\dagger}\, \Pi^2_\psi} \right) \\ &= \int \frac{\mathrm{d}^3 q}{(2\pi)^3} \left\{ -\frac{\mathrm{d}}{\mathrm{d}q^0} \left[\frac{g^2\ \partial_k R_a}{\Pi_\psi} \right]_{q^0 = -E^R_a} + \left[\frac{g^2\ \partial_k R_a}{\Pi^2_\psi} \right]_{q^0 = -E^R_a} \right\} \\ &= \int \frac{\mathrm{d}^3 q}{(2\pi)^3} \left\{ \frac{g^2\ \partial_k R_a(q,k)}{2\, E^R_a(q,k)^2} \right\}, \end{aligned} \tag{2.58}$$

where the first equality is Eq. (2.47). The integrand in the right-hand side of this equality has two terms. The first of these has a double pole inside $\mathcal{C}_u$, and the second term has a single pole. Cauchy's integral formula on the upper contour, together with $s = +1$, yields the second equality. The last equality is obtained by simplifying the previous step.

Once the q^0-integration is performed, the driving terms are given in terms of a $\mathrm{d}^3 q$-integral, where the integrands depend on the running functions and on the regulators. The regulators, and regulated energies depend on the three-momentum $\vec{q}$ only through $\|\vec{q}\|$, hence the $\mathrm{d}^3 q$-integral reduces to a integral in a single coordinate, $\|\vec{q}\|$. For some regulators this integral can be calculated exactly, but for other regulators it needs to be integrated numerically. After the q^0-integration, we solve the system of differential equations for the running functions.

[26] Instead, if the integration is performed on $\mathcal{C}_u$ and on $\mathcal{C}_l$ (respectively), then the integration paths enclose all the poles, but the contribution of these poles must vanish.

Chapter 3

Systems of bosons in vacuum

3.1 Introduction

This chapter deals with systems formed by a few—*i.e.* two, three, and four—scalar particles interacting with low energy. We focus on systems where the particle-particle interaction is close to creating two-particle bound states. The dynamics is represented by a nonrelativistic local Lagrange density, and the low-momentum quantum fluctuations are integrated using the Functional Renormalisation Group. This framework is introduced in Section 2.2.

In this framework, the scattering length, a, is the only dimensionful physical parameter related to the interaction. We define the unitary limit as $1/a \to 0$, for both signs of a. Close to the unitary limit, observable quantities should follow universal relations that depend on powers of a. In the unitary limit there are no dimensionful parameters that describe the interaction, and the behaviour of systems should be universal.[1]

This framework is independent of the detailed form of the particle-particle interaction, and in consequence, it can describe different types of systems. Some examples are low-energy nuclear physics [6, 44], systems of ^{4}He atoms at very low temperature [40], and ultra-cold atoms interacting via Feshbach resonances [20].

3.1.1 Three-particle systems and Efimov effect

A remarkable effect in systems of three particles was discovered by V. Efimov in 1970 [28, 29]. He found that, as long as the particle-particle scattering length is large enough (in absolute value), these systems possess a sequence of three-particle states. This occurs even if the interaction is too weak to form a two-particle bound

[1] Universal behaviour means that a class of systems that have some common characteristics shows the same behaviour even though some of these systems can be very different between themselves.

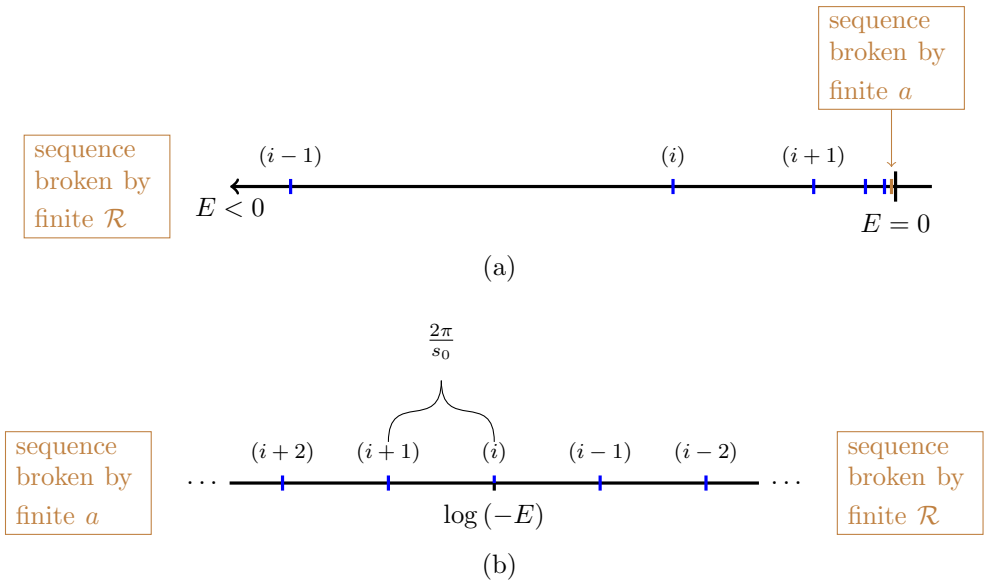

Figure 3.1: Efimov sequence as a function of the energy of the state (upper diagram) and as a function of $\log(-E)$ (lower diagram). In the upper diagram, to be able to show many states, the Efimov factor $\mathrm{e}^{-2\pi/s_0} \simeq \frac{1}{515}$ was replaced by $\mathrm{e}^{-1} \simeq \frac{1}{2.7}$.

state. In the case of identical scalar particles,[2] the binding energy of states in the sequence follows a simple law: the ratio of consecutive binding energies is a universal constant,

$$\frac{E_{i+1}}{E_i} = \mathrm{e}^{-2\pi/s_0} \simeq \frac{1}{515}, \tag{3.1}$$

where $E_i < 0$ is the binding energy of the i-th state in the sequence and $s_0 \simeq 1.006$ is a universal constant. As the Efimov sequence decreases, the binding energies become exponentially more negative, and the sequence stops when the (absolute value of the) binding energy becomes of the order of $1/(m\,\mathcal{R}^2)$, where $\mathcal{R}$ is the range of particle-particle interaction. As the sequence increases, the binding energies accumulate closer to zero, and the sequence stops when the (absolute value of the) binding energy becomes of the order of $1/(m\,|a|^2)$.

Fig. 3.1 shows an Efimov sequence plotted both as a function of the energy of the states (upper diagram) and as a function of $\log(-E)$ (lower diagram). When the states are plotted as a function of $\log(-E)$, they appear separated by a constant shift $2\pi/s_0$, *i.e.* the Efimov sequence is periodic in $\log(-E)$.

So far only the first Efimov state in the sequence has been observed. The first observation was in a gas of ultracold caesium atoms [49]. For reviews on the field see Ref. [14, 20, 31, 45].

In the unitary limit, two-particle systems do not have enough dimensionful parameters to fix physical quantities. In consequence, these quantities behave as powers

[2] When the three particles are identical, the Efimov states are totally symmetric under the interchange of particles. In contrast, Efimov states with two identical fermions are forbidden by Pauli's exclusion principle.

of the energy at with which the processes occur. These powers are dimensionless real numbers and have the same value for all systems. This is regardless of the detailed form of the two-particle potential and the mass of the particles. This power-law behaviour is known as scaling symmetry or scale invariance. It is a continuous symmetry, and a type of universal behaviour.

In the three-body system, the Efimov states break the scaling symmetry, which is reduced to a discrete symmetry. The latter symmetry is a consequence of the periodicity [in $\log(-E)$] of the Efimov states. Furthermore, because of the Efimov effect, the three-particle system does not have universal behaviour. This is because the energy of the first Efimov state provides an extra dimensionful parameter in the system, the Efimov parameter.[3] This parameter is necessary to describe a three-body system and it depends on the microscopic details of the particle-particle potential. In low-energy approaches, like the present one, the Efimov parameter is an independent parameter because it is not determined by the particle-particle scattering length.

3.1.2 Four-particle systems and tetramers

The Efimov parameter breaks the universality of three-body systems. A question arises: does the four-body system break universality any further? Or, equivalently, is it necessary to introduce an extra dimensionful parameter to describe it? Platter, *et al.* conjectured that the system does not provide further universality breaking [62, 43]. Using short-range interactions they found two four-particle states (tetramers) associated to each Efimov three-body state. Quantum mechanics calculations by von Stecher, D'Incao, Greene [71, 27], and Deltuva [21] also found two tetramers and no dependence on any four-particle parameter. These results contradict those of Hadizadeh, *et al.* [41, 42, 75]. The latter group finds nonuniversal behaviour and (up to) three tetramers in each Efimov cycle.

The four-boson system has also been studied using the FRG. In [67], R. Schmidt and S. Moroz studied a running action with atom and dimer fields. They considered up to four-body interaction terms and found one four-atom state in each Efimov cycle. However, these states where later found to be a numerical artifact.[4] In the appendix of that work, the authors extend their running action to include trimer fields. They give scale-dependence to the trimer field and use that scale dependence to eliminate the flow of some couplings. The present work builds on [67] by adding momentum dependence to the trimer and choosing to eliminate the flow of different couplings.

[3] The energy of all the other Efimov states is determined by the scaling in Eq. (3.1).

[4] This is briefly discussed in Section IV of [10] and was also clarified with R. Schmidt and S. Moroz through private communications.

3.2 Running action

This section introduces a running-action ansatz for systems of bosonic atoms.[5] This action contains three types of fields: scalar atoms, dimers, and trimers, which are respectively labelled ψ, ϕ, and χ. Dimer and trimer fields are formed by two and three atoms (respectively). Dimer fields are introduced by a Hubbard-Stratonovich transformation at the UV, see Subsection 2.2.2. Both dimer and trimer fields are included as a tool to integrate over some of the quantum fluctuations of two- and three-atom subsystems (respectively). The running action is a functional of these fields and their conjugates, $\Gamma_k = \Gamma_k[\psi, \psi^\dagger, \phi, \phi^\dagger, \chi, \chi^\dagger]$, and has the explicit form [67, 3]

$$\begin{aligned}\Gamma_k = \int \mathrm{d}^4x \Big\{ & Z_a\, \psi^\dagger \Big(\mathrm{i}\,\partial_0 + \frac{\nabla^2}{2m} \Big) \psi + Z_d\, \phi^\dagger \Big(\mathrm{i}\,\partial_0 + \frac{\nabla^2}{4m} - \frac{u_d}{Z_d} \Big) \phi \\ & + Z_t\, \chi^\dagger \Big(\mathrm{i}\,\partial_0 + \frac{\nabla^2}{6m} - \frac{u_t}{Z_t} \Big) \chi \\ & - \frac{g}{2} \big(\phi^\dagger\, \psi\, \psi + \psi^\dagger\, \psi^\dagger\, \phi \big) - \lambda\, \phi^\dagger\, \psi^\dagger\, \phi\, \psi - h \big(\chi^\dagger\, \phi\, \psi + \phi^\dagger\, \psi^\dagger\, \chi \big) \\ & - \frac{w}{4}\, \phi^\dagger\, \psi^\dagger\, \psi^\dagger\, \phi\, \psi\, \psi - \frac{v_d}{4} \big(\phi^\dagger\, \phi^\dagger\, \phi\, \psi\, \psi + \phi^\dagger\, \psi^\dagger\, \psi^\dagger\, \phi\, \phi \big) - \frac{u_{dd}}{2} \big(\phi^\dagger\, \phi \big)^2 \\ & - \frac{v_t}{2} \big(\phi^\dagger\, \psi^\dagger\, \psi^\dagger\, \chi\, \psi + \chi^\dagger\, \psi^\dagger\, \phi\, \psi\, \psi \big) - \frac{u_{dt}}{2} \big(\phi^\dagger\, \phi^\dagger\, \chi\, \psi + \chi^\dagger\, \psi^\dagger\, \phi\, \phi \big) \\ & - u_{tt}\, \chi^\dagger\, \psi^\dagger\, \chi\, \psi \Big\}, \end{aligned} \tag{3.2}$$

where all the fields are evaluated at the same space-time point, $x = (c\,t, \vec{x})$.

3.2.1 Terms in the running action

Kinetic terms

This running action contains kinetic terms for the three types of fields. These are the first three terms on the right-hand side of Eq. (3.2).

The atom inverse propagator is not renormalised. This is a consequence of atom-number conservation.[6] The kinetic terms for dimers and trimers contain four running functions. Two of them are renormalisations, one for dimers and other for trimers [$Z_d(k)$ and $Z_t(k)$ respectively]. The other two are bilinear coefficients, one for dimers and other for trimers [$u_d(k)$ and $u_t(k)$ respectively].

[5] As stated in Subsection 2.2.1, we use the word *atom* to refer to the elementary particles in this framework, but this use must not be confused with the normal use, which refers to physical atoms.

[6] The renormalisation of atom propagation is given by diagrams with a field propagating backwards in time. The latter field can be an atom, a dimer, or a trimer. However, in nonrelativistic field theories with zero density, particle-number conservation forbids such propagation. In consequence, any diagram with fields propagating backwards is zero. This includes the diagrams that renormalise the atom inverse propagator.

coupling	channels		
w	$\psi\,\psi\,\phi$	$\rightarrow$	$\psi\,\psi\,\phi$
v_d	$\psi\,\psi\,\phi$	$\rightarrow$	$\phi\,\phi$
u_{dd}	$\phi\,\phi$	$\rightarrow$	$\phi\,\phi$
v_t	$\psi\,\psi\,\phi$	$\rightarrow$	$\psi\,\chi$
u_{dt}	$\phi\,\phi$	$\rightarrow$	$\psi\,\chi$
u_{tt}	$\psi\,\chi$	$\rightarrow$	$\psi\,\chi$

Table 3.1: Four-body couplings for the running action and the channels they connect.

Interaction terms

The rest of the terms in the running action are contact interactions between the fields. There are nine of these terms, and they fall in three categories: two-, three-, and four-atom interaction terms. Interaction terms with more than two atoms are introduced in Subsection 2.2.4. The list below describes which couplings fall in each of these categories.

- **Two-atom interaction terms**: the only two-atom interaction term is the one with coupling g. This term produces a vertex where two atoms form a dimer. As a consequence of atom-number conservation in vacuum, g is constant throughout the FRG evolution.

- **Three-atom interaction terms**: there are two interaction terms of this type. They have couplings λ and h. The first coupling connects the channel atom-dimer with itself, $\psi\,\phi \rightarrow \psi\,\phi$. The second connects atom-dimer with a trimer, $\psi\,\phi \rightarrow \chi$.

- **Four-atom interaction terms**: there are six of these terms, and they connect three different four-atom channels. These four-atom channels are atom-atom-dimer (or $\psi\,\psi\,\phi$), dimer-dimer (or $\phi\,\phi$), and atom-timer (or $\psi\,\chi$). Table 3.1 shows the four-body couplings and the channels they connect.

The vertices generated by the all these interaction terms appear in Fig. 3.2.

Interaction terms not included in Γ_k

The interaction terms displayed in the running action, Eq. (3.2), are not all the possible two-, three-, and four-body terms that exist. In the two-body sector, there is a possible $-\mathfrak{g}\ \psi^\dagger\psi^\dagger\psi\psi$ term, but it was eliminated by a Hubbard-Stratonovich transformation. The three-body sector contains interaction terms with the channel $\psi\,\psi\,\psi$, and the four-body sector has interaction terms with $\psi\,\psi\,\psi\,\psi$. It is not necessary to include these terms, as they do not play a role in the FRG flow of Γ_k. This is because **a)** the couplings for all of these terms can be fixed at zero at the UV scale, and **b)**

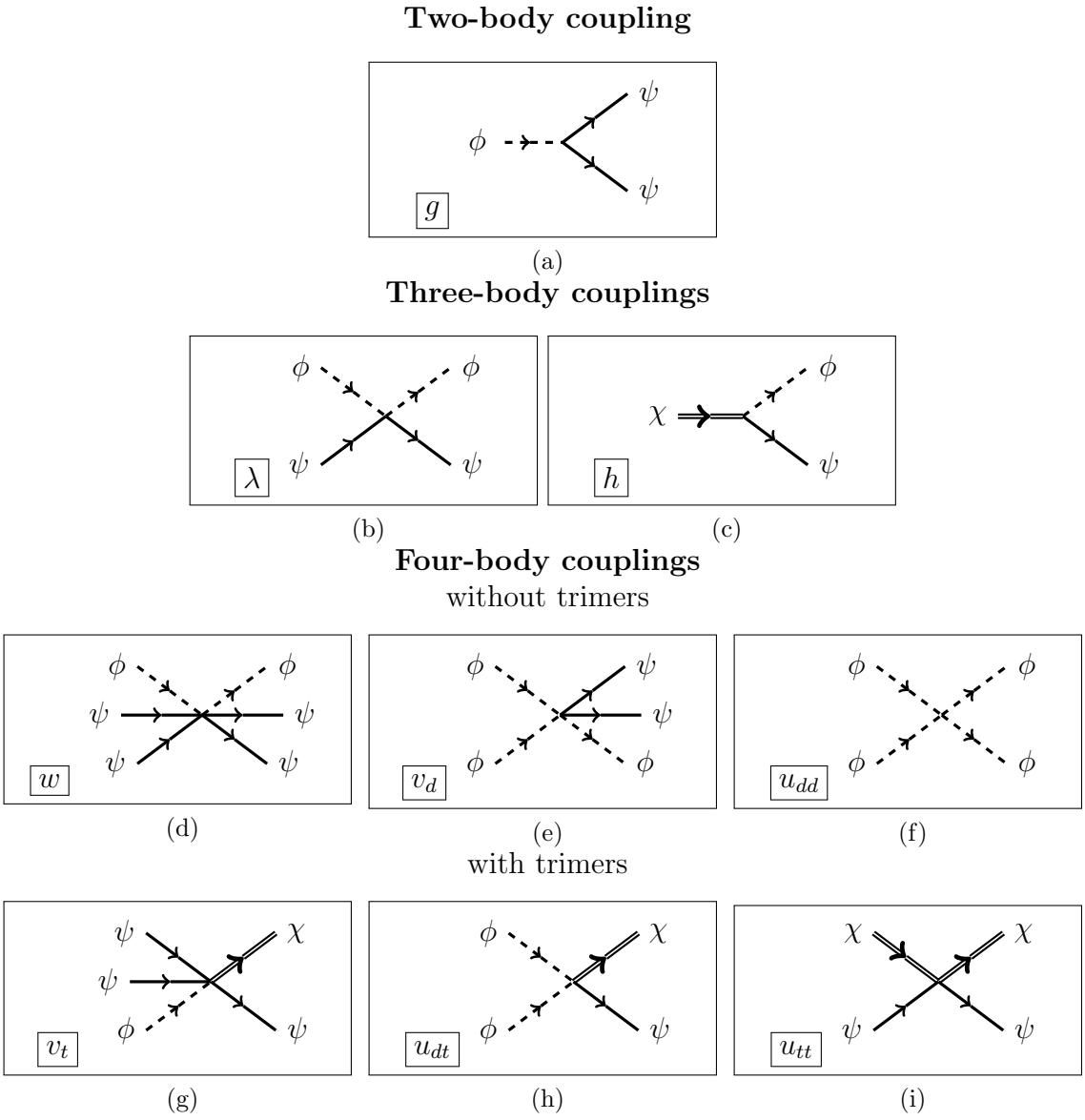

Figure 3.2: Vertices in the scalar running action and their corresponding couplings.

the flow of these couplings vanishes if all of these couplings are zero. In consequence, these couplings begin and remain at zero throughout the FRG evolution.

3.2.2 Regulators and regulated energies

At this point it is convenient to transform the running action ansatz in Eq. (3.2) to momentum coordinates. This allows us introduce the on-shell energy for the fields, which are the only terms that contain the regulators in the flow equations. These energies are important ingredients of the flow, and in this truncation they have the form

$$E_a(q,k) = \frac{q^2}{2m} + R_a(q,k) \tag{3.3a}$$

$$E_d(q,k) = \frac{q^2}{4m} + R_d(q,k) + u_d(k)/Z_d(k) \tag{3.3b}$$

$$E_t(q,k) = \frac{q^2}{6m} + R_t(q,k) + u_t(k)/Z_t(k). \tag{3.3c}$$

To evaluate the FRG flow of the running action it is necessary to chose regulators for the atom, dimer, and trimer fields. We will use regulators of the form proposed by Litim [52],

$$R_a(q,k) = \frac{k^2 - q^2}{2m}\,\theta(k-q), \tag{3.4a}$$

$$R_d(q,k) = Z_d(k)\,\frac{k^2 - q^2}{4m}\,\theta(k-q), \tag{3.4b}$$

$$R_t(q,k) = Z_t(k)\,\frac{k^2 - q^2}{6m}\,\theta(k-q). \tag{3.4c}$$

These regulators have features that simplify the calculation of flow equations for the running functions. One of these features is that for $q < k$, the (regulated) energies for atoms, dimers, and trimers are independent of q, where q is the norm of the three-momentum in the energy. Other feature is that the regulated energies are continuous (but not smooth) as they cross from $q < k$ to $k < q$.

3.3 Trimer scale dependence

The running action for scalar atoms [in Eq. (3.2)] has an interaction term with coupling g, which connects the channel $\psi\,\psi$ with the channel ϕ. This term is introduced at the UV by a Hubbard-Stratonovich transformation, see Subsection 2.2.2. This transformation also eliminates a term that connects $\psi\,\psi$ with itself, $\psi\,\psi \to \psi\,\psi$. The eliminated term has coupling $\mathfrak{g}$, which is not regenerated by the FRG flow: once $\mathfrak{g}$ is set to zero, it remains there. The $\mathfrak{g}$-term and the g-term are redundant in the sense

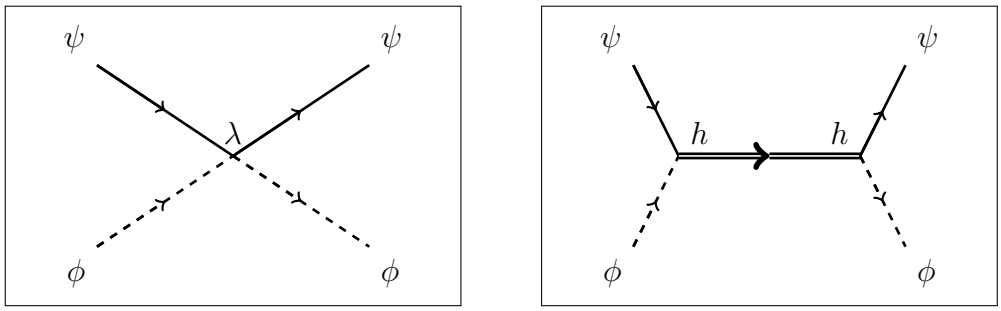

Figure 3.3: All the Feynman diagrams that describe atom-dimer scattering at tree-level with the action in Eq. (3.2). The diagram on the left is proportional to the coupling λ and has no virtual particles. The diagram on the right is proportional to h^2 and contains a virtual trimer.

that both generate tree-level Feynman diagrams for atom-atom scattering.

The running action also produces two tree-level diagrams that describe atom-dimer scattering. These diagrams appear in Figure 3.3. The diagram in the left is proportional to λ, and the diagram on the right is proportional to h^2. Analogous to the two-body case, these two diagrams are redundant in the sense that one of them is enough to describe atom-dimer scattering. At the UV scale, the coupling λ can be eliminated in favour of h. However, the FRG evolution regenerates λ, driving it out of zero. The driving terms for both h and λ must be considered.[7] It is not mandatory to eliminate the λ and h redundancy, but doing so can simplify the flow of the running action, making the system more tractable. We eliminated this redundancy by making the trimer field scale-dependent and fixing such scale dependence in a convenient way. This allows to eliminate the coupling λ and also three of the six four-body couplings in the running action. However, the driving terms for the eliminated couplings still participate in the flow of the remaining running functions.

Scale-dependent fields in the FRG have been used before. For example H. Gies and C. Wetterich used scale-dependent fields to study a transition from bound to fundamental particles as the scale changes [38]. S. Floerchinger *et al.* studied three-component Fermi gases using a scale-dependent trimer field [34, 35]. A. C. Fonseca and P. E. Shanley studied four-boson systems with atom, dimer, and trimer fields [37]. Instead of the FRG, their work relies on integral equations. However, the structure in their integrals is similar to some structures in this analysis. Furthermore, the use of scale-dependent trimer fields to eliminate couplings in this action was proposed by R. Schmidt and S. Moroz in the appendix of Ref. [67]. Our approach closely follows the ideas in such proposal.

[7] As discussed in Subsection 2.2.5, the driving terms of a running function, say $c(k)$, are the terms that give $\partial_k c(k)$. These terms are obtained from the flow equation, and are a function of the running functions, the regulated energies, and the regulators.

The FRG flow equation for scale-dependent fields is introduced in Subsection 2.1.5. This equation is

$$\partial_k \Gamma_k = -\frac{\mathrm{i}}{2}\ \mathrm{STr}\left(\partial_k \mathbf{R}\ \left(\Gamma_k^{(2)} - \mathbf{R}\right)^{-1}\right) + \sum_b \int_{\mathbf{q}'} \left(\partial_k \Phi_b(\mathbf{q}')\ \frac{\delta \Gamma_k}{\delta \Phi_b(\mathbf{q}')}\right), \tag{3.5}$$

where Φ is an array with all fields in the running action and b is an index that runs over those fields.

The k-dependence of trimer fields can be specified through their derivative in k. This derivative should be a sum of terms where each term has a product of fields times a k-dependent coefficient. Additionally, each term must have the same atom number as the trimer field. This ensures that the derivative in k has the correct atom number.[8] This chapter uses k-independent atom and dimer fields, but k-dependent trimer fields. The trimer scale-dependence has the form

$$\partial_k \chi = \zeta_1(k)\ \psi\,\phi \quad + \zeta_2(k)\ \psi^\dagger\,\psi\,\chi \ + \zeta_3(k)\ \psi^\dagger\,\phi\,\phi \ + \zeta_4(k)\ \psi^\dagger\,\psi\,\psi\,\phi, \tag{3.6a}$$

$$\partial_k \chi^\dagger = \zeta_1(k)\ \phi^\dagger\,\psi^\dagger + \zeta_2(k)\ \chi^\dagger\,\psi^\dagger\,\psi + \zeta_3(k)\ \phi^\dagger\,\phi^\dagger\,\psi + \zeta_4(k)\ \phi^\dagger\,\psi^\dagger\,\psi^\dagger\,\psi, \tag{3.6b}$$

where $\zeta_i(k)$ are four coefficients with arbitrary dependence on k. The terms in Eq. (3.6) give additional contributions to the flow of some running functions. The additional contributions are linear in the coefficients ζ_i, hence these coefficients can be set to eliminate the flow of four running functions that have additional terms.[9]

The flows receive additional contributions in the sense that the flow has the form it would have for scale-independent fields (supertrace part of the flow equation) plus terms due to the scale-dependence of trimers. The scale-independent contribution to the flow of any running function $c(k) = g, \lambda(k), h(k), \ldots$ will be denoted as $[\partial_k\, c(k)]^{\text{c.f.}}$. The flows of $\lambda, h, w, v_d, v_t, u_{tt}$ receive additional contributions, whereas the flow the other running functions in Γ_k does not change with the trimer scale dependence.

[8] There is an infinite number of terms that have the correct atom number, and that could appear in $\partial_k \chi$. For example, $\partial_k \chi$ can have terms proportional to $\psi^\dagger\,\psi\,\chi$, $(\psi^\dagger\psi)^2\chi$, $(\psi^\dagger\psi)^3\chi$, ... Nonetheless, in this case, the terms in Eq. (3.6) are sufficient. This is because only these terms give contributions to the flow of the running functions under consideration.

[9] Four of these flows can be eliminated since there are four arbitrary coefficients $\zeta_i(k)$.

The additional contributions (to the flows) have the form

$$\partial_k \lambda = [\partial_k \lambda]^{\text{c.f.}} + 2\,\zeta_1(k)\,h, \tag{3.7a}$$
$$\partial_k h = [\partial_k h]^{\text{c.f.}} + \zeta_1(k)\,u_t, \tag{3.7b}$$
$$\partial_k w = [\partial_k w]^{\text{c.f.}} + 8\,\zeta_4(k)\,h + 8\,\zeta_1(k)\,v_t, \tag{3.7c}$$
$$\partial_k v_d = [\partial_k v_d]^{\text{c.f.}} + 4\,\zeta_3(k)\,h + 4\,\zeta_1(k)\,u_{dt}, \tag{3.7d}$$
$$\partial_k v_t = [\partial_k v_t]^{\text{c.f.}} + \zeta_2(k)\,h + \zeta_4(k)\,u_t + 2\,\zeta_1(k)\,u_{tt}, \tag{3.7e}$$
$$\partial_k u_{dt} = [\partial_k u_{dt}]^{\text{c.f.}} + \zeta_3(k)\,u_t \tag{3.7f}$$
$$\partial_k u_{tt} = [\partial_k u_{tt}]^{\text{c.f.}} + 2\,\zeta_2(k)\,u_t. \tag{3.7g}$$

All the couplings whose flows receive additional contributions are zero at the ultraviolet scale. Hence if the flow of any of these couplings is eliminated the coupling would be zero throughout the FRG evolution. This can be used to simplify the system of flow equations. However, the flow of the eliminated coupling still plays a role on the flow of the running functions that were not eliminated.

We eliminate the couplings λ, w, v_d, and v_t. This is realised with the choice

$$\zeta_1(k) = -\frac{[\partial_k \lambda]^{\text{c.f.}}}{2\,h}, \tag{3.8a}$$
$$\zeta_2(k) = -\frac{[\partial_k v_t]^{\text{c.f.}}}{h} + \frac{u_{tt}\;[\partial_k \lambda]^{\text{c.f.}}}{2\,h^2} - \frac{u_t\,v_t\;[\partial_k \lambda]^{\text{c.f.}}}{2\,h^3} + \frac{u_t\;[\partial_k w]^{\text{c.f.}}}{8\,h^2}, \tag{3.8b}$$
$$\zeta_3(k) = -\frac{[\partial_k v_d]^{\text{c.f.}}}{4\,h} + \frac{u_{dt}\;[\partial_k \lambda]^{\text{c.f.}}}{2\,h^2}, \tag{3.8c}$$
$$\zeta_4(k) = -\frac{[\partial_k w]^{\text{c.f.}}}{8\,h} + \frac{v_t\;[\partial_k \lambda]^{\text{c.f.}}}{2\,h^2}. \tag{3.8d}$$

The choice to eliminate λ, w, v_d, and v_t is not unique. In Ref. [67], Schmidt and Moroz eliminated couplings λ, v_t, u_{dt}, and u_{tt}. That choice eliminates the λ and h redundancy and all the four-body couplings that include trimer fields.

The choice used here eliminates the λ and h redundancy. It also eliminates all the couplings involving the four-body channel $\psi\,\psi\,\phi$. The four-body couplings that survive are between the channels $\phi\,\phi$ and $\psi\,\chi$. This choice is inspired by the structure of the Faddeev-Yakubovsky equations [74].

Keeping only the four-body channels $\phi\,\phi$ and $\psi\,\chi$ has remarkable consequences on the structure of the FRG flow: the skeletons of the diagrams that drive the flow (of four-body couplings) have a special structure. This is discussed in more detail in Subsection 3.9.2.

3.4 Driving terms in the flow

Subsection 2.2.5 discusses a method to find driving terms for the running functions. This method involves taking field derivatives in the running action. Furthermore, the driving term for each running function involves a four-momentum integral, and Subsection 2.2.6 discusses how to evaluate the q^0 component of such integrals.

The driving terms for all the running functions form a system of differential equations.[10] Atom-number conservation in vacuum implies that n-atom running functions are completely independent of more-than-n-atom running functions. This means for example that the driving term for a two-body parameter does not involve any three-body parameters.

3.5 Two-body sector

The two-body sector comprises g, $u_d(k)$, and $Z_d(k)$. First, the coupling g is constant and it scales out of the evolution of other parameters. Its value has no effect on the flow of other running functions. Next, the flow of $u_d(k)$ and $Z_d(k)$ is described by a diagram like the one in Fig. 2.6.[11] For the regulators in this chapter, Eq. (3.4), the flow of $u_d(k)$ and $Z_d(k)$ can be analytically integrated. The integration of $u_d(k)$ uses a boundary condition that guarantees that the two-body sector yields the correct atom-atom scattering length. This condition is discussed in Subsection 2.2.3 and in Appendix B. The integration of $Z_d(k)$ uses the boundary condition $Z_d(K_0) \sim 0$, which states that the dimer has no dynamics at the UV scale. The two-body running functions have the form

$$u_d(k,a) = \frac{m\,g^2}{\pi^2}\left(\frac{k}{6} - \frac{\pi}{8\,a}\right), \tag{3.9a}$$

$$Z_d(k) = \frac{2\,m^2\,g^2}{\pi^2}\,\frac{1}{6\,k}. \tag{3.9b}$$

3.6 Three-body sector: flow equations

The FRG evolution of the three-body sector has been studied before. Ref. [67] deals with a trimerless action with scalar atoms, however, its appendix includes trimers in the action. This chapter takes the framework from such appendix, and the three-body sector in these works is identical. Ref. [34] describes the FRG flow of an action with three species of fermionic atoms.[12] That system also shows Efimov behaviour

[10] All the derivatives in the system are first-order k-derivatives.

[11] In this case, the insertion $+\frac{\mathrm{i}}{2}\,\partial_k R_a$ in Fig. 2.6 is replaced by $-\frac{\mathrm{i}}{2}\,\partial_k R_a$ because we are dealing with bosonic atoms.

[12] These species may correspond to three hyperfine states of ultracold atoms.

and the three-body flow equations are very similar to the present action.

The three-body sector comprises the couplings $\lambda(k)$ and $h(k)$, the bilinear $u_t(k)$, and the renormalisation $Z_t(k)$. However, as discussed in Section 3.3, $\lambda(k)$ is zero throughout the evolution. After being integrated over q^0, the three-body flow equations are

$$\begin{aligned} h'(k) = \int \frac{d^3q}{(2\pi)^3} \Bigg\{ & \frac{g^4 u_t}{h} \Bigg(- \frac{\partial_k R_d \; Z_d^{-2}}{8 \; (E_a)^2 \; (E_d + E_a)^2} - \frac{\partial_k R_a \; E_d \; Z_d^{-1}}{4 \; (E_a)^3 \; (E_d + E_a)^2} \Bigg) \\ & + \frac{g^4 u_t}{h} \Bigg(- \frac{3 \; \partial_k R_a \; Z_d^{-1}}{8 \; (E_a)^2 \; (E_d + E_a)^2} \Bigg) + g^2 h \Bigg(- \frac{\partial_k R_d \; Z_d^{-2}}{2 \; E_a \; (E_d + E_a)^2} \Bigg) \\ & + g^2 h \Bigg(- \frac{\partial_k R_a \; E_d \; Z_d^{-1}}{2 \; (E_a)^2 \; (E_d + E_a)^2} - \frac{\partial_k R_a \; Z_d^{-1}}{E_a \; (E_d + E_a)^2 Z_d} \Bigg) \Bigg\}, \end{aligned} \tag{3.10a}$$

$$u_t'(k) = \int \frac{d^3q}{(2\pi)^3} \Bigg\{ h^2 \Bigg(\frac{\partial_k R_d \; Z_d^{-2}}{(E_d + E_a)^2} + \frac{\partial_k R_a \; Z_d^{-1}}{(E_d + E_a)^2} \Bigg) \Bigg\}, \tag{3.10b}$$

$$Z_t'(k) = \int \frac{d^3q}{(2\pi)^3} \Bigg\{ h^2 \Bigg(- \frac{2 \; \partial_k R_d \; Z_d^{-2}}{(E_d + E_a)^3} - \frac{2 \; \partial_k R_a \; Z_d^{-1}}{(E_d + E_a)^3} \Bigg) \Bigg\}. \tag{3.10c}$$

These flow equations depend on two- and three-body running functions. They also depend on atom and dimer regulators and energies. However, they are independent of the trimer regulator and energy.

The regulated energy of an atom and a dimer, $(E_d + E_a)$, appears in several denominators in these flow equations. The combination $(E_d + E_a)$ can cross zero during the FRG evolution. The point where this happens corresponds to the atom-dimer threshold dropping below the three-atom threshold. This crossing only occurs if the atom-atom scattering length is positive, *i.e.* there is a two-atom bound state. This is because only one negative contribution to $(E_d + E_a)$ is possible,

$$\left(- \frac{2 \, m^2 \, g^2}{\pi^2} \times \frac{\pi}{4 \, a} \right) / Z_d(k),$$

which comes from the term $u_d(k)/Z_d(k)$ in the dimer energy [see Eq. (3.3)].

It is convenient to define an auxiliary function $H(k) = h^2(k)$. One of the reasons to do this will be made clear in Section 3.7: $H(k)$ changes sign periodically in $\log(k)$, hence keeping track of $H(k)$ instead of $h(k)$ means that we do not have to deal with an imaginary running function, just a negative one. Furthermore, the simultaneous differential equations for $H(k)$, $u_t(k)$, and $Z_t(k)$ are linear.

The flow of each running function is proportional to a power of g and m. These factors can be absorbed in the running functions. In the three-body sector, this leads to the introduction of g- and m-independent functions, which are denoted by a tilde,

$$\tilde{\lambda}(k) = \left(\frac{1}{g^2\, m}\right)\ \lambda(k) \tag{3.11a}$$

$$\tilde{u}_t(k) = \left(g^2\, m\right)\ u_t(k) \tag{3.11b}$$

$$\tilde{Z}_t(k) = \left(g^2\right)\ Z_t(k), \tag{3.11c}$$

where $H(k)$ does not need to absorb any of these factors to have a flow independent of g and m.

The factors of g and m on the flow of each running function can be determined **a)** by dimensional analysis on the running action or **b)** by looking at the flow of each running function. Once the powers of g and m have been absorbed in the running functions, there are only two dimensionful quantities in the flow equations: a and k.[13]

3.7 Three-body sector: scaling limit

For the FRG flow we are dealing with, the scaling limit is defined as the limit where $1/|a| \to 0$ while k remains finite. This limit corresponds to the region where $1/|a| \ll k$. There, the flow of $H(k)$, $\tilde{u}_t(k)$, and $\tilde{Z}_t(k)$ contains only one dimensionful quantity, k. Using the regulators in Eq. (3.4) and the two-body parameters in Eq. (3.9) we get the flow equations

$$\partial_k H = -\frac{312}{125\, k}\, H(k) - \frac{256}{125\, k^3}\, \tilde{u}_t(k), \tag{3.12a}$$

$$\partial_k \tilde{u}_t = \frac{56\, k}{125}\, H(k), \tag{3.12b}$$

$$\partial_k \tilde{Z}_t = -\frac{448}{625\, k}\, H(k). \tag{3.12c}$$

Assuming a power-law behaviour for $H(k)$ and $\tilde{u}_t(k)$,[14]

$$H(k) = k^d \tag{3.13a}$$

$$\tilde{u}_t(k) = D\, k^{d+2}, \tag{3.13b}$$

and substituting this in the flow equations, Eq. (3.12a) and (3.12b), we find that the power-law behaviour of $H(k)$ and $\tilde{u}_t(k)$ solves the differential equations only if two

[13] K_0 is also dimensionful, but it is a particular value of k.

[14] Dimensional analysis can be used to see that the k-exponent of $\tilde{u}_t(k)$ must be the exponent of $H(k)$ plus two, $d+2$.

conditions are fulfilled:

$$D = \frac{56}{125\ (d+2)} \tag{3.14}$$

and

$$0 = d^2 + \left(\frac{562}{125}\right) d + \frac{92\,336}{15\,625}. \tag{3.15}$$

The solutions for this quadratic are

$$d_{(\pm)} = -\frac{281}{125} \pm \mathrm{i}\,\frac{\sqrt{535}}{25}. \tag{3.16}$$

Any solution for $H(k)$ and $\tilde{u}_t(k)$ can be written as a linear combination of the solutions for $d_{(\pm)}$. The initial conditions $H(K_0)$ and $\tilde{u}_t(K_0)$ determine the two coefficients in this linear combination. The solution for $\tilde{Z}_t(k)$ provides and extra free parameter that is determined by $\tilde{Z}_t(K_0)$. However, as we will see in Subsection 3.7.2, these three initial conditions are associated with only one independent physical quantity, the Efimov parameter. The rest of the information they contain is not physical. In the next subsection, Subsection 3.7.1, we rewrite the three-body functions $H(k)$, $\tilde{u}_t(k)$, and $\tilde{Z}_t(k)$ in a way that (hopefully) makes their discussion clearer.

3.7.1 Rescaled running functions

The lack of real solutions to the power law behaviour in the three-body sector is a manifestation of the breaking of scaling symmetry. The imaginary part of $d_{(\pm)}$ will produce oscillatory behaviour in the variable

$$\tau = \log\,(k/K_0)\,. \tag{3.17}$$

This is associated with the Efimov effect and is discussed below (Subsection 3.7.2).

New three-body functions, called rescaled functions, can be defined from $H(k)$, $\tilde{u}_t(k)$, and $\tilde{Z}_t(k)$ by scaling out the real part of their corresponding power of k. For $H(k)$ and $\tilde{u}_t(k)$, this exponent is determined by the real part of $d_{(\pm)}$, [see Eq. (3.13) and (3.16)]. The real power of k for $\tilde{Z}_t(k)$ is determined by dimensional analysis and the powers of $H(k)$ and $\tilde{u}_t(k)$.

If the scaling symmetry was not broken by the Efimov effect, then there would be constant solutions for the rescaled functions. These solutions are given by the fixed points of the flow equations. The flow of systems where scaling symmetry is unbroken allows this type of solutions. For example, see Chapter 4, which deals

with a running action with fermionic atoms.[15] There, the rescaled parameters have fixed-point solutions. However, in this case, the flow equations do not allow for this type of solutions. This is because the breaking of scaling symmetry is built-in the flow equations.

These rescaled functions are also used when the atom-atom scattering length is finite. Furthermore, the powers of k that rescale the three-body sector determine analogous powers in the four-body sector.

The rescaled three-body functions are

$$\hat{H}(k) = k^{281/125}\ H(k) \tag{3.18a}$$

$$\hat{u}_t(k) = k^{31/125}\ \tilde{u}_t(k) \tag{3.18b}$$

$$\hat{Z}_t(k) = k^{281/125}\ \tilde{Z}_t(k). \tag{3.18c}$$

The flow equations for the rescaled parameters, in the scaling limit, become

$$\partial_k \hat{H} = -\frac{31}{125\ k}\ \hat{H}(k) - \frac{256}{125\ k}\ \hat{u}_t(k) \tag{3.19a}$$

$$\partial_k \hat{u}_t = +\frac{56}{125\ k}\ \hat{H}(k) + \frac{31}{125\ k}\ \hat{u}_t(k) \tag{3.19b}$$

$$\partial_k \hat{Z}_t = -\frac{448}{625\ k}\ \hat{H}(k) + \frac{281}{125\ k}\ \hat{Z}_t(k). \tag{3.19c}$$

In the scaling limit, $\hat{H}(k)$ and $\hat{u}_t(k)$ can be written as powers of k with imaginary exponents. However, there is a more convenient base to write the solutions of $\hat{H}(k)$ and $\hat{u}_t(k)$,

$$\hat{H}(k) = A_c\ \cos(\omega\ \tau) + A_s\ \sin(\omega\ \tau) \tag{3.20a}$$

$$\hat{u}_t(k) = B_c\ \cos(\omega\ \tau) + B_s\ \sin(\omega\ \tau) \tag{3.20b}$$

where k appears through the variable τ, defined in Eq. (3.17), and ω is a numeric constant

$$\omega = \mathrm{Im}\ d_{(+)} = \frac{\sqrt{535}}{25}. \tag{3.21}$$

The solution for $\hat{H}(k)$ and $\hat{u}_t(k)$ in Eq. (3.20) contains four constants, A_c, A_s, B_c, and B_s, however, only two of these constants are independent. These four constants are a linear function of the initial conditions $\hat{H}(K_0)$ and $\hat{u}_t(K_0)$.

Equation (3.20) shows solutions for $\hat{H}(k)$ and $\hat{u}_t(k)$ in terms of sine and cosine of $(\omega\,\tau)$. The most general solution for $\hat{Z}_t(k)$ is a little more complicated. It has the

[15] There is no Efimov effect in that case.

form

$$\hat{Z}_t(k) = C_0\, \mathrm{e}^{281\,\tau/125} + C_c\, \cos(\omega\, \tau) + C_s\, \sin(\omega\, \tau) \tag{3.22}$$

where C_c and C_s are linear functions of $\hat{H}(K_0)$ and $\hat{u}_t(K_0)$. In contrast C_0 is a linear function of $\hat{H}(K_0)$, $\hat{u}_t(K_0)$, and $\hat{Z}_t(K_0)$. Regardless of the value of C_0, as τ evolves towards $-\infty$ (the physical limit), the exponential term in $\hat{Z}_t(k)$ becomes unimportant. The region in k where the effect of the C_0 term is important is known as transient region.[16] For simplicity we can chose $\hat{Z}_t(K_0)$ such that $C_0 = 0$ and we will do so from now on.

The coefficients on the sine and cosine in $\hat{H}(k)$, $\hat{u}_t(k)$, and $\hat{Z}_t(k)$ are fixed by the initial conditions on $\hat{H}$ and $\hat{u}_t$. In contrast, the relative phases between the running functions are fixed by the flow equations, not by the initial conditions. Figure 3.4 shows the evolution of $\hat{H}(k)$, $\hat{u}_t(k)$ and $\hat{Z}_t(k)$ and their different relative phases.

The initial conditions on $\hat{H}$ and $\hat{u}_t$ determine two parameters, **a)** an overall phase for the oscillation of $\hat{H}(k)$, $\hat{u}_t(k)$ and $\hat{Z}_t(k)$ and **b)** an amplitude for the oscillations. The overall phase is associated with a physical parameter, the Efimov parameter, and is discussed in Subsection 3.7.2 (the next one). The amplitude of oscillations is not associated with any physical parameter and it divides out of observables calculated with the running action.

The parameters $\hat{H}(k)$ and $\hat{Z}_t(k)$ do not have the same phase. This means that there is a region in each Efimov cycle where they have opposite signs. Such region is unphysical because, there, the trimer propagator $\frac{h^2}{Z_t\, p^0 - u_t}$ has a negative residue at its pole and hence the trimer field has ghostlike character. The size of these regions is always the same—it is fixed by the flow equations, not the initial conditions—and they are smaller than the rest of the Efimov cycle. These regions are coloured with blue in Fig. 3.4.

The flow of the three-body rescaled functions can be described without specifying a value of K_0. The dimensionless variable k/K_0 is sufficient. Furthermore, the flow of four-body rescaled functions can also be determined independently of K_0. However, a particular value of K_0 is necessary to recover a dimensionful Efimov parameter (combined with the phases of the rescaled functions). Even in the case of finite a, the flow of three- and four-body functions, can be written in terms of the dimensionless combination $\frac{a^{-1}}{K_0}$.

[16] Transient regions are parts of the FRG evolution (in the scaling limit) where the initial conditions produce deviations for the scaling limit behaviour. However, as k becomes smaller the effect of initial conditions becomes unimportant.

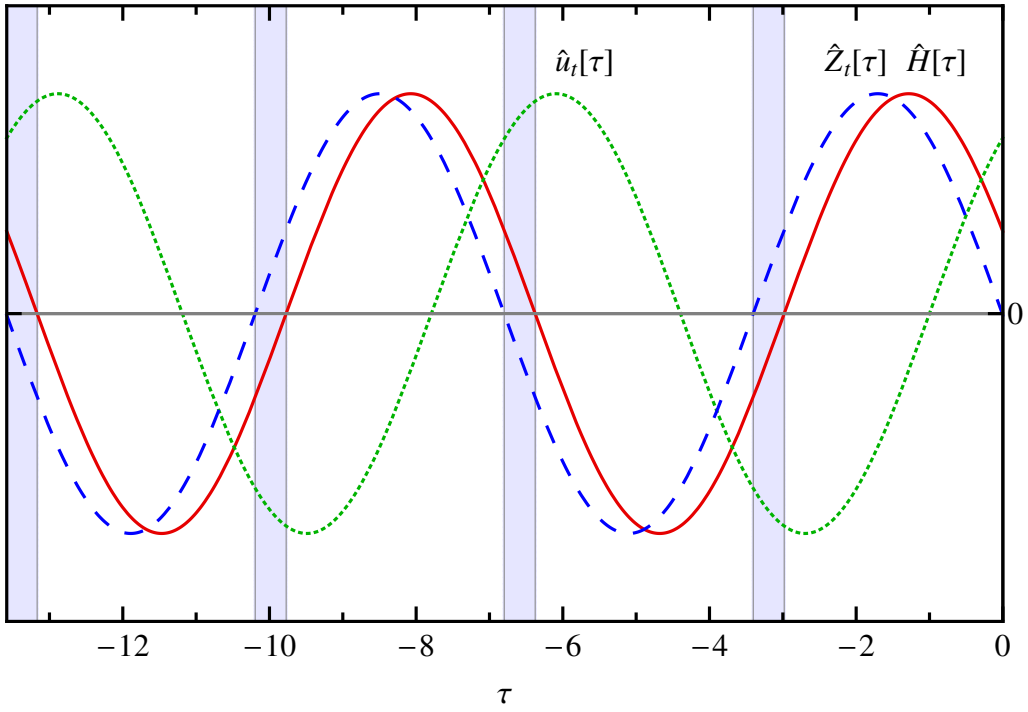

Figure 3.4: Rescaled three-body functions in the scaling limit. $\hat{H}(k)$ is the solid, red curve. $\hat{u}_t(k)$ is the dotted, green curve. $\hat{Z}_t(k)$ is the dashed, blue curve. The horizontal axis is τ, and the vertical axis corresponds to the three-body functions. These functions are divided by a numeric constant to have the same height at their respective maximums. Their relative heights are not important because they correspond to physical functions with different units. However, their relative phases are important to the FRG evolution of this system.

3.7.2 Efimov cycles

The FRG evolution goes from $k = K_0$ to $k \to 0$, or equivalently, from $\tau = 0$ to $\tau \to -\infty$. As this happens, three-body rescaled functions oscillate periodically in $(\omega\,\tau)$. Each oscillation corresponds to one Efimov cycle where the periodic behaviour of the running functions reflects the breaking of the continuous scaling symmetry to a discrete symmetry. As τ decreases, more and more quantum fluctuations are included and the running action describes shallower and shallower states.

In reality, the ratio of energies between two Efimov states is $E_{i+1}/E_i = \mathrm{e}^{-2\pi/s_0} \simeq 1/515$ or $s_0 \simeq 1.006$ [see Eq. (3.1)]. However, in the current truncation

$$s_0^\Gamma = \omega = \frac{\sqrt{535}}{25} \simeq 0.925 \tag{3.23}$$

which yields

$$\mathrm{e}^{-2\pi/\left(s_0^\Gamma\right)} \simeq \frac{1}{890}. \tag{3.24}$$

Even though the present truncation is able to describe the Efimov effect, each cycle here is considerably longer than in nature.

The choice of regulators affects the ratio between Efimov states in a FRG truncation. A different choice from the one in Eq. (3.3) could lead to different coefficients in the three-body flow equations, see Eq. (3.12). This in turn could lead to a different value of ω, see Eq. (3.21), and this would change the length of Efimov cycles in such truncation.

Position of Efimov poles

Efimov states appear as poles in the atom-dimer scattering amplitude at zero energy, which is given by

$$\frac{h^2(k)}{u_t(k)}. \tag{3.25}$$

These poles appear at the (periodic) zeros of u_t. They correspond to the point where a three-body state drops below the three-atom threshold. The position (in τ) of these zeros is determined by the phase of $\hat{u}_t$.[17] Even though this phase is dimensionless, it is associated with the Efimov parameter. This phase combined with (the dimensionful quantity) K_0 determines the energy of the deepest Efimov state. The energies of the other Efimov states are constant ratios of this energy.

Using the solutions for the three-body parameters in Eq. (3.20) and the rescalings in Eq. (3.18) we find

$$\frac{h^2(k)}{u_t(k)} = \frac{g^2\, m}{k^2}\ \left(A_\lambda + B_\lambda \tan\left(\omega\, \tau + \varphi\right)\right). \tag{3.26}$$

where A_λ, B_λ, and φ are constants that depend on the initial values of $\hat{H}$ and $\hat{u}_t$.

For a trimerless action, atom-dimer scattering is given by $\lambda(k)$. The FRG flow of such action yields a similar expression for $\lambda(k)$ as that in Eq. (3.26).[18] If the FRG flow of the trimerless action uses the regulators in Eq. (3.4a) and (3.4b), then the flow of $\lambda(k)$ is identical to the flow of $h^2(k)/u_t(k)$ in the present case.

3.7.3 Three-body sector in the scaling limit: conclusions

In the present truncation, the energy of three-body states appears with respect to a three-atom threshold that is not in the (FRG) physical limit. This is because as long as $k \ll a$, the three-body functions keep oscillating and we cannot reach the physical limit. If $a \lesssim k$ (which means that we leave the scaling limit) the Efimov

[17] This phase is in turn determined by $\hat{H}(K_0)$ and $\hat{u}_t(K_0)$.

[18] Ref. [34] discusses this for the Efimov effect with three species of fermionic atoms.

behaviour disappears.

In summary, the present FRG truncation produces Efimov-like behaviour, however, **a)** the length of Efimov cycles in the truncation is longer than the physical one and **b)** the Efimov behaviour appears out of the FRG physical limit and this is before the parameters in the running action converge.

3.8 Four-body sector: flow equations

The four-body sector is formed by six couplings. The channel $\psi\,\psi\,\phi$ participates in three: v_d, w, and v_t. These are the couplings that we chose to eliminate with the trimer scale dependence.[19] The remaining ones, u_{dd}, u_{dt}, and u_{tt}, connect only the channels $\phi\,\phi$ and $\psi\,\chi$. Their flow is given by one-loop FRG diagrams and extra terms from the trimer scale dependence. For more details on couplings and channels see Subsection 3.2.1.

The Faddeev-Yakubovsky equations [74] have an structure that is driven by the four-body channels $\phi\,\phi$ and $\psi\,\chi$. Such structure inspires our choice to keep the couplings u_{dd}, u_{dt}, and u_{tt}. The flow equations for these running couplings are in Appendix D.

The driving terms in the four-body flow equations have denominators with integer powers of E_a, E_d, $(E_a + E_d)$, and $(E_a + E_t)$. The energy $(E_a + E_t)$ corresponds to the (regulated) energy of an atom and a trimer. During the FRG evolution this energy can be zero. When this happens, an atom-trimer threshold drops below the four-atom threshold. Right before the crossing,[20] the atom-trimer threshold is above the four-atom threshold. As k decreases, the atom-trimer threshold goes below the four-atom threshold.

At each crossing we expect contributions to the imaginary parts of the four-body couplings. These imaginary parts signal the opening of a new channel with an Efimov state. The four-body flow equations have denominators with powers of $(E_a + E_t)$, which diverge at these crossings. In our scheme, these divergences will provide the expected imaginary contributions to the four-body couplings.

The four-body flow equations contain two sources of divergences. **a)** Denominators with powers of $(E_a + E_t)$, discussed above. **b)** Terms with $1/h(k)$, which originate from the trimer scale dependence.[21] The trimer scale dependence eliminates divergences in the flow of $\lambda(k)$, but as a tradeoff, it introduces divergences via terms with $1/h(k)$.

[19] Any explicit participation of couplings with the $\psi\,\psi\,\phi$ channel was eliminated from the four-body flow equations. However, their effects still appear implicitly through extra terms to the flow of the remaining ones. These extra terms are generated by the trimer scale dependence.

[20] That is, when k is slightly larger than the point where $(E_a + E_t)$ crosses zero.

[21] This is because $h(k)$ vanishes once in each Efimov cycle.

3.8.1 Four-body couplings: rescalings

The constant parameters g and m can be removed from the flow of the running functions in the running action. To eliminate g and m from the four-body flow equations, we define new couplings

$$\tilde{u}_{dd}(k) = \left(g^{-4}\, m^{-3}\right)\; u_{dd}(k) \tag{3.27a}$$

$$\tilde{u}_{dt}(k) = \left(g^{-1}\, m^{-1}\right)\; u_{dt}(k) \tag{3.27b}$$

$$\tilde{u}_{tt}(k) = \left(g^{2}\, m\right)\; u_{tt}(k), \tag{3.27c}$$

which have flows independent of both g and m.

We also define a new flowing four-body parameter

$$\tilde{U}_{dt}(k) = h(k) \times \tilde{u}_{dt}(k). \tag{3.28}$$

This new parameter will be used instead of $\tilde{u}_{dt}$. This is because the flow of $\tilde{u}_{dt}$ contains terms with $h(k) = \sqrt{H(k)}$, whereas the flow of $\tilde{U}_{dt}$ does not need those square roots, even though it contains terms with $H(k)$. By using $\tilde{U}_{dt}$ we avoid dealing with an imaginary $h(k)$ in the regions where $H(k)$ is negative.

Now that we have four-body flows independent of g and m, the only dimensionful parameters in the flow are k and a. A real power of k can still be scaled out of each four-body parameter. These powers are determined by the scalings for the three-body running functions in Eq. (3.18). The four-body scalings can be determined by using the three-body scalings and dimensional analysis on the running action or from the four-body flow equations. These scalings are

$$\hat{u}_{dd}(k) = k^{3}\; \tilde{u}_{dd}(k) \tag{3.29a}$$

$$\hat{U}_{dt}(k) = k^{531/250}\; \tilde{u}_{dt}(k)\, h(k) \tag{3.29b}$$

$$\hat{u}_{tt}(k) = k^{406/125}\; \tilde{u}_{tt}(k), \tag{3.29c}$$

where the powers of g, m, and k that are absorbed by the three- and four-body parameters are Eq. (3.11) and (3.27) respectively.

3.9 Four-body sector: scaling limit

In the scaling limit there is only one dimensionful parameter in the flow, k. The flow of the four-body rescaled couplings, $\hat{u}_{tt}(k)$, $\hat{U}_{dt}(k)$, and $\hat{u}_{dd}(k)$, is fully determined by **a)** the dimensionless variable τ, **b)** the flow of two- and three-body rescaled running functions, and **c)** the initial conditions on the four-body couplings, $\hat{u}_{tt}(K_0)$, $\hat{U}_{dt}(K_0)$, and $\hat{u}_{dd}(K_0)$.

As we will see in Subsection 3.9.1, the initial conditions on the four-body couplings become unimportant as τ decreases. We find that the four-body system does not introduce any new physical parameter. In the present truncation the four-body sector is universal. This is in contrast with the three-body sector, where the Efimov parameter is needed to describe the system.

The four-body flow equations in the scaling limit appear in Section D.1 of Appendix D. These flow equations contain terms with the rescaled atom-trimer energy, defined as

$$\hat{E}_{at}(k) = \frac{2}{3} + \frac{\hat{u}_t(k)}{\hat{Z}_t(k)}. \tag{3.30}$$

This energy has one zero in each Efimov cycle, which corresponds to an atom-trimer threshold dropping below the four-atom threshold. This is discussed in page 73.

There are terms with factors of $1/\hat{E}_{at}(k)$ and $1/\hat{H}(k)$ which create divergences in the four-body flow equations. The differential flow equations are evaluated numerically, hence it is necessary to regulate these divergences. To achieve this, we set the initial conditions on the three-body sector as complex numbers, where the imaginary part is much smaller than the real part. Additionally, the imaginary parts of $\hat{H}(k)$ and $\hat{u}_t(k)$ must be out of phase with the real parts. If this is the case, the running functions $\hat{H}(k)$, $\hat{u}_t(k)$, and $\hat{Z}_t(k)$ are never zero: when the real part vanishes, the imaginary part is nonzero.

These small imaginary parts are a way to regulate the divergences in the flow.[22] However, the FRG can be meaningful only if the flow is independent of the size of these imaginary regulators. We are interested on the flow in the limit where the imaginary regulators approach zero. We evaluate the four-body flows numerically, thus, we try to make sure that the four-body flows are independent of the size of the imaginary regulators. Roughly speaking, we find this limit numerically.

3.9.1 Results on four-body sector in the scaling limit

We numerically integrated the four-body flow equations in the scaling limit, Eq. (D.3). We found that the four-body couplings inherit the Efimov periodicity from the three-body running functions. This is unsurprising because the four-body driving terms have Efimov periodicity.

In principle, the four-body flow depends on its initial conditions. Nonetheless, it becomes independent of the initial conditions after the first zero of $\hat{E}_{at}(k)$.[23] The dependence on (four-body) initial conditions is transient; it disappears as the FRG

[22] There may be more than one way to regulate these divergences.

[23] The position of the zeros of $\hat{E}_{at}(k)$ is determined by the Efimov parameter, but it is independent of four-body physics parameters.

evolves. The four-body flow is independent of four-body parameters. This is a case of universal behaviour.

Before the first zero of $\hat{E}_{at}(k)$, the four-body couplings are real.[24] At this zero, the four-body couplings develop a finite imaginary part which is independent of the (size of the) imaginary regulators.

In this truncation some running functions alternate sign between each Efimov cycle while others do not. For example, the three-body running functions $\hat{H}(k)$, $\hat{u}_t(k)$, and $\hat{Z}_t(k)$ change sign between each Efimov cycle. The four-body running functions $\hat{U}_{dt}$ and $\hat{u}_{tt}$ also alternate sings, but $\hat{u}_{dd}$ does not.

Fig. 3.5 displays the flow of $\hat{u}_{tt}$ through a few Efimov cycles. The four-body flow in these plots was calculated using the same three-body physics as in Fig. 3.4. Some features on the evolution of four-body couplings are described below.

Features of the evolution: $\hat{H}(k) = 0$

At each zero of $\hat{H}(k)$, the four-body flow equations have singularities associated with $1/\hat{H}(k)$. These singularities are regulated by the imaginary parts in the three-body running functions. There, the couplings $\hat{u}_{dd}(k)$ and $\hat{U}_{dt}(k)$ show a glitch, whereas $\hat{u}_{tt}(k)$ has peaks which are more complicated than a simple pole. In Fig. 3.5 the zeros of $\hat{H}(k)$ are signaled by vertical, dashed, grey lines. They appear at $\tau = -3.0, -6.40, -9.79$.

The vanishing of $\hat{H}(k)$ in the FRG evolution is not a related to any physical threshold. We regard the associated peaks and glitches as unphysical. They appear at the start of an unphysical region where $\hat{Z}_t(k)$ and $\hat{H}(k)$ have opposite signs, causing the trimer to behave like a ghost field. This region is coloured with blue in Fig. 3.4.

Features of the evolution: super Efimov four-body states

Before each zero of $\hat{E}_{at}(k)$ there is a series of peaks in the couplings. These peaks are generated by the flow, not by divergences in the flow equations. Except for the transient region, the (positions of these) four-body peaks are fixed relative to the zeros of $\hat{E}_{at}(k)$. The peaks have the form of simple poles,[25] which means they have properties of four-body states.

In Fig. 3.5 the zeros of $\hat{E}_{at}(k)$ are signaled by vertical, solid, grey lines. The first zero after the transient region appears at $\tau = -4.85$. In the same Efimov cycle, three peaks are visible to the right of that zero. The largest one appears at $\tau = -3.83$.

[24] To be more precise, these couplings are real in the limit where the imaginary regulators (in the three-body running functions) approach zero. As discussed above, in page 75, we are interested in the limit where these imaginary regulators approach zero.

[25] This means that the imaginary part has only one spike, whereas the real part has one positive and one negative spikes.

Then there is a smaller peak at $\tau = -4.67$. Additionally, there is a barely visible glitch right before the zero of $\hat{E}_{at}(k)$.

A closer look reveals more peaks that accumulate right before each zero of $\hat{E}_{at}(k)$. As the sequence increases, the peaks are lower, more narrow, and increasingly closer to the zero. More zoom reveals more peaks: the sequence is infinite![26]

Let τ_{a+t} be the position of one zero of $\hat{E}_{at}(k)$, and τ_n be the position of the n-th peak in the sequence, where n grows as the peaks approach τ_{a+t}. Then, the position of the peaks follows the relation

$$\frac{\tau_n - \tau_{a+t}}{\tau_{n+1} - \tau_{a+t}} = 7.8. \tag{3.31}$$

This means that the sequence is periodic in $x = \log(\tau - \tau_{a+t})$. One of these sequences of peaks is displayed in Fig. 3.6. There, a coupling is plotted in the region right before one zero of $\hat{E}_{at}(k)$. These sequences and how they are generated is discussed in the next subsection (Subsection 3.9.2).

In Ref. [56], Nishida, Moroz, and Son study the three-body physics of a two-dimensional system. They also found infinite sequences of peaks that (like x) are periodic in a variable that is a double logarithm of k.

Events in the evolution: atom-trimer threshold behaviour

At each zero of $\hat{E}_{at}(k)$, the regulated atom-trimer energy drops below the regulated four-atom energy, and the atom-trimer channel opens. The flow of couplings reflects that this point is a threshold for the atom-trimer channel. The couplings receive additional imaginary contributions signalling the opening of the new channel.

At the zeros of $\hat{E}_{at}(k)$, the right-hand sides of the four-body flow equations are divergent. The couplings, however, are finite and the real parts of the couplings cross the threshold smoothly. In contrast, the imaginary parts abruptly start to increase after the threshold.[27] The threshold is a continuous but nondifferentiable point for the imaginary parts. One example of this behaviour is in Fig. 3.7.

3.9.2 Behaviour near atom-trimer threshold

As discussed above, in Subsection 3.9.1, the four-body couplings have an infinite sequence of peaks before each atom-trimer threshold. These sequences are produced by the four-body flow equations in the scaling limit [Eq. (D.3) in Appendix D].

[26] Our integration of the four-body equations is numeric, hence we do not find infinitely many peaks, just a high number. The number of peaks we find is limited by the resolution of the numerical integration. In Subsection 3.9.2 we explain the claim that the sequence is infinite.

[27] Because of the three-body imaginary regulators, the term $\hat{E}_{at}(k)$ is not really zero at the threshold. It is a small imaginary number. There, the terms proportional to $1/\hat{E}_{at}(k)$ and $1/\hat{E}_{at}(k)^2$ in the flow equations give large imaginary contributions to the couplings.

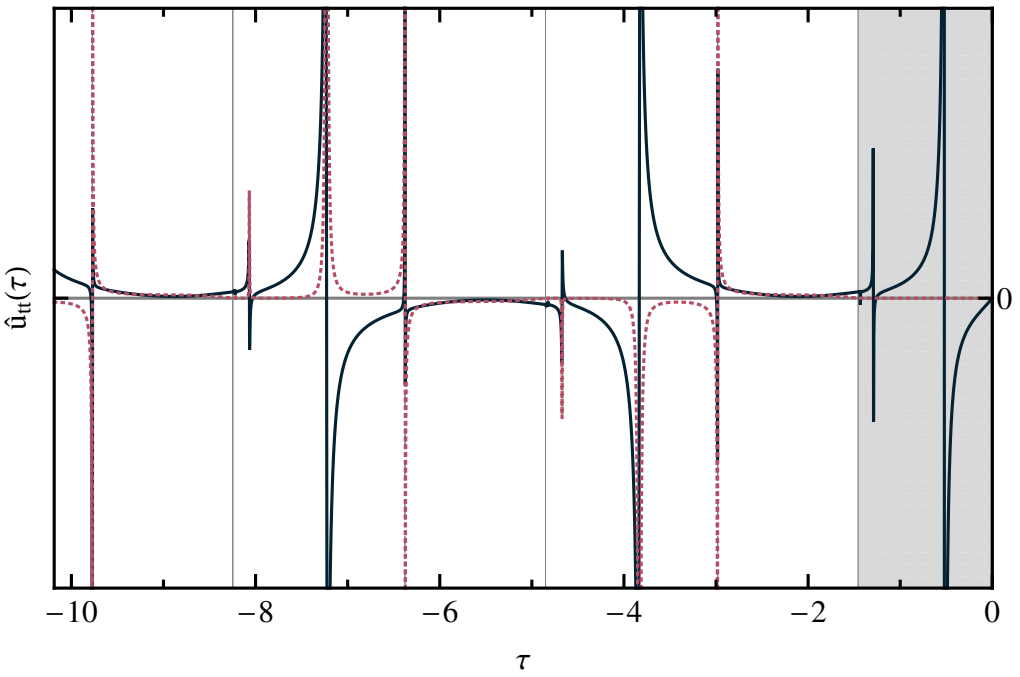

Figure 3.5: Four-body rescaled coupling $\hat{u}_{tt}$ (vertical axis) as a function of τ (horizontal axis) going through a few Efimov cycles. The real part of $\hat{u}_{tt}$ is the solid, blue curve, whereas the imaginary part is the dotted, pink curve. There are three zeros of $\hat{H}$. They appear right before $\tau = -3$, between $\tau = -6$ and -7, and between $\tau = -9$ and -10. There are three atom-trimer thresholds. They are signaled by vertical, solid, grey lines. The region coloured in grey goes from the start of the evolution to the first atom-trimer threshold. There, the couplings have not (yet) reached Efimov periodicity.

However, due to the complicated structure of these equations, it is hard to understand their behaviour near the threshold.

We calculated the flow of each four-body coupling while artificially fixing the other four-body couplings at zero. The flows for $\hat{U}_{dt}(k)$ and $\hat{u}_{tt}(k)$ by themselves do not produce super Efimov behaviour. In contrast, the evolution of $\hat{u}_{tt}(k)$ does. The latter has similar qualitative features to the evolution with all couplings, but its quantitative features are different. Even though the evolution of each isolated four-body coupling does not give any quantitative information, it suggests that the super Efimov behaviour is driven by the flow of $\hat{u}_{tt}(k)$.

To explore the flow of $\hat{u}_{tt}(k)$ near one of the atom-trimer thresholds with a simpler equation,[28] we expand the driving term of $\partial_\tau \hat{u}_{tt}$ [right-hand side of Eq. (D.3c)] as a series in τ_{th}. Here, $\tau_{th} = \tau - \tau_{a+t}$, and τ_{a+t} is the position (in τ) of the threshold around which the expansion is centred.[29]

The full flow equation for $\hat{u}_{tt}(k)$ has terms proportional to $1/\hat{E}_{at}^2$ and $1/\hat{E}_{at}$.

[28] Simpler than the full four-body flow equations, Eq. (D.3).

[29] We can use any atom-trimer threshold except the first one. There, transient effects are still in play.

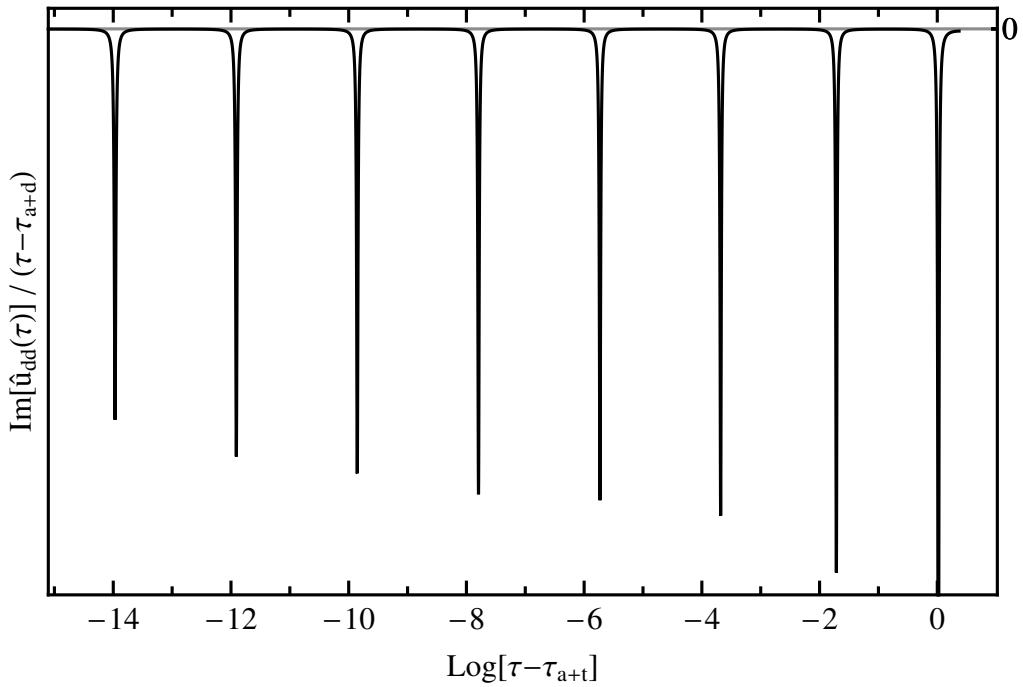

Figure 3.6: Sequence of super Efimov peaks right before an atom-trimer threshold. The vertical axis is $\mathrm{Im}\left[\hat{u}_{tt}\right]/\left(\tau-\tau_{a+t}\right)$, and the horizontal axis is $x=\log\left(\tau-\tau_{a+t}\right)$. The distance in x between peaks is $\log(7.8)=2.0$. The coupling $\hat{u}_{tt}$ is divided by $\tau-\tau_{a+t}$ to compensate for the decreasing height of the peaks.

These terms will produce terms proportional to $1/\left(\tau_{th}\right)^2$ and $1/\left(\tau_{th}\right)$ in the series expansion. Near the threshold the latter terms dominate, hence we keep powers of zero or less in the variable τ_{th}.

The expansion around threshold yields

$$\begin{aligned}\partial_{\tau_{th}}\hat{u}_{tt}=&\left(\frac{h_7}{(\tau_{th})^2}+\frac{h_8}{\tau_{th}}+h_9\right)+\left(\frac{h_4}{(\tau_{th})^2}+\frac{h_5}{\tau_{th}}+h_6\right)\,\hat{u}_{tt}(\tau_{th})+g_2\,\hat{U}_{dt}(\tau_{th})^2\\&+\left(\frac{h_1}{(\tau_{th})^2}+\frac{h_2}{\tau_{th}}+h_3\right)\,\hat{u}_{tt}(\tau_{th})^2+g_1\,\hat{U}_{dt}(\tau_{th}),\end{aligned}\tag{3.32}$$

where h_i and g_i are constant coefficients in the expansion. To evaluate these coefficients, the two- and three-body parameters must be evaluated at the threshold.[30]

To study $\hat{u}_{tt}(\tau_{th})$ in the expansion we switch to the variable $x=\log(\tau_{th})$. The super Efimov behaviour is periodic in x, hence $\hat{u}_{tt}(x)$ should have that periodicity. We also introduce an auxiliary function

$$G(x)=\mathrm{e}^x\,\left(\frac{h_1}{\mathrm{e}^{2x}}+\frac{h_2}{\mathrm{e}^x}+h_3\right)\,\hat{u}_{tt}(x)+A(x),\tag{3.33}$$

[30] The coefficients h_i and g_i should be independent of the Efimov parameter. This is because the driving terms in the four-body flow equations are determined by the three-body flowing parameters, which have fixed values with respect to the atom-trimer threshold.

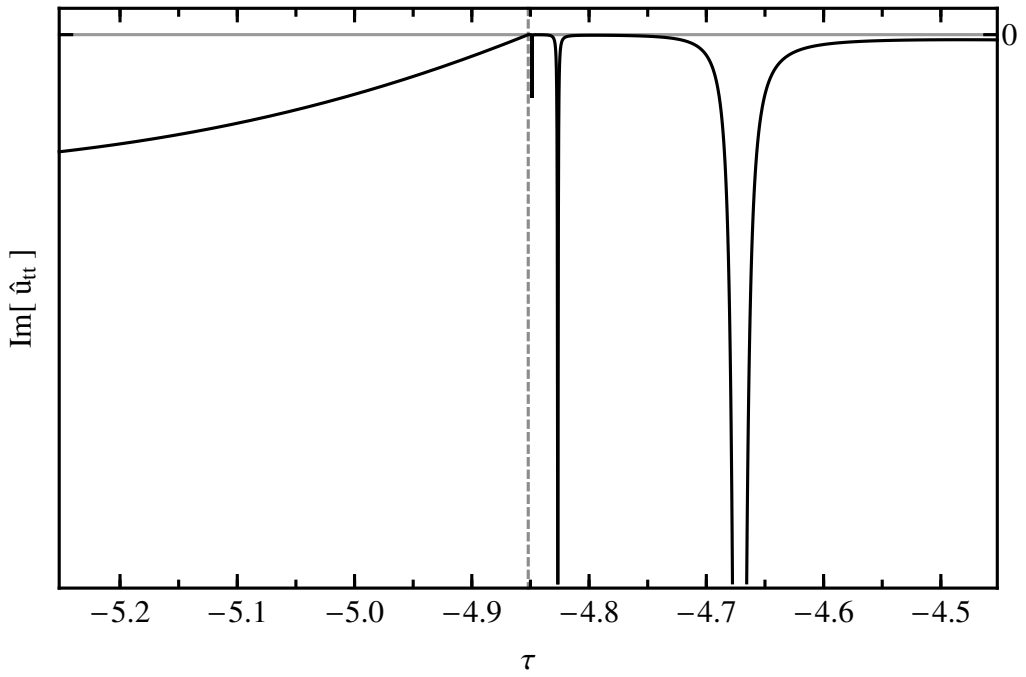

Figure 3.7: Four-body coupling crossing an atom-trimer threshold. The vertical axis is $\mathrm{Im}[\hat{u}_{tt}]$, and the horizontal axis is τ. The atom-trimer threshold is signaled by a vertical, dashed, grey line. Three peaks in the super Efimov sequence are visible to the right of the threshold. At the threshold, the atom-trimer channel opens. This is reflected by the sudden growth of the imaginary part of $\hat{u}_{tt}(k)$. The plot corresponds to the same evolution as that in Figure 3.5.

where $A(x)$ depends on x, on the coefficients h_i and g_i, and on $\hat{U}_{dt}(x)$. However, $A(x)$ does not depend on $\hat{u}_{tt}$. The functions $G(x)$ and $\hat{u}_{tt}(x)$ are equivalent; if $G(x)$ has a periodic divergence in x, then so does $\hat{u}_{tt}(x)$. The differential equation for $G(x)$ has the form

$$\mathrm{d}_x G = G(x)^2 + \left(\omega_{\mathrm{sE}}(x)\right)^2 , \tag{3.34}$$

where $\omega_{\mathrm{sE}}(x)$ depends on $\hat{U}_{dt}(x)$. Since $\hat{U}_{dt}$ does not generate the super Efimov behaviour, we substitute it for its numerical value at the threshold from the full evolution of the four-body couplings. In such case

$$\lim_{x\to-\infty} \left(\omega_{\mathrm{sE}}\right)^2 = \left(\omega_{\mathrm{sE}}^{-\infty}\right)^2 \tag{3.35}$$

is a positive constant. Then,

$$\mathrm{d}_x G = G(x)^2 + \left(\omega_{\mathrm{sE}}^{-\infty}\right)^2 . \tag{3.36}$$

is solved by

$$G(x) = \tan\left(\omega_{\mathrm{sE}}^{-\infty}\ x + \varphi\right), \tag{3.37}$$

where $G(x)$ has periodic peaks in x. The angular frequency, $\omega_{\mathrm{sE}}^{-\infty}$, fixes the ratio of the positions of two consecutive super Efimov peaks. It yields

$$\exp\left\{\pi/\omega_{\mathrm{sE}}^{-\infty}\right\} = 7.9, \tag{3.38}$$

which is close to the result for the full evolution, 7.8 in Eq. (3.31).

For arbitrary values of the coefficients h_i, the function $(\omega_{\mathrm{sE}}(x))^2$ has terms proportional to e^{-2x} and e^{-x}. These terms diverge when $x \to -\infty$, destroying the super Efimov behaviour. However, for the values of h_i in the expansion around any atom-trimer threshold, the coefficients next to e^{-2x} and e^{-x} vanish. This allows $\left(\omega_{\mathrm{sE}}^{-\infty}\right)^2$ to be finite, and preserves the super Efimov behaviour.

The terms proportional to e^{-2x} and e^{-x} in $(\omega_{\mathrm{sE}}(x))^2$ arise from the combination

$$\begin{aligned}&\mathrm{e}^{2x}\left(\frac{h_7}{\mathrm{e}^{2x}} + \frac{h_8}{\mathrm{e}^{x}} + h_9 + g_1\,\hat{U}_{dt}(x) + g_2\,\hat{U}_{dt}^2(x)\right)\left(\frac{h_4}{\mathrm{e}^{2x}} + \frac{h_5}{\mathrm{e}^{x}} + h_6\right)\\ &-\frac{1}{4}\mathrm{e}^{2x}\left(\frac{h_1}{\mathrm{e}^{2x}} + \frac{h_2}{\mathrm{e}^{x}} + h_3\right)^2.\end{aligned} \tag{3.39}$$

Even though the h_i seem independent, the cancellation of the coefficients of e^{-2x} and e^{-x} in the above combination is not a coincidence. This cancellation arises from the structure of the flow equations, in particular from terms with $\hat{E}_{at}(k)$ in the denominator.

In the flow equations, all terms with $\hat{E}_{at}(k)$-denominators come from skeleton diagrams with a particular structure.[31] These diagrams are generated by pasting together the coupling-like structures in Fig. 3.8. The resulting skeleton diagrams appear in Fig. 3.9. The contribution from these diagrams to the flow of $u_{tt}(k)$ has the form

$$\partial_k u_{tt} \supset \partial R_k\ \frac{\delta}{\delta R_k}\left(c_2\ (u_{tt})^2 + c_1\ u_{tt} + c_0\right) \tag{3.40}$$

where the coefficients c_2, c_1, and c_0 are the coefficients of u_{tt} on the quadratic $\mathcal{A}^2$ (see Fig. 3.8).

The quadratic character of the c_i is inherited into the flow equation of $\hat{u}_{tt}$. In consequence, the divergent terms in Eq. (3.39) cancel, making the super Efimov

[31] Skeleton diagrams are not the diagrams that contribute to the flow of a running function. The latter are obtained by differentiating the former with respect to k, but only those k in a regulator R_k, not the k on the running functions and parameters in Γ_k. This operation is equivalent to taking $\partial R_k\ \frac{\delta}{\delta R_k}(\cdot)$.

behaviour possible.

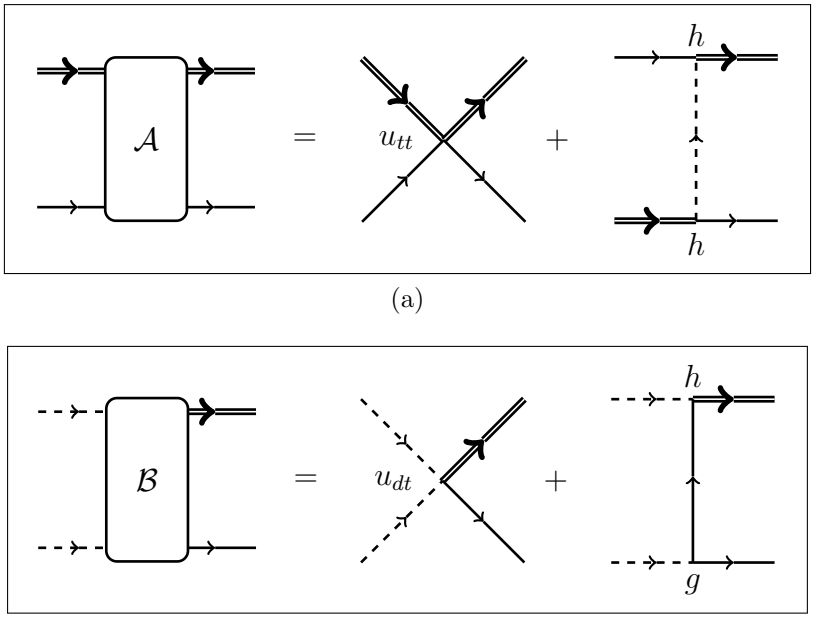

Figure 3.8: Coupling-like structures $\mathcal{A}$ and $\mathcal{B}$, which connect the four-body channels in the FRG flow. Structure $\mathcal{A}$ connects the channel $\psi\,\chi$ to $\psi\,\chi$, whereas $\mathcal{B}$ connects $\psi\,\chi$ to $\phi\,\phi$. These structures do not generate all the terms in the four-body flow equations, but they generate all the terms with atom-trimer energies in the denominator.

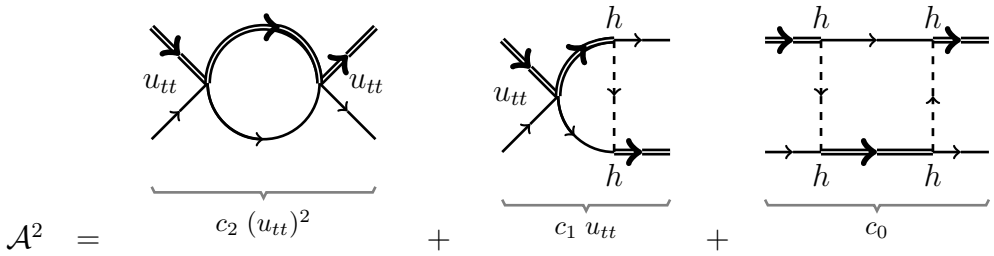

Figure 3.9: Skeletons of some of the diagrams in the flow of u_{tt}, which couples the channel $\psi\,\chi$ to $\psi\,\chi$. They are produced by the structure $\mathcal{A}\times\mathcal{A}$. These are not all the skeleton diagrams in $\partial_k u_{tt}$, but they produce all the terms with atom-trimer energies in the denominator. The quadratic structure of the coefficients c_i, is an important ingredient of the super Efimov behaviour.

3.9.3 Four-body sector in the scaling limit: conclusions

We integrated the four-body flow equations in the scaling limit and found that the flow has Efimov periodicity. Additionally, the flow is independent of the initial conditions on the four-body couplings. This means that the four-body system is universal, at least in the present truncation. We also found the expected threshold behaviour

when the atom-trimer energy drops below the four-atom energy. Furthermore, we found an infinite sequence of peaks right before each of these thresholds.

The introduction of **a)** the trimer field and **b)** the flow-structure of the couplings that connect the $\psi\,\chi$ and $\phi\,\phi$, are important ingredients for the super Efimov behaviour. In contrast, this behaviour does not appear in the FRG flow of a similar, but trimerless action.

The peaks in the super Efimov sequences have state-like character. Nonetheless, we cannot regard them as physical states because they appear for values of k where the FRG has not converged. This lack of convergence is a consequence of the Efimov effect in the scaling limit, where parameters oscillate for arbitrarily small values of k.

To obtain a FRG evolution that converges (in this truncation), it is necessary to introduce an extra dimensionful parameter. This is discussed next, in Section 3.10. In such case, as the FRG converges, the super Efimov peaks might move relative to the atom-trimer threshold and (some of) these peaks might become virtual states. The rest may correspond to physical states. Furthermore, not all the super Efimov states on top a of each trimer can be physical. This is forbidden by a theorem by Amado and Greenwood [2]. Nonetheless, these virtual states might be relevant to the four-body spectrum out of the scaling limit. For example, for a large and positive atom-atom scattering length, Deltuva found towers of four-body states right below the atom-atom-dimer threshold [22].

3.10 Evolution with finite scattering length

Up to this point, this chapter **a)** introduces a running action for scalar atoms, and **b)** deals with its flow. The flow of the three- and four-body sectors has Efimov periodicity, which persists for arbitrarily low values of k. In consequence, the flow never converges. This section discusses the flow with an extra dimensionful parameter, a finite atom-atom scattering length. The flow is no longer in the scaling limit.

The scattering length disrupts the Efimov behaviour when the energy (of the Efimov states) becomes of the order of $-1/(m\,a^2)$.[32] This disruption is reflected in the FRG flow: when k reaches values $\sim 1/|a|$, the Efimov periodicity disappears. For $k \ll 1/|a|$, the three- and four-body flows converge.

3.10.1 Three-body parameters

The flow of the three-body parameters, $H(k)$, $\tilde{u}_t(k)$, and $\tilde{Z}_t(k)$ is given by the flow equations in Eq. (3.10). Those equations need the input of two-body physics, which

[32] As the Efimov sequence advances, the energy of the Efimov states approaches 0, but this energy always remains negative, see Fig. 3.1.

is given by $u_d(k,a)$ and $Z_t(k)$ in Eq. (3.9). The atom-atom scattering length is the only two-body physical parameter in this truncation. It appears in the flow equations through $u_d(k,a)$, which is part of the dimer energy.

The atom-atom scattering length can either be positive or negative. If it is negative there is no atom-atom bound state. If it is positive, there is such state. An atom-atom bound state affects the energy spectrum of the three-body system. The (atom-atom) binding energy becomes the threshold for the continuum in the three-body system. Below the dimer binding energy, only discrete (Efimov) states exist. Above (the dimer binding energy), the three-body system can be formed by a dimer and a free atom.

This atom-dimer threshold is reflected in the FRG evolution of the three-body system. If $a > 0$, then at some point in the evolution the atom-dimer energy, $(E_a + E_d)$, crosses zero. This creates a divergence in the three-body flow equations.

In contrast, for $a < 0$, the atom-dimer energy does not cross zero during the FRG evolution. To avoid the atom-dimer threshold, in this section (Section 3.10) we deal exclusively with the case $1/a \leq 0$.

Three-body parameters: results

Using different values for the atom-atom scattering length and Efimov parameter, we (numerically) integrated the three-body flow equations [in Eq. (3.10)]. The three-body parameters show different behaviour in different regions. At the beginning of the evolution, when $k \gg 1/|a|$, the system is close to the scaling limit and shows Efimov behaviour. There, it is convenient to use the rescaled parameters $\hat{H}(k)$, $\hat{u}_t(k)$, and $\hat{Z}_t(k)$. As the FRG evolution advances, k decreases and eventually becomes $\sim 1/|a|$. There, the parameters switch to a different behaviour. Fig. 3.10 shows the flow of the three-body rescaled running functions $\hat{H}(k)$, $\hat{u}_t(k)$, and $\hat{Z}_t(k)$.

For $k \ll 1/|a|$, the scaling of the running functions changes. The rescaled running functions (those with a hat) are no longer the best functions to describe the three-body physics. It is convenient to switch back to nonrescaled functions, $H(k)$, $\tilde{u}_t(k)$, and $\tilde{Z}_t(k)$.

We expand the three-body flow equations in Eq. (3.10) as a series in powers of k. The expansion is valid for very small k, and it helps understand the behaviour of $H(k)$, $\tilde{u}_t(k)$, and $\tilde{Z}_t(k)$ near the physical limit. This expansion yields

$$\frac{\mathrm{d}H}{\mathrm{d}k} = \frac{16\, a\, \tilde{u}_t(k)}{3\, \pi\, k^2} + \mathcal{O}(k^{-1}), \qquad \frac{\mathrm{d}\tilde{u}_t}{\mathrm{d}k} = \mathcal{O}(k^3), \qquad \frac{\mathrm{d}\tilde{Z}_t}{\mathrm{d}k} = \mathcal{O}(k^2),$$

which means

$$\lim_{k\to 0} H = -\frac{16\, a\, \tilde{u}_t}{3\, \pi\, k}, \qquad \lim_{k\to 0} \tilde{u}_t = \text{constant}, \qquad \lim_{k\to 0} \tilde{Z}_t = \text{constant}. \tag{3.41}$$

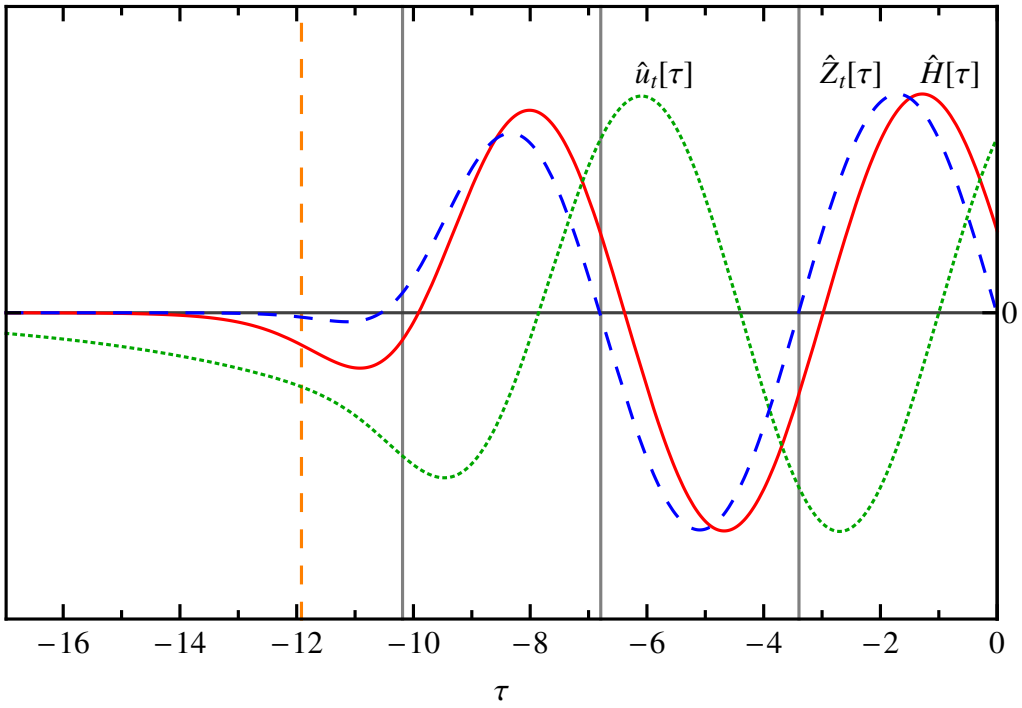

Figure 3.10: Flow of three-body rescaled running functions $\hat{H}(k)$, $\hat{u}_t(k)$, and $\hat{Z}_t(k)$ with a finite scattering length. They are respectively a solid, red curve; a dotted, green curve; and a dashed, blue curve. The horizontal axis is τ, and the vertical axis corresponds to the three-body functions. These functions have different units, and they are divided by a numeric constant to have the same height at their respective maximums. The length of three Efimov cycles is signaled by grey, solid, vertical lines. During the third cycle, the Efimov behaviour starts to distort. The vertical, dashed, orange line corresponds to $k = 1/|a|$. For $k \lesssim 1/|a|$, the Efimov behaviour is lost and the rescaled running functions approach zero for $k \to 0$. The Efimov region in this plot is similar to Fig. 3.4, which is in the scaling limit.

We find that $H(k)$ has $1/k$ behaviour in the physical limit, whereas $\tilde{u}_t$ and $\tilde{Z}_t$ converge to constants. Fig. 3.11 shows the flow of $k \times H(k)$, $\tilde{u}_t(k)$, and $\tilde{Z}_t(k)$ with a negative scattering length.

The values of $k\,H$, $\tilde{u}_t$, and $\tilde{Z}_t$ in the physical limit are not independent. They are regulated by two parameters, the atom-atom scattering length and the Efimov parameter. The scattering length determines where (in k) does the Efimov behaviour stop. The Efimov parameter moves the phase of the Efimov cycles. Either of these parameters can be used to tune the three-body functions in the physical limit.

As discussed in Subsection 3.7.2, the trimer states appear as poles in h^2/u_t. $\tilde{u}_t$ can be tuned so that it vanishes in the physical limit. The corresponding scattering length and Efimov parameters produce a zero-energy, three-body state in the physical limit. Trimer states have been observed in gases of ultracold atoms. Ref. [49] reports the first observation, and Ref. [14, 31, 45] are reviews on the field.

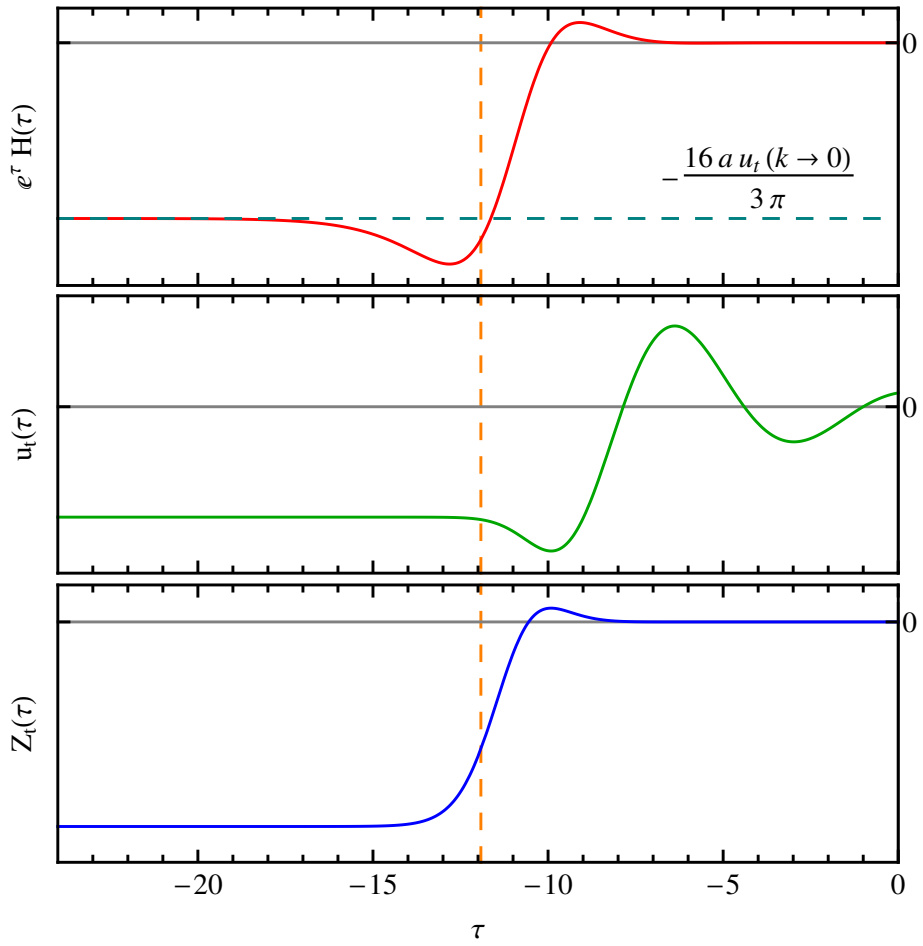

Figure 3.11: Flow of the three-body parameters $k\,H(k)$, $\tilde{u}_t(k)$, and $\tilde{Z}_t(k)$ with a negative scattering length. The vertical axes corresponds to these parameters, and the horizontal axis corresponds to τ. The vertical, dashed, orange line corresponds to $k = 1/|a|$. $k\,H(k)$, $\tilde{u}_t(k)$, and $\tilde{Z}_t(k)$ converge to a constant in the physical limit. This happens for $k \ll 1/|a|$.

3.10.2 Four-body parameters

Using the flow of two- and three-body parameters as input, we integrated the four-body flow equations [in Eq. (3.8)]. At the beginning to the evolution, when $1/|a| \ll k$, the flow is similar to the flow in the scaling limit. There, it is convenient to use rescaled parameters. However, as k approaches $\sim 1/|a|$, the Efimov behaviour is disrupted and it is more convenient to switch to nonrescaled parameters.

We explore the behaviour of four-body couplings for $k \ll 1/|a|$, by expanding the flow equations [in Eq. (3.8)] as a power series in k. This yields

$$\frac{\mathrm{d}\tilde{u}_{dd}}{\mathrm{d}k} = \frac{1}{k^3} + \mathcal{O}(k^{-2}), \qquad \frac{\mathrm{d}\tilde{U}_{dt}}{\mathrm{d}k} = \frac{256\,a^2\,\tilde{u}_t}{9\,\pi^2\,k^2} + \mathcal{O}(k^{-1}),$$
$$\frac{\mathrm{d}\tilde{u}_{tt}}{\mathrm{d}k} = -\frac{48\,a\,\pi\,\tilde{u}_t}{k^2} + \mathcal{O}(k^{-1}),$$

which means

$$\lim_{k\to 0} \tilde{u}_{dd} = -\frac{1}{2\,k^2}, \qquad \lim_{k\to 0} \tilde{U}_{dt} = -\frac{256\,a^2\,\tilde{u}_t}{9\,\pi^2\,k}, \qquad \lim_{k\to 0} \tilde{u}_{tt} = \frac{48\,a\,\pi\,\tilde{u}_t}{k}. \tag{3.42}$$

This power-law behaviour changes when $\tilde{u}_t(k \to 0) = 0$. In such case, $\tilde{U}_{dt}$ and $\tilde{u}_{tt}$ become constant as $k \to 0$. For a finite scattering length, the four-body parameters near the physical limit behave like powers of k, but not the powers that correspond to the rescaled parameters.

Four-body parameters: results

We tune the atom-atom scattering length such that $\tilde{u}_t(k \to 0) = 0$.[33] This means that there is a zero-energy trimer in the physical limit. In consequence, the last atom-trimer threshold of the FRG evolution appears at the physical limit as well.

We integrated the four-body couplings in the case with a zero-energy trimer at the physical limit. Three four-body states are present before the last atom-trimer threshold. These states appear in a regime where the FRG evolution converges, and they might correspond to physical four-body states, or tetramers. Furthermore, there is no conflict with Amado and Greenwood's theorem because the number of tetramers on top of each trimer is finite [2]. The flow of one four-body coupling in this case is in Figure 3.12.

We denote the scattering length that produces a zero-energy trimer as a_3. If we integrate the flow with a slightly above a_3,[34] then the four-body peaks move closer to the physical limit. By carefully decreasing a, we find the scattering lengths at which these states cross the four-atom threshold:

$$\frac{a_4^{(0)}}{a_3} = 0.438, \qquad \frac{a_4^{(1)}}{a_3} = 0.887, \qquad \frac{a_4^{(2)}}{a_3} = 0.997. \tag{3.43}$$

These three scattering lengths produce zero-energy, four-atom states in the physical limit. Two of these states, corresponding to $a_4^{(0)}$ and $a_4^{(1)}$, are predicted by quantum mechanics calculations [21, 41], and also have been observed in gases of ultracold atoms [30]. The ratios $a_4^{(0)}/a_3$ and $a_4^{(1)}/a_3$ in Eq. (3.43) are within 5% agreement with Ref. [21, 41, 30].

The last four-atom state, corresponding to $a_4^{(2)}$, could either be a real state, or an artifact of the FRG truncation. This state lies very close to the atom-trimer threshold. Hence, if it is real, it would be difficult to observe it.

[33] Due to Efimov periodicity, there is more than one value of a that produces such behaviour. If a_3 is one of these scattering lengths, then $a_3\,\mathrm{e}^{n\,\pi/s_0}$ (for $n = 2, 3, \ldots$) also produce $\tilde{u}_t(k \to 0) = 0$. In this truncation, $s_0^{\Gamma} = 0.925$.

[34] In all these integrations we use the same initial conditions for the three-body parameters. This is because these initial conditions also affect the values of the parameters in the physical limit.

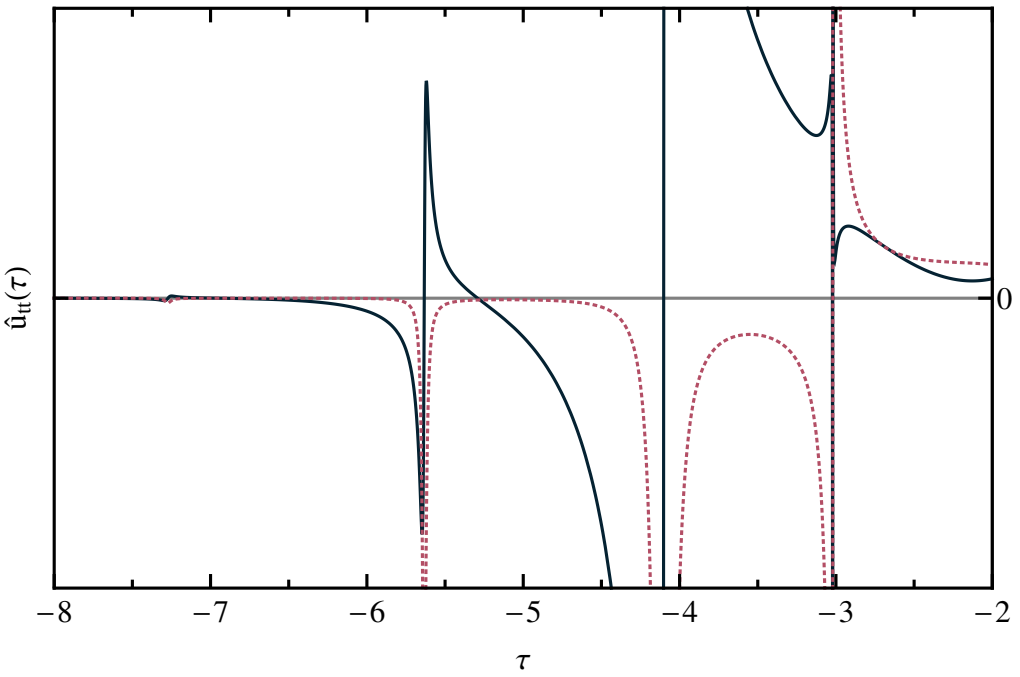

Figure 3.12: Flow of $\hat{u}_{tt}$ (vertical axis) as a function of τ (horizontal axis). The real part of $\hat{u}_{tt}$ is the solid, blue curve, and the imaginary part is the dotted, pink curve. The two- and three-body physics is tuned such that there is a zero-energy trimer at the physical limit. The coupling has (unphysical) peaks at $H(\tau) = 0$, right after $\tau = -3$. There are also three peaks corresponding to four-body states. They appear at $\tau^{(2)} = -4.1$, at $\tau^{(1)} = -5.6$, and (barely visible) at $\tau^{(0)} = -7.1$.

3.11 Evolution with a finite external energy

Up to this point, this chapter discusses a running action ansatz for scalar atoms. This section extends this ansatz by adding an external energy to the inverse propagators.

We regard the inverse propagators in the ansatz (for the running action) as a series expansion (in q^0) of the inverse propagators in the exact effective action. The form of the latter action is unknown, which is why we resort to an ansatz.

In the running action used so far [in Eq. (3.2)], the atom inverse propagator is expanded around $q^0 = 0$ while keeping (up to) linear terms in q^0.[35] In contrast, for the extended ansatz in this section, the atom inverse propagator is expanded around $q^0 = -\varepsilon/2 \geq 0$. As a consequence of energy conservation, dimer and trimer inverse propagators should be expanded around $q^0 = -\varepsilon$ and $q^0 = -3\,\varepsilon/2$. However, these energies are absorbed, respectively, by dimer and trimer bilinears. Therefore, kinetic

[35] If inverse propagators have up to linear terms in q^0, then Galilean invariance restricts $\|\vec{q}\|$ terms to be quadratic.

terms in the new running action are

$$\psi^* \left(q^0 + \frac{\varepsilon}{2} - \frac{q^2}{2\,m} \right) \psi \tag{3.44a}$$

$$\phi^* \left(Z_d \left(q^0 - \frac{q^2}{4\,m} \right) - u_d \right) \phi \tag{3.44b}$$

$$\chi^* \left(Z_t \left(q^0 - \frac{q^2}{6\,m} \right) - u_t \right) \chi. \tag{3.44c}$$

The rest of the extended running action (the interaction terms) has the same form as the previous running action, in Eq. (3.2).

In the present truncation, each atom, dimer, or trimer has a fixed energy of $-\varepsilon/2$, $-\varepsilon$, or $-3\,\varepsilon/2$, respectively. Feynman diagrams constructed with the new ansatz have a finite energy flowing through them. Each initial atom in the diagram contributes $-\varepsilon/2$ to the total energy flowing through, whereas each initial dimer or trimer contributes $-\varepsilon$ or $-3\,\varepsilon/2$, respectively.

In this truncation, the flow receives contributions from q^0 that do not correspond to the kinetic energy, for example the value of q^0 that contributes in an atom propagator does not correspond to $q^0 = \frac{\vec{q}^{\,2}}{2\,m}$. Instead, the quantity $q^0 + \frac{\varepsilon}{2}$ corresponds to the kinetic energy of an atom. This shift gives a finite energy to every atom line in every Feynman diagram.

We must be careful when comparing running actions with different values of ε: these actions correspond to different truncations that (try to) describe the same physical systems. Some values of ε describe some physical processes better, but in the end they correspond to different expansions of the same physics.

Instead of ε, we use an auxiliary parameter with units of momentum, $\gamma > 0$, defined as $-\varepsilon = \frac{\gamma^2}{m}$. Now, the regulated energies that correspond to the kinetic terms in Eq. (3.44) are

$$E_a = \frac{q^2}{2\,m} + \frac{R_a(q,k)}{Z_a(k)} - \frac{\varepsilon}{2} \qquad = \frac{q^2}{2\,m} + \frac{R_a(q,k)}{Z_a(k)} + \frac{\gamma^2}{2\,m} \tag{3.45a}$$

$$E_d = \frac{q^2}{4\,m} + \frac{R_d(q,k)}{Z_d(k)} + \frac{u_d(k)}{Z_d(k)} \tag{3.45b}$$

$$E_t = \frac{q^2}{6\,m} + \frac{R_t(q,k)}{Z_d(k)} + \frac{u_t(k)}{Z_t(k)}\,. \tag{3.45c}$$

Flow equations for the running parameters are obtained by taking functional derivatives in the running action. These flow equations use the regulated energies above, combined with the regulators in Eq. (3.4).

3.11.1 Two-body sector

The flow of two-body parameters with a finite γ can be integrated exactly. The boundary condition on the dimer bilinear is

$$u_d(k=0,\gamma,a) = \frac{m\,g^2}{\pi^2}\left(-\frac{\pi}{8\,a}+\frac{\pi\,\gamma}{8}\right). \tag{3.46}$$

This condition produces a divergence in the dimer propagator when **a)** the dimer is a bound state and **b)** the energy carried by each atom is half the binding energy of the dimer. This corresponds to $\varepsilon = -\gamma^2/m = -\frac{1}{m\,a^2}$, or $\gamma = 1/a$. This condition on u_d means that the pole in the dimer propagator appears at the correct energy.

The flow of $Z_d(k,\gamma)$ is fully determined by the condition $Z_d(k\to\infty)\to 0$. Furthermore, $Z_d(k\to 0,\gamma>0)$ is finite, whereas $Z_d(k\to 0,\gamma=0)$ diverges as $\propto 1/k$.

The explicit expressions for the two-body functions are

$$u_d(k,\gamma,a) = \frac{m\,g^2}{\pi^2}\left(\frac{1}{12}\left[3\,k-\frac{k^3}{k^2+\gamma^2}-3\,\gamma\,\mathrm{ArcTan}\,(k/\gamma)\right]-\frac{\pi}{8\,a}+\frac{\pi\,\gamma}{8}\right) \tag{3.47a}$$

$$Z_d(k,\gamma) = \frac{2\,m^2\,g^2}{\pi^2}\left(\frac{\pi}{32\,\gamma}+\frac{1}{48}\left[\frac{5\,k^3+3\,k\,\gamma^2}{\left(k^2+\gamma^2\right)^2}-\frac{3\,\mathrm{ArcTan}\,(k/\gamma)}{\gamma}\right]\right). \tag{3.47b}$$

In the limit $\gamma\to 0$, we recover the two-body functions for the running action without γ, which are discussed in Section 3.5.

3.11.2 Three-body sector

The three-body sector for the running action with a finite external energy shows an atom-dimer threshold and trimer states with Efimov periodicity.

The atom-dimer threshold should appear when the energy of three atoms is equal to the dimer binding energy.[36] There, the three-atom system is formed by a dimer and a free atom, both with zero kinetic energy. In this truncation atoms, dimers, and trimers carry a fixed energy, and the energy of a three-atom system is $3\,\varepsilon/2$. In consequence, the atom-dimer threshold should appear for $3\,\varepsilon_{a+d}/2 = -\frac{1}{m\,a^2}$, which is equivalent to $\gamma_{a+d} = \sqrt{3/2}\,a^{-1} \simeq 0.816\ a^{-1}$. However, the atom-dimer threshold is the solution of the equation

$$\left(E_a + E_d\right)_{q=0,\,k=0} = 0. \tag{3.48}$$

The value of γ that solves this equation is $\gamma_{a+d}^{\mathrm{trunc.}} = 4/5\,a^{-1} = 0.8\ a^{-1}$.[37] This means that, in the present truncation, the atom-dimer threshold does not appear at its

[36] This requires that the dimer is a bound state, or $a>0$.

[37] This is obtained by substituting Eq. (3.45) and (3.47) in the equation above.

exact value. There is a deviation of about 2%. This threshold appears in Fig. 3.13 as an orange, solid line.

We now turn to the trimer states. In the present truncation, this states appear for $u_t(k \to 0) = 0$. Given some fixed initial conditions in the three-body sector, the trimer states form curves in the $\left(-\sqrt{-m\,E}, 1/a\right)$ plane.

For $\gamma = 0$, the trimer appears for $a < 0$.[38] Say a_3 is a scattering length that produces a trimer for $\gamma = 0$. Then, because of the Efimov periodicity in the flow equations, there is one trimer state for every value of $a = a_3\ \mathrm{e}^{-\pi\, n/s_0^\Gamma} = \left(\frac{1}{29.8}\right)^n$, where $n = 1, 2, \ldots$, and where s_0^Γ is defined in Eq. (3.23). The curve corresponding to each of these trimer states merges with the atom-dimer threshold. Fig. 3.13 shows one of these trimer states as a black, dashed curve.

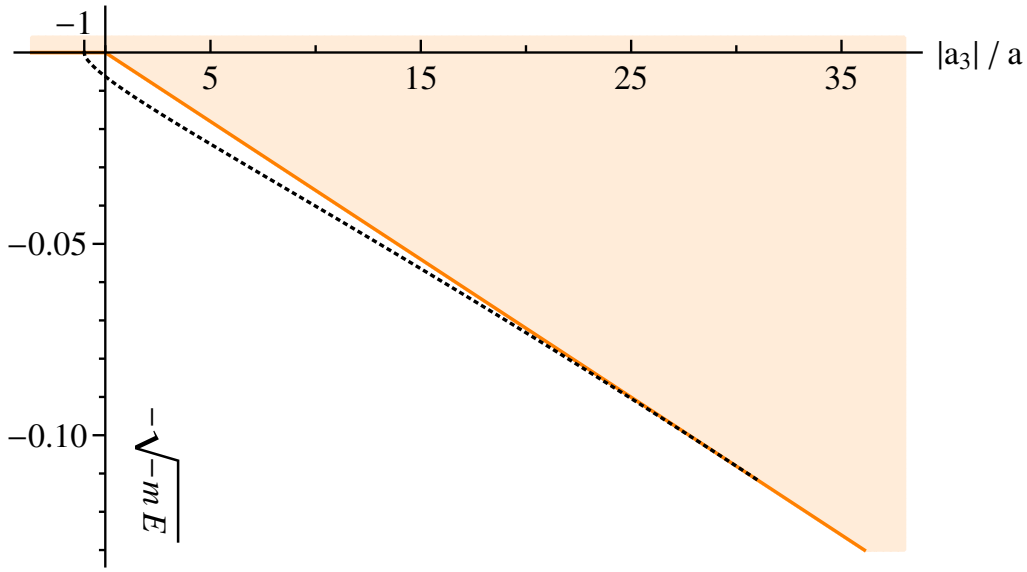

Figure 3.13: Plot with the three-body physics in the plane $(\,|a_3|/a,\ -\sqrt{-m\,E}\,)$. The horizontal axis corresponds to the inverse atom-atom scattering length, or $1/a$, in units of $|a_3|$. The latter is the (absolute value of the) atom-atom scattering length that produces a zero-energy trimer state. The vertical axis is proportional to (minus) the square root of the total energy in the system. For three-atom systems, this is $-\sqrt{-3\,m\,\varepsilon/2} = -\sqrt{3\,m}\,\gamma$.
The atom-dimer threshold is the solid, orange line and has slope $\sqrt{4/5}\,|a_3|$.
The trimer state is the black, dashed curve. It appears when the system has a total energy below the atom-dimer threshold. For $\gamma = 0$, the trimer appears for $|a_3|/a = -1$, but as $1/a$ increases the trimer state becomes more deeply bound, until it intersects the atom-dimer threshold.

[38] For $\gamma = 0$, the value of $a < 0$ that produces a trimer state depends in the three-body initial conditions.

3.11.3 Four-body sector

The four-body sector inherits the Efimov periodicity of the three-body sector. For each Efimov cycle there is an atom-trimer threshold and three tetramer states. The four-body sector also shows a dimer-dimer threshold. In this truncation, the latter threshold appears for

$$2\ (E_d)_{q=0,\,k=0} = 0, \tag{3.49}$$

which is solved by $\gamma_{d+d} = 1/a$.[39] Fig. 3.14 shows the dimer-dimer threshold as a blue, solid line.

For each Efimov cycle, the atom-trimer threshold appears for $\gamma = 0$ and $a = a_3 < 0$. As $1/a$ increases, this threshold forms a curve that eventually intersects the dimer-dimer threshold (for some $a > 0$). This threshold is given by the solution of

$$(E_a + E_t)_{q=0,\,k=0} = 0, \tag{3.50}$$

and it is displayed as the green, solid curve in Fig. 3.14.

The tetramer states appear for the values of a and γ that produce a divergence in the four-body couplings in the limit $k \to 0$. As discussed in Section 3.10, for $\gamma = 0$ we find three tetramer states for each trimer. The scattering lengths that produce these tetramers appear in Eq. (3.43). These tetramers are labeled, from deepest to shallowest, (0), (1), and (2). The shallowest of these tetramers, (2), appears very close to the atom-trimer threshold and it quickly merges with it. This tetramer only appears for a very narrow region in $1/a$. In contrast, the two deepest tetramers, (0) and (1), appear for a longer range of $1/a$. Both of them remain below the atom-trimer threshold, even though (1) runs very close to the threshold. Furthermore, as $1/a$ increases the tetramers eventually intersect the dimer-dimer threshold. Tetramers are (0) and (1) similar to the ones found in Ref. [43, 71]. They are displayed as red, dashed curves in Fig. 3.14 and 3.15.

3.11.4 Evolution with a finite external energy: conclusions

This section, Section 3.11, extends the running action ansatz for scalar atoms. The extension shifts the parameter q^0 in the propagators for the fields. This gives a finite energy that flows through each atom, dimer, or trimer in every Feynman diagram. Despite the incomplete momentum dependence, the truncation qualitatively produces the expected structure for three- and four-atom systems.

[39] This threshold matches the points where the energy of four atoms, $4\ \frac{\varepsilon}{2}$, is equal to twice the binding energy of two dimers, $-2\ \frac{1}{m\,a^2}$. Unlike the atom-dimer threshold, the dimer-dimer threshold appears at the position that is expected on physical grounds.

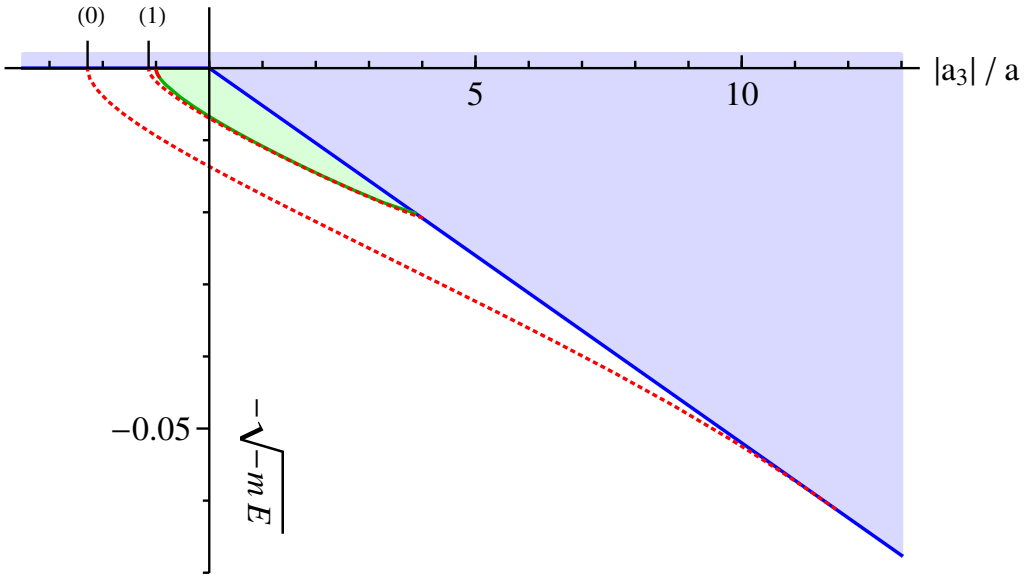

Figure 3.14: Plot of the states for systems of four scalar atoms. The horizontal axis corresponds to the inverse atom-atom scattering length, or $1/a$, in units of $|a_3|$. The latter is the (absolute value of the) atom-atom scattering length that produces a zero-energy trimer state. The vertical axis is proportional to (minus) the square root of the total energy in the system. For four-atom systems, this is $-\sqrt{-4\,m\,\varepsilon/2} = -2\,\sqrt{m}\,\gamma$. The dimer-dimer threshold is the blue, solid line, and the atom-trimer threshold is the green, solid curve.
Two of three tetramers are visible as red, dashed curves. They are labeled as (0) and (1). The third tetramer, (2), is barely visible. It is close to $E = 0$ and the atom-trimer threshold.

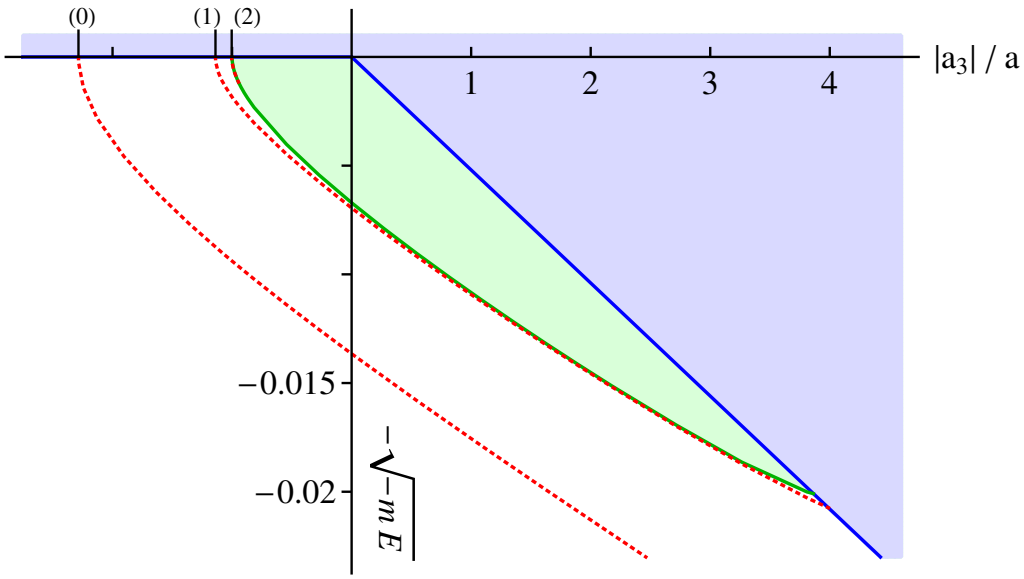

Figure 3.15: Zoom of Fig. 3.14 where the three tetramers are visible. They are labeled (from deepest to shallowest) as (0), (1), and (2).

In the three-body sector we find the atom-dimer threshold (with a small deviation from its physical value) and trimer states with Efimov periodicity. The latter states

merge with the atom-dimer threshold.

In the four-body sector we find both a dimer-dimer threshold and an atom-dimer threshold. We also find three tetramer states for each Efimov trimer. One of these states quickly merges with the atom-trimer threshold, and might be an artefact of our truncation, which produces unphysically long Efimov cycles. The other two tetramer states remain below the atom-trimer threshold [43, 71].

Chapter 4

Systems of fermions in vacuum

> Symmetry is what we see at a glance; based on the fact that there is no reason for any difference...
>
> **Blaise Pascal**

4.1 Introduction

This chapter studies systems formed by two, three, or four fermions with very low energy. The treatment is similar to the one in Chapter 3, but here we deal with spin-$\frac{1}{2}$ atoms instead of spin-0.[1] For few-particle systems the density is zero, and we refer to the study of these systems as vacuum case, or zero-density case.[2]

We deal with nonrelativistic atoms, where the dynamics is represented by a local Lagrange density. We integrate low-momentum quantum fluctuations using the FRG. This framework is introduced in Chapter 2. Section 2.1 deals with the FRG in general, and Section 2.2 describes techniques to study nonrelativistic atoms.

We describe systems with very low energy, and where the atom-atom interaction produces a scattering length, a, much larger (in absolute value) than the range. In the unitary limit, $|a| \to \infty$, the interaction does not provide any dimensionful parameters. We expect universal behaviour in systems of three and four atoms. This is because Pauli's exclusion principle forbids any states that could bring extra dimensionful parameters into the system. This is in contrast with systems of scalar atoms (discussed in Chapter 3) where the Efimov effect introduces a dimensionful parameter in three-body systems. In the unitary limit, fermion systems should display scaling symmetry. This means that physical quantities behave as powers of the

[1] The use of the word *atom* refers to the elementary particles in this framework. This use must not be confused with the normal use, which refers to physical atoms. This appears throughout this thesis.

[2] Dense-matter systems of spin-$\frac{1}{2}$ atoms are studied in Chapter 5.

energy at which physical processes occur. Close to the unitary limit, some physical quantities may behave as powers of a.

The two-particle system is studied in Ref. [11], which finds the fixed points of the Renormalisation Group of two-body scattering. Three-fermion systems are studied in References [58, 61], which calculate the atom-dimer scattering length and other three-body quantities relevant to ultracold atomic gases. Ref. [53] also calculates the atom-dimer scattering length, but for systems confined to one dimension. The latter three references use Schrödinger-equation calculations. Ref. [1] calculates the atom-dimer scattering length when the mass of one species of atoms is much larger than the other. Ref. [58] also uses different masses for atom species. The latter work uses the Skorniakov and Ter-Martirosian approach. In 1956 G. V. Skorniakov and K. A. Ter-Martirosian calculated for the first time the atom-dimer scattering for systems with a zero-range interparticle interaction [69]. Ref. [26] also calculates the atom-dimer scattering length, but it relies on the Functional Renormalisation Group.

The four-fermion system is studied in Ref. [60], which uses the Schrödinger equation to calculate the dimer-dimer scattering length. Ref. [50] uses the FRG to calculate the same quantity, and Ref. [9] verifies the convergence on the FRG flow of such systems. References [59, 23] are reviews of few-body systems. The former one relies on quantum mechanics calculations, and the latter one relies on FRG analysis. Finally, Ref. [10] studies a more complicated system, the FRG flow of systems formed of nucleons. This adds a degree of freedom to the fermions, the isospin.

4.2 Running action

This section introduces an ansatz for the running action. The ansatz contains atom and dimer fields with kinetic terms for both of them. A dynamical dimer field is introduced as a way to account for (some of) the energy dependence from two-atom subsystems. This running action also contains interaction terms with two-, three-, and four-atom physics. The explicit form of the ansatz is [9]

$$\begin{aligned}\Gamma_k = \int \mathrm{d}^4x \Bigg\{ & \sum_{i=1,2}\left(\psi_i^\dagger\left(\mathrm{i}\,\partial_0 + \frac{\nabla^2}{2\,m}\right)\psi_i\right) + Z_d\,\phi^\dagger\left(\mathrm{i}\,\partial_0 + \frac{\nabla^2}{4\,m} - \frac{u_d}{Z_d}\right)\phi \\ & - g\left(\phi^\dagger\,\psi_1\,\psi_2 + \psi_2^\dagger\,\psi_1^\dagger\,\phi\right) - \lambda\sum_{i=1,2}\left(\phi^\dagger\,\psi_i^\dagger\,\psi_i\,\phi\right) - w\left(\phi^\dagger\,\psi_2^\dagger\,\psi_1^\dagger\,\psi_1\,\psi_2\,\phi\right) \\ & - \frac{v}{2}\left(\phi^\dagger\,\phi^\dagger\,\psi_1\,\psi_2\,\phi + \phi^\dagger\,\psi_2^\dagger\,\psi_1^\dagger\,\phi\,\phi\right) - \frac{u_{dd}}{2}\left(\phi^\dagger\,\phi\right)^2\Bigg\},\end{aligned} \tag{4.1}$$

where all the fields are evaluated at the same space-time point, $x = (c\,t, \vec{x})$.

The fields are independent of the scale k, but the rest of the parameters in

this ansatz may have scale dependence. We refer to these parameters as running functions.

4.2.1 Terms in the running action

Kinetic terms

The first and second terms in the ansatz are, respectively, kinetic terms for atom and dimer fields. The kinetic term for atoms could contain a renormalisation, $Z_a(k)$. However, the flow of Z_a is zero, and this renormalisation remains at its UV value throughout the FRG evolution, $Z_a = 1$. This is a consequence of atom-number conservation in nonrelativistic systems with zero density.[3]

The dimer kinetic term contains two running functions, the renormalisation $Z_d(k)$ and the bilinear $u_d(k)$. At the UV scale, the dimers have no dynamics, hence $Z_d(K_0)$ should be (close to) zero. As k decreases, more and more low-momentum quantum fluctuations are integrated over, and $Z_d(k)$ becomes finite. The bilinear $u_d(k)$ appears in the dimer propagator, hence it is related with atom-atom scattering, see Subsection 2.2.3.

Interaction terms

The rest of the terms in the running action are interaction terms. There is a two-atom term (third term), a three-atom term (fourth), and three four-atom terms (fifth to seventh). A channel notation for these terms is introduced in Subsection 2.2.4.

The two-atom term corresponds to a $\psi_1\,\psi_2 \to \phi$ vertex. It has coupling g, which remains frozen throughout the FRG evolution. This is a consequence of atom-number conservation. The three-atom term describes atom-dimer scattering. It has coupling $\lambda(k)$, which has nonzero FRG flow. The four-body terms (fifth to seventh) have couplings $w(k)$, $v(k)$, and $u_{dd}(k)$, and also have nonzero FRG flow. The vertices that correspond to these interaction terms are displayed in Fig. 4.1.

The interaction terms in the running-action ansatz, Eq. (4.1), are all the possible two-, three-, or four-body interaction terms that can be generated without adding a more complicated momentum-dependence on the couplings.[4] This is because any term with a repeated atom field, *e.g.* $\propto \ldots\psi_1\ldots\psi_1\ldots$, must be zero. This is a

[3] In a nonrelativistic theory with zero density, atom-number conservation implies that particles cannot propagate backwards in a Feynman diagram. In consequence, the diagrams that renormalise Z_a vanish. This also happens for scalar atoms (Chapter 3) but not for fermionic atoms with a finite density (Chapter 5). There, the propagation of holes in the Fermi surface gives finite contributions to the atom renormalisation.

[4] Except for a term $-\mathfrak{g}\,\psi_2^\dagger\psi_1^\dagger\,\psi_1\psi_2^\dagger$, which was removed by a Hubbard-Stratonovich transformation at the UV, see Subsection 2.2.2. This term is not included because, out of the UV, the FRG flow does not regenerate it.

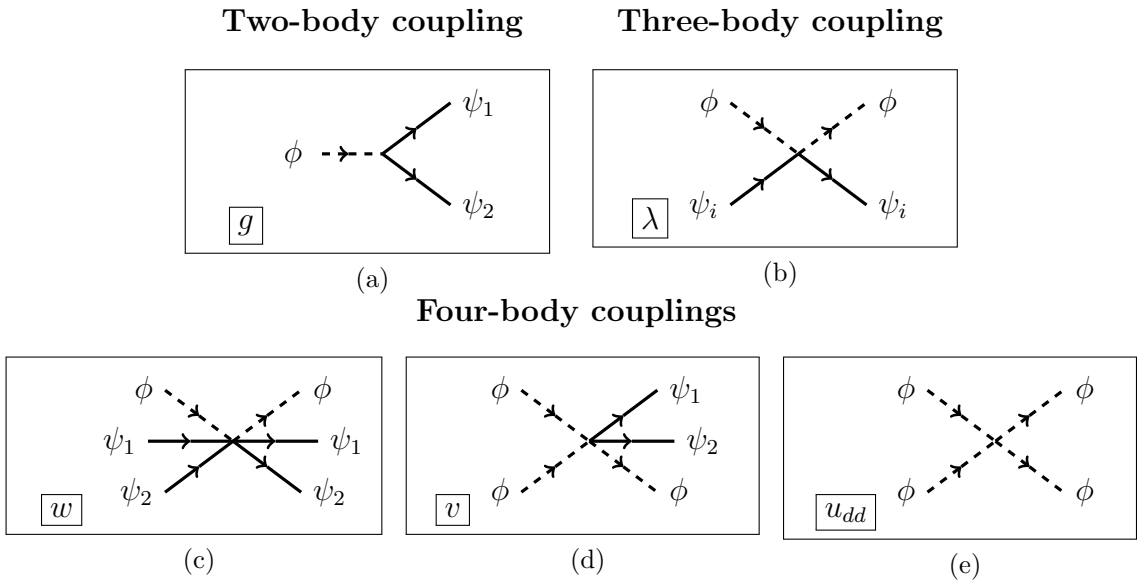

Figure 4.1: Vertices in the running action for fermionic atoms and their corresponding couplings.

consequence of the anticommutation of fermionic fields.[5]

4.2.2 Regulators and regulated energies

The running action in Eq. (4.1) is written in terms space-time coordinates. However, to use the FRG as presented in Chapter 2, we need to transform the running action to momentum coordinates. After this transformation, it is easier to write the regulated energies for atom and dimer fields, which appear in the flow equations for the running functions. These energies are

$$E_a(q,k) = \frac{q^2}{2m} + R_a(q,k) \tag{4.2a}$$

$$E_d(q,k) = \frac{q^2}{4m} + R_d(q,k) + u_d(k)/Z_d(k), \tag{4.2b}$$

and we use the regulators[6]

$$R_a(q,k) = \frac{k^2 - q^2}{2m}\,\theta(k-q) \tag{4.3a}$$

$$R_d(q,k) = Z_d(k)\,\frac{k^2 - q^2}{4m}\,\theta(k-q), \tag{4.3b}$$

which greatly simplify the three-momentum integration in the flow equations. This is because in the region where the regulators are nonzero, the regulated energies are independent of the three-momentum, $\|\vec{q}\| = q$.

[5] Furthermore, the n-body interaction terms are limited when $n \geq 3$. For odd n, there is only one possible interaction term. For even n, there are three possible terms.

[6] These regulators are optimal for convergence to physical results [52].

4.3 Two-body sector

The two-body physics is encoded in three parameters in the running action, g, $u_d(k)$, and $Z_d(k)$. As discussed above, at zero density, g is frozen throughout the evolution. In contrast, $u_d(k)$ and $Z_d(k)$ flow.

The flow equations for $u_d(k)$ and $Z_d(k)$ can be obtained by inserting the running action ansatz in the flow equation and taking the appropriate field derivatives. This procedure is used for all the running functions, and is described in Subsection 2.2.5. These flow equations [for $u_d(k)$ and $Z_d(k)$] are also described by one diagram, which is displayed in Fig 2.6. This diagram has one loop, and an insertion proportional to $\partial_k R_a$ in one of its virtual particles.[7]

Boundary conditions are necessary to integrate the flow of $u_d(k)$ and $Z_d(k)$. Fixing the atom-atom scattering to yield the correct scattering length gives a boundary condition for $u_d(k=0)$. This is discussed in Subsection 2.2.3. The boundary conditions on $Z_d(k)$ are simpler. The latter must be (close to) zero at the UV scale because, there, the dimer fields do not have dynamics.

Using the regulators in Eq. (4.3) to integrate the flow equations yields

$$u_d(k) = \frac{m\,g^2}{\pi^2}\left(\frac{k}{3} - \frac{\pi}{4\,a}\right) \tag{4.4a}$$

$$Z_d(k) = \frac{2\,m^2\,g^2}{\pi^2}\left(\frac{1}{3\,k}\right). \tag{4.4b}$$

The flow of $Z_d(k)$ is independent of a, but the flow of $u_d(k)$ is not. If $a > 0$, there is a two-atom bound state, and $u_d(k)$ crosses zero during the FRG evolution. In consequence, $E_d(k)$ and $E_{a+d}(k)$ also cross zero for one value of k (there is one crossing for each of these energies). These crossings are associated with the opening of the dimer-dimer and atom-dimer channels. In contrast, if $a < 0$, there is no two-atom bound state, and $u_d(k)$, $E_d(k)$, $E_{a+d}(k)$ remain nonzero throughout the evolution.

4.4 Three-body sector: flow equations

The three-body sector consists of the coupling $\lambda(k)$. Its flow equation has the form

$$\lambda'(k) = \int \frac{\mathrm{d}^3 q}{(2\pi)^2}\left\{ g^4\,\frac{Z_d\,(3\,E_a + 2\,E_d)\,\partial_k R_a + E_a\,\partial_k R_d}{4\,E_a^3\,(E_{a+d})^2\,Z_d^2} + \lambda^2\,\frac{Z_d\,\partial_k R_a + \partial_k R_d}{(E_{a+d})^2\,Z_d^2} \right.$$
$$\left. + g^2\,\lambda\,\frac{Z_d\,(2\,E_a + E_d)\,\partial_k R_a + E_a\,\partial_k R_d}{E_a^2\,(E_{a+d})^2\,Z_d^2} \right\}. \tag{4.5}$$

[7] All FRG diagrams have exactly one loop.

The atom-dimer regulated energy, E_{a+d}, appears in the denominator of several terms in the flow equation for $\lambda(k)$. For a positive atom-atom scattering length, this energy will vanish for some value of $k > 0$, producing a divergence in the flow equation. Such divergence is associated with the opening of the atom-dimer channel. If the atom-atom scattering is not positive, then E_{a+d} remains finite throughout the FRG evolution and the flow of $\lambda(k)$ is free from divergences.

The parameters g and m are constant throughout the evolution, and they can be divided out of the flow equations of all the running functions. For $\lambda(k)$, this can be achieved with the definition

$$\tilde{\lambda}(k) = \frac{1}{g^2\, m}\, \lambda(k), \tag{4.6}$$

where the flow of $\tilde{\lambda}$ is independent of g and m. Throughout this work we use the following convention, the tilde denotes functions where the appropriate powers of g and m where divided out, in consequence their flows are independent of g and m.

4.5 Three-body sector: scaling limit

We define the scaling limit of the flow as the limit where $1/|a| \to 0$ while k remains finite. Here, the flow of the running action has only one dimensionful parameter, the scale k.[8] Furthermore, the Fermi exclusion principle forbids any states formed by three (or more) atoms. In consequence, there should not exist any states that fix a dimensionful scale in the three-body system. This is in contrast with the case of scalar atoms discussed in Chapter 3, where three-body Efimov states break the continuous scaling symmetry to a discrete symmetry.

In the scaling limit, we expect the flow to have scaling symmetry, and we also expect each running function—*e.g.* $u_d(k)$, $\lambda(k)$, $w(k)$—to behave as a real power of k times a dimensionless coefficient. For each running function, the exponent of k can be obtained by dimensional analysis, either on the running action, or on the flow equations. This power-of-k behaviour is a type of universality: all the atom-atom microscopic potentials with infinite scattering length have the same low-momentum quantum corrections, which are free from dimensionful parameters. In this analysis, the dimensionless coefficients (next to the power of k) are not so universal: they have some dependence on the choice of regulators.

Each running function can absorb the power of k that determines its scaling-limit behaviour. This introduces new functions, called rescaled functions, which are denoted by a hat.

[8] This is because g and m can be divided out of all the flow equations with the appropriate redefinitions. The redefined, running functions are denoted by a tilde, *e.g.* $\tilde{\lambda}(k)$ in Eq. (4.6).

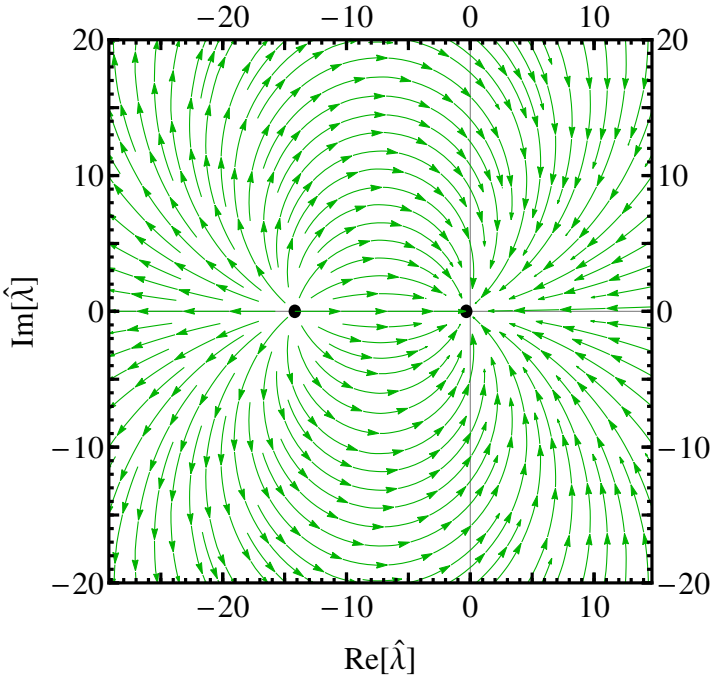

Figure 4.2: Flow of $\hat{\lambda}$ on the complex plane. The horizontal and verticals axes correspond to the real and imaginary parts of $\hat{\lambda}$. The black point on the left is the repulsive fixed point, $\hat{\lambda}^{(\text{fp-1})}$, whereas the black point on the right (close to the origin) is the attractive fixed point, $\hat{\lambda}^{(\text{fp-2})}$.

The rescaled flow equations should have fixed-point solutions. For each rescaled coupling, an attractive, fixed-point solution corresponds to the universal coefficient next to the power of k in the nonrescaled coupling. The approach of rescaled couplings and fixed points is a reformulation of the expected power-of-k behaviour of nonrescaled functions.

For the three-body sector, the rescaled atom-dimer coupling is

$$\hat{\lambda}(k) = \frac{k^2}{g^2\, m}\, \lambda(k), \tag{4.7}$$

and the flow equation for $\hat{\lambda}(k)$ in the scaling limit is

$$\mathrm{d}_\tau\, \hat{\lambda} = \frac{28}{125}\, \hat{\lambda}^2 + \frac{406}{125}\, \hat{\lambda} + \frac{128}{125}, \tag{4.8}$$

where $\tau = \log(k/K_0)$.

This equation has two fixed points. They are the roots of the quadratic on the right-hand side of Eq. (4.8). One of the fixed points is attractive while the other is

repulsive. These fixed points are

$$\hat{\lambda}^{(\text{fp-1})} = -\frac{29}{4} - \frac{5}{4}\sqrt{\frac{215}{7}} \simeq -14.2 \qquad \text{(repulsive)} \tag{4.9a}$$

$$\hat{\lambda}^{(\text{fp-2})} = -\frac{29}{4} + \frac{5}{4}\sqrt{\frac{215}{7}} \simeq -0.322 \qquad \text{(attractive)}. \tag{4.9b}$$

We are interested on the convergence of the flow when $\tau \to -\infty$ (the physical limit). In consequence, the eigenvalues of the matrix of derivatives at an attractive fixed point are all negative. In contrast, the eigenvalues at a repulsive fixed point are all positive.[9]

The flow of $\hat{\lambda}(k)$ is displayed in Fig. 4.2. This figure shows the attractive and repulsive fixed points.

4.6 Four-body sector: flow equations

The four-body sector is formed by three couplings, $w(k)$, $v(k)$, and $u_{dd}(k)$. Their flow equations are in Appendix E. The flow equation for w is free from the coupling u_{dd} because all the diagrams for the flow of w that involve the coupling u_{dd} require the propagation of an antiparticle, and therefore vanish. Similarly the flow of u_{dd} is free from w. In contrast the coupling v, which mixes the channels $\phi\,\phi$ and $\phi\,\psi_1\,\psi_2$, appears in the flow of all four-body channels.

The four-body driving terms [Eq. (E.1)] have denominators with (factors of) E_d and E_{a+d}. If the scattering length is positive, these regulated energies will vanish at some point in the flow. This can produce divergences in the four-body couplings. Such divergences are associated with the opening of the channel $\phi\,\phi$. In the physical limit, this threshold appears when the total energy of the system is twice the dimer binding energy.

The tilded four-body couplings are

$$\tilde{w}(k) = \frac{1}{m\,g^2}\,w(k), \tag{4.10a}$$

$$\tilde{v}(k) = \frac{1}{m^2\,g^3}\,v(k), \tag{4.10b}$$

$$\tilde{u}_{dd}(k) = \frac{1}{m^3\,g^4}\,u_{dd}(k), \tag{4.10c}$$

where the flow of $\tilde{w}(k)$, $\tilde{v}(k)$, and $\tilde{u}_{dd}(k)$ is free of g and m.

[9] In the usual language of fixed-point solutions, eigenvalues (of the matrix of derivatives) of an attractive fixed point are positive, and eigenvalues of a repulsive fixed point are negative. However, in the usual language, convergence is expected for $\tau \to +\infty$. FRG analysis looks for convergence at $\tau \to -\infty$. That is why the signs of the eigenvalues are the opposite as in many discussions of fixed points.

fixed point		$\hat{w}$	$\hat{v}$	$\hat{u}_{dd}$	eigenvalues		
fp-1	(repulsive)	-66500	-835	-7.79	-6.11,	-5.15,	-4.19
fp-2	(attractive)	-10.5	0.102	0.0357	+6.11,	+5.15,	+4.19
fp-3	(mixed)	-4640	-207	-4.61	-6.11,	-0.959,	+4.19
fp-4	(mixed)	-431	-51.7	-3.15	+6.11,	+0.959	-4.19

Table 4.1: Fixed points of four-body couplings and eigenvalues of the matrix of derivatives at each of these points.

4.7 Four-body sector: scaling limit

The power-of-k behaviour in the four-body couplings in the scaling limit is

$$\hat{w}(k) = k^5\,\tilde{w}(k), \tag{4.11a}$$

$$\hat{v}(k) = k^4\,\tilde{v}(k), \tag{4.11b}$$

$$\hat{u}_{dd}(k) = k^3\,\tilde{u}_{dd}(k), \tag{4.11c}$$

which was obtained by dimensional analysis.

In the scaling limit, the flow equations for the four-body, rescaled couplings depend on the couplings themselves and on $\hat{\lambda}$. However, as discussed in Section 4.4, $\hat{\lambda}$ flows toward the attractive fixed point $\hat{\lambda}^{(\text{fp-2})}$. Hence, it is convenient to replace $\hat{\lambda}$ by this fixed point. Then, the four-body flow equations have the form

$$\begin{aligned} \mathrm{d}_\tau \hat{w} = {} & \left(1 + \frac{4}{5}\sqrt{\frac{301}{5}}\right)\hat{w} + \frac{\pi^2}{15}\,\hat{v}^2 + \left(\frac{20\,\pi^2}{3} - \frac{124\,\pi^2}{525}\sqrt{1505}\right)\hat{v} \\ & + \left(\frac{55533\,\pi^2}{35} - \frac{4273\,\pi^2}{105}\sqrt{1505}\right) \end{aligned} \tag{4.12a}$$

$$\begin{aligned} \mathrm{d}_\tau \hat{v} = {} & \frac{2}{3\,\pi^2}\,\hat{w} + \frac{2\,\pi^2}{15}\,\hat{w}\,\hat{v} + \left(2 + \frac{2}{5}\sqrt{\frac{301}{5}}\right)\hat{v} + \left(\frac{20\,\pi^2}{3} - \frac{124\,\pi^2}{525}\sqrt{1505}\right)\hat{u}_{dd} \\ & - \frac{1549}{7} + \frac{1003}{5}\sqrt{\frac{43}{35}} \end{aligned} \tag{4.12b}$$

$$\mathrm{d}_\tau \hat{u}_{dd} = \frac{2}{3\,\pi^2}\,\hat{v} + \frac{2\,\pi^2}{15}\,\hat{u}_{dd}^2 + 3\,\hat{u}_{dd} + \frac{364 - 10\sqrt{1505}}{21\,\pi^2} \tag{4.12c}$$

The right-hand sides of these equations are quadratic on the rescaled couplings. The fixed points of the three four-body couplings are encoded on a system of coupled, quadratic equations. There are four solutions to these equations. They are displayed in Table 4.1. We calculate the matrix of derivatives for the system in Eq. (4.12). Then, we evaluate this matrix at each of the four four-body fixed points and calculate the corresponding eigenvalues. These eigenvalues reveal that one of the fixed points is repulsive, other is attractive, and the other two are mixed. They are displayed in Table 4.1.

In the scaling limit, the flow of the running action is free from any dimensionful parameter, and the three- and four-body sectors flow towards their attractive fixed points. The existence and uniqueness[10] of these attractive fixed points is a manifestation of universal behaviour. This confirms the hypothesis that, in the scaling limit, the running functions behave as a real power of k, times a dimensionless and universal[11] coefficient.

4.8 Finite scattering length

A finite atom-atom scattering length provides a dimensionful physical scale in the flow. This parameter breaks the scaling symmetry at $k \sim 1/|a|$, thus changing the behaviour of the running functions. In the physical limit, the running functions are more complicated that the power-of-k behaviour of the scaling limit. However, with a finite scattering length, some running functions behave as $\propto k^\alpha\, a^\beta$, where the power of k is different from the one in the scaling limit.

A finite scattering length gives a term $-\frac{m\,g^2}{4\,\pi\,a}$ in $u_d(k)$ (the two-body sector is discussed in Section 4.3). This modifies the dimer energy, and for a positive scattering length the regulated energies E_d and E_{a+d} cross zero during the evolution. These crossings are associated with the opening of the channels $\phi\,\phi$ and $\phi\,\psi_a$. The three- and four-body flow equations have divergences at these crossings, and to (numerically) evaluate the flow equations, it is necessary to regulate such divergences. This is performed by adding a small imaginary part to the regulated dimer energy,[12]

$$E_d \to \frac{q^2}{4\,m} + \frac{u_d}{Z_d} - \mathfrak{i}\,\epsilon. \tag{4.13}$$

The magnitude of ϵ is unphysical, hence we look for the evolution in the (numerically obtained) limit $\epsilon \to 0$. This is similar to the imaginary regulator in Section 3.9. If the scattering length is negative, this imaginary regulator is unnecessary.

4.8.1 Three-body sector

The flow of $\lambda(k)$ with a finite scattering length differs from the flow in the scaling limit. However, near the UV scale, k is much larger than $1/|a|$, and the flow is still very close to the scaling limit. We use the attractive fixed point $\hat{\lambda}^{(\text{fp-2})}$ as the initial condition of $\hat{\lambda}$.[13] Departure from the scaling limit occurs when k decreases and becomes comparable with $1/|a|$.

[10] For the three- and four-body sectors there are more than one fixed-point solutions. However, only one of these fixed points is attractive.

[11] These universal coefficients have some regulator dependence.

[12] There are other possible schemes to regulate the divergences.

[13] Setting $\hat{\lambda}$ close to its attractive fixed point means that for $1/|a| \ll k$ the flow of $\hat{\lambda}$ remains flat.

For a positive scattering length, E_{a+d} crosses zero near $k = 1/|a|$. This crossing produces a divergence in the flow equation of $\tilde{\lambda}(k)$. There, $\mathrm{Im}\big[\tilde{\lambda}\big]$ grows suddenly, signalling the opening of the channel $\phi\,\psi_a$. Near the crossing, the real and imaginary parts of $\tilde{\lambda}(k)$ show one peak (each) with finite height and width; the shape of the peaks is independent of the imaginary regulator. After this region, k becomes much smaller than $1/|a|$, and the flow approaches physical-limit behaviour. The upper plot in Fig. 4.3 shows $\tilde{\lambda}$ with a positive scattering length.

For a negative scattering length, $\tilde{\lambda}(k)$ remains real (if the initial conditions are real), and does not need an imaginary regulator. When the scale k approaches $1/|a|$, the flow smoothly changes behaviour. When k is much smaller than $1/|a|$, the flow displays physical-limit behaviour. The lower plot in Fig. 4.3 shows $\tilde{\lambda}$ with a negative scattering length.

The behaviour of the flow near the physical limit is determined by the flow equations with $k \ll 1/|a|$. We expand the driving terms of the flow equations around $k = 0$, which yields

$$\mathrm{d}_k\tilde{\lambda} = -\frac{8\,a}{3\,\pi\,k^2} + \mathcal{O}(k^{-1}). \tag{4.14}$$

Therefore, near the physical limit, $\tilde{\lambda}(k)$ behaves like

$$\tilde{\lambda}(k) \sim \frac{8\,a}{3\,\pi\,k}, \tag{4.15}$$

which is a both a power of k and a power of a. In the physical limit, $(\mathrm{e}^{\tau}\,\tilde{\lambda})$ converges to a finite quantity, which has the sign of the atom-atom scattering length.

4.8.2 Four-body sector

Near the UV scale, the behaviour of four-body couplings is close the scaling-limit case. Therefore, the attractive fixed point $(\hat{w}^{(\text{fp-2})}, \hat{v}^{(\text{fp-2})}, \hat{u}_{dd}^{(\text{fp-2})})$ is used as initial condition for $(\hat{w}, \hat{v}, \hat{u}_{dd})$. As k approaches $1/|a|$, the couplings switch to a different behaviour.

For a positive scattering length, there are two divergences in the flow equations, both near $k = 1/|a|$. The first one corresponds to the crossing of $E_{a+d} = 0$, and the other one to the crossing of $E_{d+d} = 0$. The latter crossing corresponds to the threshold of the channel $\phi\,\phi$. The imaginary regulator introduced in Subsection 4.8.1 is used to integrate through this divergences.

For a negative scattering length, there are no divergences in the flow equations, and the transition between scaling-limit behaviour and physical-limit behaviour is smooth.

For $k \ll 1/|a|$, the flow switches to a different behaviour. The driving terms of

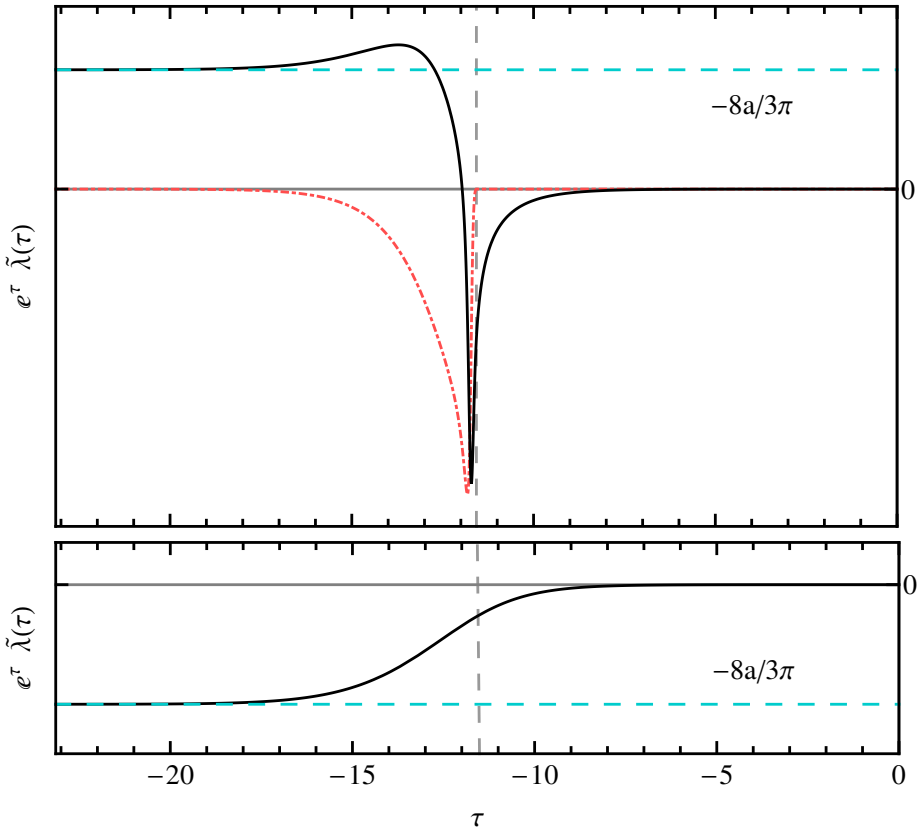

Figure 4.3: Plots with the evolution of $e^\tau\ \tilde{\lambda}(\tau)$ with positive (upper plot) and negative scattering lengths (lower plot). These scattering lengths are given by $a^{-1}K_0 = \pm 10^{-5}$. The vertical axis is $e^\tau\ \tilde{\lambda}(\tau)$, and the horizontal axis is τ. The vertical and horizontal scales are the same in the two plots. The black, solid curve corresponds to the real part of $e^\tau\ \tilde{\lambda}(\tau)$, whereas the red, dotted curve corresponds to the imaginary part. A grey, vertical, dashed line signals $E_{a+d} = 0$, which also corresponds to $k \sim 1/|a|$. The cyan, horizontal, dashed lines signal $-8\,a/3\,\pi$, which is the value of $e^\tau\ \tilde{\lambda}$ in the physical limit.

the flow equations expanded around $k = 0$ describe the physical-limit behaviour of the couplings. This expansion yields

$$\mathrm{d}_k\tilde{w} = \frac{32\,a^2}{k^4} + \mathcal{O}(k^{-3}), \tag{4.16a}$$

$$\mathrm{d}_k\tilde{v} = \frac{32\,a\,\tilde{\lambda}(k)}{3\,\pi\,k^2} + \frac{128\,a^2\,\tilde{\lambda}(k)}{5\,\pi^2\,k} - \frac{32\,a^2}{3}\,\tilde{u}_{dd}(k) - \frac{8\,a}{3\,\pi}\,\tilde{v}(k) + \frac{2}{3\,\pi^2}\,\tilde{w}(k) + \frac{1408\,a^3}{27\,\pi^3}\,\tilde{\lambda}(k) + \frac{16\,a}{3\,\pi}\,\tilde{\lambda}^2(k) + \mathcal{O}(k), \tag{4.16b}$$

$$\mathrm{d}_k\tilde{u}_{dd} = -\frac{2}{\pi^2\,k^4} + \mathcal{O}(k^{-3}). \tag{4.16c}$$

In consequence, in the physical limit, the couplings behave like

$$\tilde{w}(k) \sim -\frac{32\,a^2}{3\,k^3} \tag{4.17a}$$

$$\tilde{v}(k) \sim -\frac{64\,a^2}{9\,\pi^2\,k^2} \tag{4.17b}$$

$$\tilde{u}_{dd}(k) \sim \frac{2}{3\,\pi^2\,k^3}, \tag{4.17c}$$

where the products $(\mathrm{e}^{3\tau}\ \tilde{w})$, $(\mathrm{e}^{2\tau}\ \tilde{v})$, $(\mathrm{e}^{3\tau}\ \tilde{u}_{dd})$ approach finite constants, which are independent of the sign on the scattering length. The constants corresponding to $(\mathrm{e}^{3\tau}\ \tilde{w})$ and $(\mathrm{e}^{2\tau}\ \tilde{v})$, are proportional to a^2, whereas the constant corresponding to $(\mathrm{e}^{3\tau}\ \tilde{u}_{dd})$ is independent of a.

The coupling $\tilde{u}_{dd}(k)$, has the same power-of-k behaviour both in the scaling limit, see Eq. (4.11c), and near the physical limit with a finite scattering length. This appears in both the upper and lower plots in Fig. 4.4. There, for $-8 < \tau$, $(\mathrm{e}^{3\tau}\ \tilde{u}_{dd}) = \hat{u}_{dd}$ is still near the scaling limit, and $\hat{u}_{dd}$ remains close to $\hat{u}_{dd}^{(\text{fp-2})} \simeq 0.0357$. For $\tau < -16$, $(\mathrm{e}^{3\tau}\ \tilde{u}_{dd}) = \hat{u}_{dd}$ is close to the physical limit, and $\hat{u}_{dd}$ is near $\frac{2}{3\,\pi^2}$. This is not the case of the other four-body couplings.

Figure 4.4 shows the flow of $(\mathrm{e}^{3\tau}\ u_{dd})$, both with positive and negative scattering lengths.

4.9 External energy

This section extends the running action for fermionic atoms, Eq. (4.1), by adding a fixed energy into the propagators of the fields. This energy shifts the zero of q^0. A similar modification is introduced for an action with scalar atoms in Section 3.11. In the running action used in the previous parts of this chapter, the atom kinetic term is expanded linearly around $q^0 = 0$. In this section it is expanded around $q^0 = -\varepsilon/2 \geq 0$. Because of energy conservation the dimer kinetic term is now expanded around $q^0 = -\varepsilon$. However, the extra term ε in the dimer inverse propagator is absorbed by $u_d(k)$. The kinetic terms in the new running action are

$$\psi_a^\dagger \left(q^0 + \frac{\varepsilon}{2} - \frac{q^2}{2\,m} \right) \psi_a \tag{4.18a}$$

$$\phi^\dagger \left(Z_d \left(q^0 - \frac{q^2}{4\,m} \right) - u_d \right) \phi. \tag{4.18b}$$

The rest of the running action has the same interaction terms as in Eq. (4.1).

As discussed in page 89, we must be careful when comparing running actions with different values of ε: these actions correspond to different truncations that (try to) describe the same physical systems. Some values of ε describe some physical

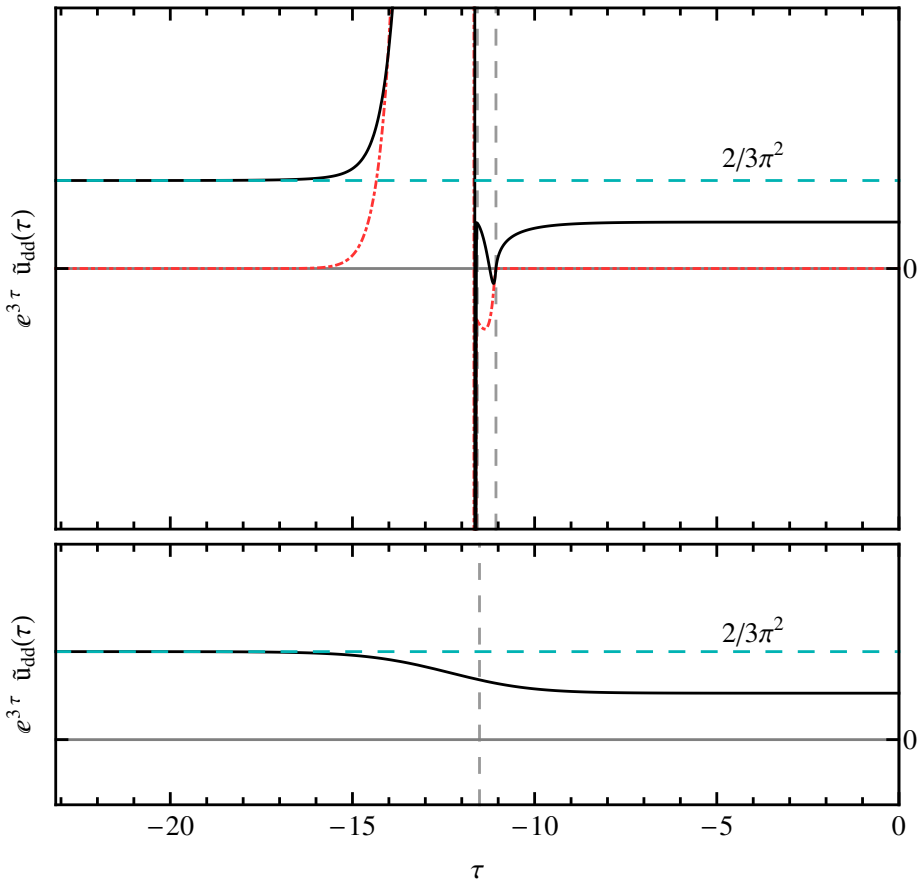

Figure 4.4: Evolution of $e^{3\tau}\ \tilde{u}_{dd}$ with positive (upper plot) and negative (lower plot) scattering lengths. These are given by $a^{-1}K_0 = \pm 10^{-5}$. The black, solid curve corresponds to the real part, whereas the red, dotted curve corresponds to the imaginary part. The horizontal axis is τ. In the positive-scattering-length plot there are two grey, vertical lines. The left one signals $E_{a+d} = 0$, and the right one signals $E_{d+d} = 0$. In the negative-scattering-length plot there is one grey, vertical line. It signals $k = 1/|a|$. In both plots, the cyan, horizontal, dashed line signals $2/3\pi^2$, which is the value of $e^{3\tau}\ \tilde{u}_{dd}$ in the physical limit.

processes better, but in the end they correspond to different expansions of the same physics.

We introduce the auxiliary definition,

$$\varepsilon = -\frac{\gamma^2}{m} < 0, \tag{4.19}$$

where $\gamma > 0$ and has units of momentum. The regulated energies now are

$$E_a = \frac{q^2}{2\,m} + R_a(q,k) - \frac{\varepsilon}{2} \qquad = \frac{q^2}{2m} + R_a(q,k) + \frac{\gamma^2}{2\,m} \tag{4.20a}$$

$$E_d = \frac{q^2}{4\,m} + \frac{R_d(q,k)}{Z_d(k,\gamma)} + \frac{u_d(k,a,\gamma)}{Z_d(k,\gamma)}. \tag{4.20b}$$

Flow equations for the parameters in this new running action are obtained by

taking the appropriate field derivatives of the flow equation.

We use the dimensionless auxiliary parameters,

$$f = \frac{\gamma}{a^{-1}} \tag{4.21a}$$

$$r_a = \frac{a^{-1}}{K_0}, \tag{4.21b}$$

to write results independent of unphysical (but dimensionful) parameters.

4.9.1 Two-body sector

A finite γ modifies the boundary condition on $u_d(k, a, \gamma)$, which is set at

$$u_d(k = 0, \gamma, a) = \frac{m\, g^2}{\pi^2} \left(-\frac{\pi}{4\, a} + \frac{\pi\, \gamma}{4} \right). \tag{4.22}$$

This condition produces a pole in the dimer propagator when each atom carries half the binding energy of the dimer. This condition is $\gamma = 1/a$.

The two-body running functions are

$$u_d(k, a, \gamma) = \frac{g^2\, m}{\pi^2} \left(\frac{k}{2} - \frac{\pi}{4\, a} + \frac{\pi\, \gamma}{4} - \frac{k^3}{6\, (k^2 + \gamma^2)} - \frac{\gamma}{2} \operatorname{ArcTan}(k/\gamma) \right) \tag{4.23a}$$

$$Z_d(k, \gamma) = \frac{2\, m^2\, g^2}{\pi^2} \left(\frac{3\, \pi\, k^4 + 10\, \gamma\, k^3 + 6\, \pi\, \gamma^2\, k^2 + 6\, \gamma^3\, k + 3\, \pi\, \gamma^4}{48\, \gamma\, \left(k^2 + \gamma^2\right)^2} - \frac{\operatorname{ArcTan}(k/\gamma)}{8\, \gamma} \right). \tag{4.23b}$$

These running functions are an important ingredient in the driving terms of the flow in the three- and four-body sectors.

In the physical limit, these running functions are

$$\lim_{k \to 0} u_d(k, a, \gamma) = \frac{m\, g^2}{\pi^2} \left(-\frac{\pi}{4\, a} + \frac{\pi\, \gamma}{4} \right) \tag{4.24a}$$

$$\lim_{k \to 0} Z_d(k, \gamma) = \frac{2\, m^2\, g^2}{\pi^2} \left(\frac{\pi}{16\, \gamma} \right). \tag{4.24b}$$

If the boundary conditions are chosen carefully, these physical-limit values do not depend on the form of the regulators in Eq. (4.3).

4.9.2 Three-body sector

The three-body sector comprises $\lambda(k)$, which couples the atom-dimer channel with itself. When dimers are bound states ($a > 0$), there is an atom-dimer threshold.[14]

[14] In contrast, when dimers are not physical states ($a < 0$), there is no atom-dimer threshold.

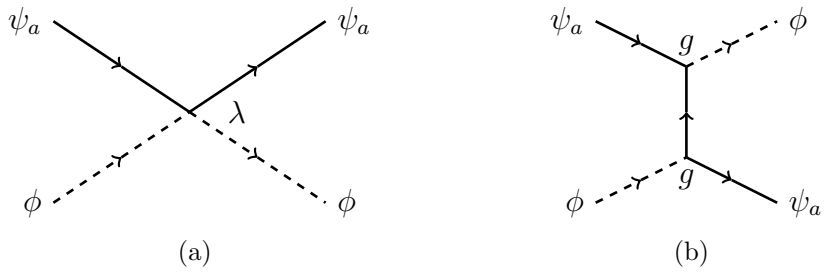

(a) (b)

Figure 4.5: Tree-level diagrams for atom-dimer scattering.

$r_a^2 \left[\mathrm{e}^{-2\tau}\,\hat{\lambda}(\tau)\right]_{\tau\to-\infty}$	f
-0.836	0.8 (ψ-ϕ trunc. threshold)
-0.618	$\sqrt{2/3}$ (ψ-ϕ phys. threshold)
-0.258	1 (dimer threshold)

Table 4.2: Physical limit of $r_a^2 \left[\mathrm{e}^{-2\tau}\,\hat{\lambda}(\tau)\right]$ for different values of f.

In the present truncation, this threshold appears for the values of γ and that solve

$$(E_a + E_d)_{q=0,k=0} = 0. \tag{4.25}$$

This equation is solved by $\gamma_{a+d}^{\text{trunc.}} = \frac{4}{5}\,a^{-1} = 0.8\,a^{-1}$, which is not the correct position for the atom-dimer threshold. It should appear when the energy of three atoms is the same as dimer binding energy, or

$$3 \times \left(\frac{\epsilon}{2}\right) = -\frac{1}{m\,a^2}, \tag{4.26}$$

which implies $\gamma_{a+d} = \sqrt{2/3}\,a^{-1} \simeq 0.816\,a^{-1}$. This discrepancy between the physical threshold and the threshold in our truncation is generated by the incomplete energy-dependence in our truncation. However, the discrepancy does not depend on the explicit choice of regulators. This is because in the present truncation, the threshold is set by the physical limit of the two-body functions, Eq. (4.24a).

Atom-dimer scattering

An important parameter in three-atom systems is the atom-dimer scattering length, $a_{\psi\phi}$, which is a function of the atom-atom scattering length. The ratio $a_{\psi\phi}/a = 1.2$ has been calculated in different ways [69, 58, 61, 26, 1]. We proceed to calculate this ratio in the present truncation, which yields $a_{\psi\phi}/a = 1.56$.

The amplitude for atom-dimer scattering is

$$T_{\psi\phi}(p) = -\frac{2\,\pi}{\mu_{\psi\phi}}\left(\frac{1}{-\mathrm{i}\,p - 1/a_{\psi\phi} + \ldots}\right) \to \frac{3\,\pi}{m}\,a_{\psi\phi} \tag{4.27}$$

where $\mu_{\psi\phi} = 2\,m/3$ is the reduced mass of the atom-dimer system, and $a_{\psi\phi}$ is the atom-dimer scattering length. This process, $\phi\,\psi_a \to \phi\,\psi_a$, is independent of the atom spin.

This amplitude can be obtained from tree-level diagrams in the running action (evaluated at the physical limit). Two diagrams contribute to this process. They appear in Fig. 4.5. The contribution to the amplitude of atom-dimer scattering from the diagram on the left is

$$\lim_{k\to 0}\frac{\lambda}{\left(\sqrt{Z_d}\right)^2} = \frac{8\,\pi\,f}{m}\,\left(r_a^2\,\lim_{\tau\to-\infty}\left[\mathrm{e}^{-2\,\tau}\,\hat{\lambda}(\tau)\right]\right)\,a, \tag{4.28}$$

where f and r_a are dimensionless parameters introduced in Eq. (4.21). The quantity

$$\left(r_a^2\,\lim_{\tau\to-\infty}\left[\mathrm{e}^{-2\,\tau}\,\hat{\lambda}(\tau)\right]\right), \tag{4.29}$$

depends on the ratio f, but does not depend on the atom-atom scattering length directly. Its value in (terms of f) is displayed in Table 4.2.

Now, the contribution from the diagram on the right in Fig. 4.5 is

$$\lim_{k\to 0}\frac{\frac{g^2}{-\varepsilon}}{\left(\sqrt{Z_d}\right)^2} = \frac{8\,\pi}{m\,f}\,a. \tag{4.30}$$

Adding the contribution of the two diagrams yields

$$T_{\psi\phi} = \frac{8\,\pi}{m}\left(\frac{1}{f} + f\,\left(r_a^2\,\lim_{\tau\to-\infty}\left[\mathrm{e}^{-2\,\tau}\,\hat{\lambda}(\tau)\right]\right)\right)\,a, \tag{4.31}$$

and in consequence,

$$\frac{a_{\psi\phi}}{a_{\psi\psi}} = \begin{cases} 1.56 & \text{for } f = 4/5 \text{ (trunc. threshold)} \\ 1.92 & \text{for } f = \sqrt{2/3} \text{ (phys. threshold)} \end{cases}. \tag{4.32}$$

Using γ corresponding to the threshold truncation gives a better value than using γ corresponding to the physical threshold. However, this value has a 30% deviation from the exact value $a_{\psi\phi}/a_{\psi\psi} = 1.2$ [69, 58, 61, 26, 1].

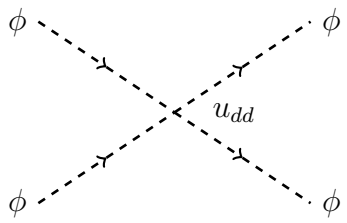

Figure 4.6: Tree-level diagram for dimer-dimer scattering.

4.9.3 Four-body sector

The four-atom sector comprises two channels: $\psi_1\,\psi_2\,\phi$ and $\phi\,\phi$. In this work we focus on the latter one. If the dimer is a bound state, the dimer-dimer channel has a threshold, which appears when the total energy of the system is twice the dimer binding energy. In our truncation the threshold is set at

$$2\,E_d(q=0,k=0)=0. \tag{4.33}$$

The corresponding value of γ is $\gamma = a^{-1}$, which is also the physical position of the threshold.

Dimer-dimer scattering

The dimer-dimer scattering length, $a_{\phi\phi}$, was calculated by Petrov, Salomon, and Shlyapnikov using the Schrödinger equation. They found the exact value $a_{\phi\phi}/a = 0.6$ [60]. This ratio was also calculated using the FRG in [50, 9] where the result in the latter reference matches that in [60].

The dimer-dimer scattering length in terms of the amplitude is

$$T_{\phi\phi} = \frac{4\,\pi}{\mu_{\phi\phi}}\,a_{\phi\phi} = \frac{4\,\pi}{m}\,a_{\phi\phi}, \tag{4.34}$$

where the reduced mass of the dimer-dimer system is $\mu_{\phi\phi} = m$. In our truncation, dimer-dimer scattering is given by the tree-level diagram in Fig. 4.6. The amplitude of this diagram is

$$T_{\phi\phi} = \lim_{k\to 0}\frac{2\,u_{dd}}{(\sqrt{Z_d})^4} = \frac{128\,\pi^2\,f^2}{m}\,\left(r_a^3\lim_{\tau\to-\infty}\left[\mathrm{e}^{-3\,t}\,\hat{u}_{dd}(\tau)\right]\right)\,a, \tag{4.35}$$

where f and r_a are dimensionless parameters defined in Eq. (4.21). The combination

$$\left(r_a^3\lim_{\tau\to-\infty}\left[\mathrm{e}^{-3\,t}\,\hat{u}_{dd}(\tau)\right]\right) \tag{4.36}$$

depends on f, but does not directly depend on a.

The dimer-dimer threshold appears for $f = 1$, and there

$$\frac{a_{\phi\phi}}{a_{\psi\psi}} = 0.57, \tag{4.37}$$

which is close to the exact result, $a_{\phi\phi}/a_{\psi\psi} = 0.6$ [60].

4.10 Systems of fermions in vacuum: conclusions

Near the unitary limit, low-energy systems of spin-$\frac{1}{2}$ atoms display universal behaviour. The FRG flow in this chapter is consistent with the expected universality. In the scaling limit, we find one attractive fixed point for the flow of each parameter from the three- and four-atom sectors. Away from the scaling limit, where $|a|$ is large but finite, we find power law behaviour in a in the three- and four-atom parameters.

Finally, we extend the running-action ansatz to include some energy dependence. This dependence fixes the atom-atom threshold at its correct energy. Next, we calculate the atom-dimer and dimer-dimer scattering lengths.

We find an atom-dimer scattering length with an important deviation (of about 30%) from the exact value [69, 58, 61, 1]. Ref. [26] uses the FRG and finds an atom-dimer scattering length consistent with the exact value. The latter study incorporates an extra (unphysical) parameter that effectively changes the value of the FRG scale in the dimer regulator compared with the scale in the atom regulator. The variation with respect to this parameter estimates the error associated with the truncation. The atom-dimer scattering length in this chapter is within the errors found in Ref. [26]. Allowing for a more general momentum dependence in the propagators could reduce errors associated with unphysical changes in the regulators.

In the four-body sector, we find $a_{\phi\phi}/a_{\psi\psi} = 0.57$ for the ratio of the dimer-dimer to atom-atom scattering lengths, which is close to the exact value 0.6 [60]. Even though we find a result close to the exact value, we should further study the error in the truncation, which would be reflected in a dependence on the choice of regulators, R. Ref. [9] performs such analysis, and for some region of parameters the authors find small dependence ($\lesssim 8\%$) on unphysical parameters.

In summary, a simple and helpful extension to the work in this chapter would be to use a more general parametrisation of the regulators to monitor the regulator dependence of results in the physical limit.

Chapter 5

Fermion matter

[Calvin is outside, looking up at the stars.]
Calvin: I'M SIGNIFICANT!...screamed the dust speck.

Bill Watterson, *There's Treasure Everywhere*, page 30

5.1 Introduction

This chapter deals with systems of infinitely many spin-$\frac{1}{2}$ particles homogeneously distributed in space. We study systems with a finite density of particles. Individually these particles are the same as the atoms discussed in Chapter 4. However, dense-matter systems (or finite-density systems) have crucial differences compared with few-body systems. The two main differences are **a)** the presence of a Fermi surface for atoms, and **b)** the possibility of spontaneous symmetry breaking through a nonzero classical dimer field. The latter is a signal of superfluidity in the system.

The dynamics of finite-density systems of fermions is introduced in Section 1.1, and the discussion is expanded in Section 1.3 in the context of nuclear matter. This chapter studies fermions with two species, which we regard as spin-up and spin-down degrees of freedom. In contrast, nucleons have an extra degree of freedom, the isospin, and the nucleon-nucleon interaction has two different scattering lengths. Here, there is only one atom-atom scattering length. The work in this chapter does not describe symmetric nuclear matter. Instead, it describes a two-species Fermi gas near the unitary limit. This description can be applied to neutron matter or ultracold gases of atoms.

As discussed in Section 1.1, ultracold gases of atoms allow to tune the atom-atom interaction by external magnetic fields. This allows experimentalists to explore the thermodynamics of Fermi gases near the unitary limit [47, 54, 55, 51].

Fermi gases near the unitary limit can be studied with different approaches. These approaches include quantum Monte Carlo methods [16, 18, 19, 17, 15]; Luttinger-Ward variational many-body methods [46]; and Renormalisation Group methods,

which include the FRG [8, 24, 25, 32, 5, 33, 12, 13]. The latter reference uses regulators that suppress both momentum and energy modes. Ref. [23] provides a review to the FRG study of Fermi gases near the unitary limit.

5.2 Running action

5.2.1 Running-action ansatz

We use an ansatz (for the running action) that contains atom and dimer fields. It is an extension of the ansatz in Chapter 4, which describes few-atom systems. This extension incorporates a Fermi surface for atoms, and allows a nonzero classical dimer field. The ansatz we use for the running action is

$$\begin{aligned}\Gamma_k = \int \mathrm{d}^4x \Big\{ & Z_a \sum_{i=1,2} \Big(\psi_i^\dagger \Big(\mathrm{i}\,\partial_0 + \frac{\nabla^2}{2\,m} + \frac{p_F^2}{2\,m} \Big) \psi_i \Big) + Z_d\, \phi^\dagger \Big(\mathrm{i}\,\partial_0 + \frac{\nabla^2}{4\,m} \Big) \phi \\ & - g \left(\phi^\dagger\, \psi_1\, \psi_2 + \psi_2^\dagger\, \psi_1^\dagger\, \phi \right) - \lambda \sum_{i=1,2} \Big(\phi^\dagger\, \psi_i^\dagger\, \psi_i\, \phi \Big) - w \left(\phi^\dagger\, \psi_2^\dagger\, \psi_1^\dagger\, \psi_1\, \psi_2\, \phi \right) \\ & - \frac{v}{2} \left(\phi^\dagger\, \phi^\dagger\, \psi_1\, \psi_2\, \phi + \phi^\dagger\, \psi_2^\dagger\, \psi_1^\dagger\, \phi\, \phi \right) - U(\phi^\dagger, \phi) \Big\}, \end{aligned} \tag{5.1}$$

where all the fields are evaluated at the same space-time point, $x = (c\,t, \vec{x})$.

In previous approaches to study finite-density Fermi gases, the running-action ansätze do not incorporate all possible four-atom interaction terms [8, 33, 13]. In contrast, the ansatz in Eq. (5.1) incorporates these terms. This is the main difference between this ansatz and ansätze in previous approaches. In zero-density systems, including all the four-atom interaction terms helps find results that are independent of unphysical changes in the regulators [9]. A similar situation might occur in finite-density systems, where (including all) four-atom terms might play a role in the convergence of results.

5.2.2 Potential and its expansion

The term $U(\phi^\dagger, \phi)$ in Eq. (5.1) is a potential. It depends on ϕ and $\phi^\dagger$, but it is independent of the atom fields. The dependence on the dimer fields only appears through the combination $\phi^\dagger\phi$ because of a global $U(1)$ symmetry in the running action. The shape of U (for arbitrary $\phi^\dagger\phi$) can change with every value of k. Furthermore, the classical values of $\phi^\dagger$ and ϕ are determined by the minimum of U. This is where the possibility of spontaneous symmetry breaking arises: $U(\phi^\dagger\phi)$ can have degenerate minima while respecting the $U(1)$ symmetry. See for example the potential in Fig. 5.1.

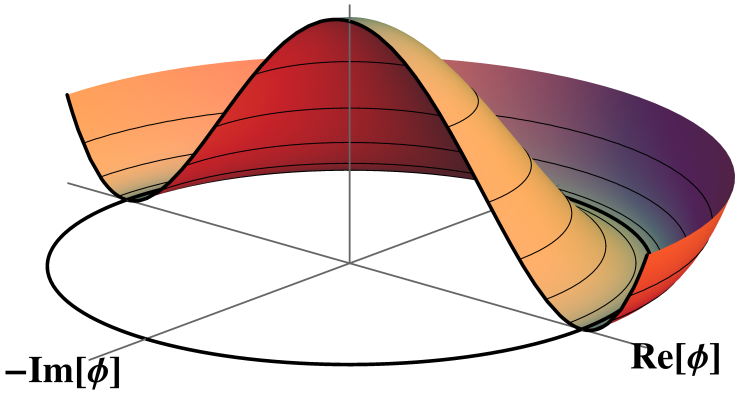

Figure 5.1: Potential with degenerate minima and a rotational symmetry around the z axis.

It might be possible to calculate the flow of Γ_k with a general form for U. This would involve solving partial differential equations in the variables k and $\rho = \phi^\dagger\phi$. To avoid this complication, we give an explicit form to U by expanding it around its minimum. This expansion has the form

$$U(\phi^\dagger\phi) = u_d(k)\left(\phi^\dagger\phi - \phi_0^2\right) + \frac{u_{dd}(k)}{2}\left(\phi^\dagger\phi - \phi_0^2\right)^2, \tag{5.2}$$

where we chose one particular minimum of U, the one that satisfies $\phi_{\text{clss}} = \phi^\dagger_{\text{clss}} = \phi_0$. If we chose any other minimum, then ϕ_0^2 in Eq. (5.2) should be replaced by $\phi^\dagger_{\text{clss}} \times \phi_{\text{clss}}$. This expansion does not allow to find the full form of the potential, but it allows to find the classical dimer field. It also allows to approximate the potential when the dimer fields are close to their classical value.

We set the running action such that at the UV, the classical value of the dimer is zero, $\phi_0 = 0$. In that case, the potential has the form

$$U(\phi^\dagger\phi) = u_d(k)\ \phi^\dagger\phi + \frac{u_{dd}(k)}{2}\left(\phi^\dagger\phi\right)^2, \tag{5.3}$$

and we follow the flow of $u_d(k)$ and $u_{dd}(k)$. At the UV, u_d is positive, but as k decreases, u_d crosses zero. After that point, the potential has degenerate minima with finite values for the classical dimer fields. At that point, we change the expansion in Eq. (5.3), so that U is expanded around ϕ_0. This leads to

$$U(\phi^\dagger\phi) = \frac{u_{dd}(k)}{2}\left(\phi^\dagger\phi - \phi_0^2\right)^2, \tag{5.4}$$

which has the same form as Eq. (5.2), but with $u_d(k) = 0$. Keeping u_d at zero implies

that

$$\left.\frac{\mathrm{d}U}{\mathrm{d}\phi}\right|_{\phi^\dagger,\phi=\phi_0} = 0, \tag{5.5}$$

which means that the potential has a minimum at $\phi = \phi^\dagger = \phi_0$. In the broken phase we treat ϕ_0 as a running function that tracks the minimum of U.[1]

5.2.3 Running functions and parameters in the flow

Running functions

This subsection discusses which parts of the running action are treated as running functions, and which ones are treated as independent parameters.

- The expansion for the potential (discussed in Subsection 5.2.2) yields **two** running functions. In the symmetric phase they are $u_d(k)$ and $u_{dd}(k)$. In the broken phase they are $\phi_0(k)$ and $u_{dd}(k)$.

- The running action in Eq. (5.1) contains **four** interaction terms: their corresponding couplings are running functions. These are $g(k)$, $\lambda(k)$, $w(k)$, and $v(k)$. These four interaction terms are analogous to the interaction terms in Chapter 4, which deals with systems in vacuum. The vertices of these interaction terms are displayed in Fig. 4.1.[2]

- The kinetic terms in the running action yield **three** more running functions. Two of them are the atom and dimer renormalisations, $Z_a(k)$ and $Z_d(k)$. The third one comes from the atom inverse-propagator, which contains a term $(p_F^2/2\,m)$. At the UV, $(p_F^2/2\,m)$ is equal to the atom chemical potential, μ. However, the flow generates a bilinear term in the atom inverse-propagator, and we keep track of this term by treating p_F as a running function. This does not mean that the chemical potential flows; μ is an external parameter. The flow of p_F keeps track of the Fermi surface as the FRG flows.

The flow of the running functions forms a system of coupled, ordinary, first-order differential equations. Both in the symmetric and in the broken phases, nine functions run simultaneously. These functions are summarised in Table 5.1.

[1] It is not mandatory to use ϕ_0 as a running function. An alternative approach would consist of calculating the evolution with a constant but nonzero ϕ_0. There, we could use the expansion of U with $u_d(k) \neq 0$ and $\phi_0 \neq 0$, displayed in Eq. (5.2). The condition that ϕ_0 is a minimum of the potential would be applied only at the physical limit, $u_d(k \to 0) \to 0$. This approach has the advantage that it eliminates the running of ϕ_0. The tradeoff is that the condition $u_d(k \to 0) \to 0$ is satisfied after the flow is calculated, which means that many different values of ϕ_0 need to be tried until the condition $u_d(k \to 0) \to 0$ is satisfied. However, as stated above, we use a different approach where ϕ_0 is a minimum of U for every value of k.

[2] The term $-u_{dd}(k)\,\phi^\dagger\phi^\dagger\,\phi\phi$ in the potential is also an interaction term, and its corresponding vertex also appears in Fig. 4.1.

one-atom sector	$p_{\scriptscriptstyle F}(k)$, $Z_a(k)$
two-atom sector	
symmetric phase	$g(k)$, $u_d(k)$, $Z_d(k)$
broken phase	$g(k)$, $\phi_0(k)$, $Z_d(k)$
three-atom sector	$\lambda(k)$
four-atom sector	$w(k)$, $v(k)$, $u_{dd}(k)$

Table 5.1: List of running functions in the running action for dense-matter.

The running action has a global $U(1)$ symmetry, which produces atom-number conservation. The flow also inherits this symmetry. However, unlike zero-density systems, the flow of n-atom parameters can depend on more-than-n-atom parameters. There are two features in the flow that allow this mixing. **a)** Both in the symmetric and broken phases, the Fermi surface for atoms allows the propagation of particle-hole states. This allows backward propagation (of fields) in Feynman diagrams. In consequence, there are diagrams for the flow of n-body functions, which depend on parameters from more-than-n-body sectors.[3] **b)** In the broken phase, diagrams can have insertions from the nonzero background field, the classical dimer. This produces diagrams for the flow of n-body parameters which contain more-than-n-body parameters.

Parameters in the flow

The flow receives physical information from two dimensionful parameters, the atom-atom scattering length, denoted as a, and the atom chemical potential, denoted as μ. The scattering length enters the flow through the initial conditions on $u_d(k)$—this is discussed below, in Section 5.3—and the chemical potential introduces a momentum scale through the initial value of $p_{\scriptscriptstyle F}$. The latter is $p_{\scriptscriptstyle F}(K_0) = \sqrt{2\,m\,\mu}$.

There are other dimensionful parameters in the flow, g at the UV (or $g_{\scriptscriptstyle UV}$), the atom mass (or m), and the UV momentum scale (or K_0). For each running function we can divide out certain powers of $g_{\scriptscriptstyle UV}$, m, and K_0. These powers are the same as in the vacuum case, and they are summarised in Table 5.2. If these powers are divided out of the running functions, then the flow can be expressed in terms of the dimensionless ratios k/K_0, a^{-1}/K_0, and $\sqrt{2\,m\,\mu}/K_0$, and it can be calculated independently of $g_{\scriptscriptstyle UV}$, m, and K_0.[4]

[3] The propagation of holes also gives nonzero flow to parameters that are frozen in zero-density systems, *e.g.* $g(k)$ and $Z_a(k)$. This is discussed in more detail below.

[4] The initial conditions from the rest of the running functions do not introduce more dimensionful parameters. This is discussed below, in Section 5.3.

one-atom sector	
$p_{F}(k)$	K_0
$Z_a(k)$	1

two-atom sector	
$g(k)$	g_{UV}
$u_d(k)$	$m\, g_{UV}^2\, K_0$
$Z_d(k)$	$m^2\, g_{UV}^2 / K_0$
$\phi_0(k)$	$K_0^2 / m\, g_{UV}$

three-atom sector	
$\lambda(k)$	$m\, g_{UV}^2 / K_0^2$

four-atom sector	
$w(k)$	$m\, g_{UV}^2 / K_0^5$
$v(k)$	$m^2\, g_{UV}^3 / K_0^4$
$u_{dd}(k)$	$m^3\, g_{UV}^4 / K_0^3$

Table 5.2: Powers of m, g_{UV}, and K_0 in the running functions.

5.2.4 Matrix of derivatives of the running action

Up to this point, this chapter has relied on fields represented in space-time coordinates. However, to use the FRG as it is formulated in Chapter 2, in consequence, the rest of this chapter uses quantities expressed in terms of momentum coordinates.

Symmetric phase

In the symmetric phase of dense-matter systems, the matrix $\big(\Gamma_k^{(2)} - \mathbf{R}\big)^{-1}_{\text{clss}}$ and the field propagators, $1/\Pi_{\psi,\psi^\dagger,\phi,\phi^\dagger}$, have the same form as in zero-density systems,[5] Eq. (2.41) and (2.42) respectively. The regulated energies in dense-matter, however, are different from those in zero-density. This is because, in dense-matter, the atom energy has a Fermi-surface term. The regulated energies in the symmetric phase are

$$E_a(q,k) = \frac{q^2}{2\,m} - \frac{p_F^2}{2\,m} + \frac{R_a(q,k,p_F)}{Z_a} \tag{5.6a}$$

$$E_d(q,k) = \frac{q^2}{4\,m} + \frac{R_d(q,k)}{Z_d} + \frac{u_d}{Z_d}, \tag{5.6b}$$

where the second term in $E_a(q,k)$ is the Fermi-surface term. When $q < p_F$ the atom energy is below the Fermi surface. There, this energy is negative because both $\big(\frac{q^2}{2\,m} - \frac{p_F^2}{2\,m}\big)$ and $R_a(q,k,p_F)$ are negative.[6] When $p_F < q$ the atom energy is above the Fermi surface and it is positive.

We obtain driving terms for each running function by taking functional derivatives on the flow equation.[7] Each driving term involves a four-momentum integration. The q^0 component of these integrals is performed using Cauchy's integral formula by

[5] The label clss denotes an object evaluated at the classical fields.
[6] The regulators are discussed below, in Subsection 5.2.5.
[7] This method is described in Chapter 2, Subsection 2.2.5.

looking at the poles in the propagators in each driving term.[8]

In finite-density systems, the poles in the q^0-integral (on the driving terms) depend on $\mathrm{sign}\big(E_a\big)$. The latter function distinguishes contributions above and below the Fermi surface. Contributions above the Fermi surface have a similar form to contributions in zero-density systems because the poles in the propagators are the same. However, contributions below the Fermi surface have different poles. The latter contributions give nonzero flow to objects that are frozen in zero-density systems, *e.g.* $Z_a(k)$ and $g(k)$.

Broken phase

Some of the entries in $\big(\Gamma_k^{(2)} - \mathbf{R}\big)_{\text{clss}}$ which are zero in the symmetric phase become finite in the broken phase. In consequence, in the broken phase the structure of the inverse matrix, $\big(\Gamma_k^{(2)} - \mathbf{R}\big)^{-1}_{\text{clss}}$, is more complicated than in the symmetric phase. The explicit form of these matrices appears in Appendix F.

Both in the symmetric and in the broken phases, we find the driving terms for the running functions by taking functional derivatives on both sides of the flow equation.[9] To evaluate these functional derivatives, we use the explicit form of $\big(\Gamma_k^{(2)} - \mathbf{R}\big)^{-1}_{\text{clss}}$. The form of this matrix (and the flow equations) changes between the symmetric and broken phases.

After the functional derivatives are evaluated, we find the driving terms for each running function. Each of these driving terms involves a four-momentum integral. In the broken phase the structure of the driving terms is more complicated than in the symmetric phase. In consequence, integrating the q^0 component of the driving terms is slightly more complicated in the broken phase. This is discussed in Appendix F.

In the broken phase, the atom and dimer energies have the form

$$E_{a,1} = \frac{q^2}{2\,m} - \frac{p_{\scriptscriptstyle F}^2}{2\,m} + \frac{\lambda\,\phi_0^2}{Z_a} + \frac{R_\psi(q,k)}{Z_a} \tag{5.7a}$$

$$E_{d,1} = \frac{q^2}{4\,m} + \frac{R_\phi(q,k)}{Z_d} + \frac{u_{dd}\,\phi_0^2}{Z_d}. \tag{5.7b}$$

These energies appear in the driving terms.

Throughout the flow, we use the running quantity $p_{\scriptscriptstyle F}(k)$ to track the Fermi surface. In the broken phase, the atom energy receives an extra contribution, $\lambda\,\phi_0^2/Z_a$. This creates an effective Fermi surface, with radius [33]

$$p_{\scriptscriptstyle F}^{\text{eff}} = \sqrt{p_{\scriptscriptstyle F}^2 - 2\,m\,\lambda\,\phi_0^2/Z_a}. \tag{5.8}$$

In the broken phase, the atom regulator is evaluated at $p_{\scriptscriptstyle F}^{\text{eff}}$ instead of $p_{\scriptscriptstyle F}$.

[8] This integration is described in Chapter 2, Subsection 2.2.6.

[9] This method is described in Chapter 2, Subsection 2.2.5.

A nonzero classical dimer field changes the atom spectrum with respect to the symmetric phase. This is because the matrix of inverse-propagators, $\big(\Gamma_k^{(2)} - \mathbf{R}\big)_{\text{clss}}$, has entries with

$$\left[\left(\frac{\delta}{\delta\psi_1}\big(\Gamma_k\big)\right)\frac{\overleftarrow{\delta}}{\delta\psi_2}\right]_{\text{clss}} = -g\,\phi_0 - \frac{v}{2}\,(\phi_0)^3, \tag{5.9}$$

and these entries create a gap in the atom spectrum. We define this gap as

$$\Delta = g\,\phi_0 + \frac{v}{2}\,(\phi_0)^3. \tag{5.10}$$

The ratio Δ/μ is a physical quantity for the unitary Fermi gas. This ratio can be calculated with different approaches. These include the FRG [5, 33, 13], quantum Monte Carlo methods [16, 18], and many-body variational methods [46].

Elements with

$$\left[\left(\frac{\delta}{\delta\phi}\big(\Gamma_k\big)\right)\frac{\overleftarrow{\delta}}{\delta\phi}\right]_{\text{clss}} = -u_{dd}\,\phi_0^2 \tag{5.11a}$$

in $\big(\Gamma_k^{(2)} - \mathbf{R}\big)_{\text{clss}}$ also produce a gap in the dimer propagator. However, as we discuss in Section 5.5, the dimer gap vanishes in the physical limit.

The q^0-integration of the driving terms produces denominators with

$$E_{a,2} = \sqrt{(E_{a,1})^2 + \left(\frac{\Delta}{Z_a}\right)^2} \tag{5.12a}$$

$$E_{d,2} = \sqrt{(E_{d,1})^2 - \left(\frac{u_{dd}\,\phi_0^2}{Z_d}\right)^2}, \tag{5.12b}$$

where the term $(\Delta/Z_a)^2$ in the square root in Eq. (5.12a) arises as a consequence of the atom gap. The term $-\left(u_{dd}\,\phi_0^2/Z_d\right)^2$ is a consequence of the dimer gap.

5.2.5 Regulators

The driving terms for the running functions involve a d^3q-integral.[10] In Chapters 3 and 4, for systems in vacuum, analogous integrations are performed analytically. However, in this chapter, the structure of the driving terms is more complicated, and the d^3q-integration is performed numerically. To do so, we use smooth regulators. These regulators depend on smoothed step functions, which depend on a parameter σ. This parameter controls the smoothness of the regulators. In the limit $\sigma \to 0$,

[10] The driving terms are spherically symmetric in $\vec{q}$, hence the d^3q-integral reduces to a one-dimensional integral.

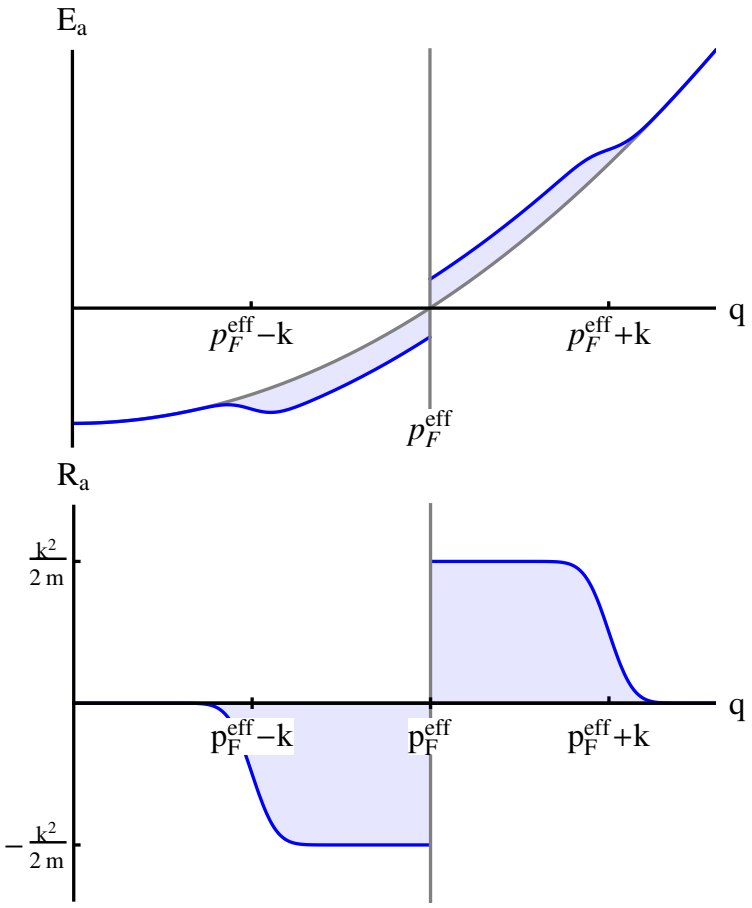

Figure 5.2: Regulated atom energy (upper plot) and atom regulator (lower plot). The horizontal axis is the module of three-momentum, $\|\vec{q}\| = q$, and the vertical grey line signals $q = p_F^{\text{eff}}$. In the upper plot the unregulated energy is the grey solid curve, and the regulated energy is the blue solid curve, which is discontinuous at $q = p_F^{\text{eff}}$.

the step functions become sharp, and the regulators become

$$\lim_{\sigma\to 0} R_a(q,k,p_F^{\text{eff}}) = \begin{cases} 0 & \text{for } q<0 \text{ and for } q < p_F^{\text{eff}} - k \\ -Z_a(k)\,\frac{k^2}{2m} & \text{for } \text{Max}\left(p_F^{\text{eff}}-k,0\right) < q < p_F^{\text{eff}} \\ +Z_a(k)\,\frac{k^2}{2m} & \text{for } p_F^{\text{eff}} < q < p_F^{\text{eff}} + k \\ 0 & \text{for } p_F^{\text{eff}} + k < q \end{cases} , \quad (5.13a)$$

and

$$\lim_{\sigma\to 0} R_d(q,k) = \begin{cases} +Z_d(k)\,\frac{k^2}{4m} & \text{for } 0<q<k \\ 0 & \text{for } k<q \end{cases} . \quad (5.13b)$$

The full form of the smooth regulators is displayed in Appendix G.

Dimers are scalar fields, and hence do not have a Fermi surface. Low-momentum

dimer fluctuations occur close to (but above) the zero of energy. The dimer regulator needs the same features as the regulators in few-particle systems: for $q \ll k$, the regulator is close to $Z_d \frac{k^2}{4m}$, and for $k \ll q$ it is zero.

Atoms propagate as fluctuations above the (effective) Fermi surface, and holes propagate below the (effective) Fermi surface.[11] Low-momentum fluctuations occur around the Fermi surface, not around the zero-energy states (these states are occupied). To suppress low-momentum fluctuations, the atom regulator needs to act above and below the Fermi surface. Above the Fermi surface, when q is close to p_F^{eff}, the regulator is close to $+\frac{k^2}{2m} Z_a$. When q is much larger than $p_F^{\text{eff}} + k$, the regulator is zero. Below the Fermi surface, when q is close to p_F^{eff}, the regulator is close to $-\frac{k^2}{2m} Z_a$. The atom regulated energy and the smooth atom regulator are displayed in Fig. 5.2.

5.3 Initial conditions on the flow

To calculate the flow, it is necessary to find initial conditions for the nine running functions in the symmetric phase. These functions are summarised in Table 5.1.[12]

At the UV, atoms are dynamical fields, and their renormalisation is fixed at $Z_a(K_0) = 1$. The atom energy, $p_F^2/2m$, is fixed at the atom chemical potential, $p_F^2(K_0)/2m = \mu$.

In zero-density systems the boundary condition

$$u_d(k \to 0) = -\frac{g^2\, m}{4\,\pi\, a}. \tag{5.14}$$

guarantees that the action yields the correct atom-atom scattering length.[13] We calculate the flow of $u_d(k)$ at zero density (analytically) and find the exact value of $u_d^{\text{vac}}(K_0)$ that satisfies this condition. Next, we use a modified version of the FRG flow equation to evolve from zero-density regulators to finite-density regulators. This evolution does not involve $\partial_k R$. Instead, it contains μ' derivatives at constant $k = K_0$, $\partial_{\mu'} R_a$. We calculate the flow in $\partial_{\mu'}\Gamma_{k=K_0}$ from $\mu' = 0$ to $\mu' = \mu$.[14] This yields a finite contribution

$$\Delta_{\mu'=0}^{\mu'=\mu} \left(u_d(K_0)\right), \tag{5.15}$$

[11] In the symmetric phase, the radius of the Fermi surface is given by $p_F(k)$, but in the broken phase, we use the effective radius of the Fermi surface, $p_F^{\text{eff}}(k)$, which is defined in Eq. (5.8).

[12] The flow begins in the symmetric phase.

[13] This is discussed in Subsection 2.2.3.

[14] The parameter μ' is not a physical quantity. It is just an auxiliary parameter that changes the chemical potential in the regulators. This change is only in the atom regulator, and not in the Fermi energy in the atom inverse propagator. If we try to evolve the Fermi energy with μ', the μ'-flow equation diverges.

which is proportional to $p_{_F}(K_0)$. This accounts for the change from zero-density to finite-density regulators. We use

$$u_d(K_0) = u_d^{\text{vac}}(K_0) + \Delta_{\mu'=0}^{\mu'=\mu}\left(u_d(K_0)\right) + 2\,\mu \tag{5.16}$$

as initial condition, where the last term is the dimer chemical potential at the UV.

The scaling limit of the FRG consists of the limit where k is the only dimensionful parameter in the flow. This happens when $k \sim K_0$ and both $\frac{a^{-1}}{K_0} \to 0$ and $\frac{\sqrt{2\,m\,\mu}}{K_0} \to 0$. In this limit, the running functions $Z_d(k)$, $\lambda(k)$, $w(k)$, $v(k)$, and $u_{dd}(k)$ behave as a negative power of k, times some constant. These constants are attractive fixed points of the flow in the scaling limit. For these running functions, the initial conditions are not relevant because the flow in the scaling limit takes the coupling to the attractive fixed point.[15]

Finally, the initial value of g, $g_{_{UV}}$, is a dimensionful parameter, but it can be divided out of all the running functions, see Table 5.2 in Subsection 5.2.3.

5.4 Flow

5.4.1 Two-body contact term

Subsection 2.2.2 discusses how an interaction term $-\mathfrak{g}\;\psi_2^\dagger\psi_1^\dagger\,\psi_1\,\psi_2$ is eliminated in favour of $-g\;\left(\phi^\dagger\,\psi_1\psi_2 + \psi_2^\dagger\psi_1^\dagger\,\phi\right)$. In zero-density systems, the former term is not regenerated by the flow. There, once $\mathfrak{g}$ is eliminated (at the UV) it remains at zero. In contrast, in finite-density systems, the flow gives nonzero driving terms for $\partial_k\mathfrak{g}$. Fig. 5.3 displays a diagram that contributes to the flow of $\mathfrak{g}$. In the symmetric phase, all the contributions to $\partial_k\mathfrak{g}$ come from diagrams with two holes, and we expect such contributions to be smaller than for g. In this work we neglect the regenerated coupling. However, it is possible to keep $\mathfrak{g}$ at zero throughout the flow with k-dependent rebosonisation techniques [33].[16]

5.4.2 Flow in the symmetric phase

Near the UV, a^{-1} and μ are neglectable, and the flow has a behaviour similar to the scaling limit. However, as k decreases the scales given by μ and a^{-1} become important, and the behaviour of the flow changes. We deal with systems near the unitary limit, and in consequence $\sqrt{2\,m\,\mu} > |a^{-1}|$, *i.e.* the finite-$\mu$ behaviour dominates the finite-a behaviour.

[15] Sections 4.5 and 4.7 in Chapter 4 discuss the flow in the scaling limit. There, we find one attractive fixed point for every running function.

[16] These techniques use extra constraints to keep $\mathfrak{g}$ at zero while including its contribution in the flow equations.

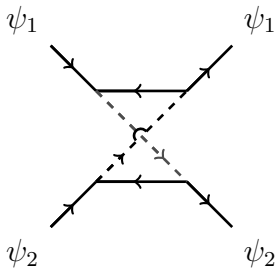

Figure 5.3: Diagram that contributes to the regeneration of $\mathfrak{g}$.

In this region, there is always one value of $k = k_{\mathrm{sb}}$, for which $u_d(k_{\mathrm{sb}}) = 0$. This scale is $k_{\mathrm{sb}} \sim \sqrt{2\,m\,\mu}$. At that point, the potential U has degenerate minima, which produce a finite classic dimer field.

5.4.3 Flow in the broken phase

In the broken phase, the driving terms of $p_{_F}(k)$ and $g(k)$ receive contributions proportional to $\partial_k\lambda$ and $\partial_k v$ respectively. These contributions arise from taking field derivatives of $\partial_k\Gamma_k$, which have the form

$$\left[\delta_{\psi_2}\delta_{\psi_1}\delta_{\phi^\dagger}\left(\partial_k\Gamma_k\right)\right]_{\mathrm{clss}} = -\partial_k g - (\phi_0)^2\,\partial_k v, \tag{5.17}$$

$$\left[\delta_{\psi_1}\delta_{\psi_1^\dagger}\left(\partial_k\Gamma_k\right)\right]_{\mathrm{clss}} = \frac{Z_a\,p_{_F}}{m}\,\partial_k p_{_F}(k) + \frac{p_{_F}^2}{2\,m}\,\partial_k Z_a - (\phi_0)^2\,\partial_k\lambda. \tag{5.18}$$

The respective terms are the last ones on the right-hand sides of Eq. (5.17) and (5.18). These terms would not appear if the interaction terms with dimer and atom fields where expanded around ϕ_0.[17] However, if all the interaction terms are expanded around ϕ_0, it would be necessary to introduce new running functions in the ansatz. For example, we would have to include a running function that accounts for the atom gap.

If the terms $-(\phi_0)^2\,\partial_k v$ and $-(\phi_0)^2\,\partial_k\lambda$ are included in the flow of $p_{_F}(k)$ and $g(k)$ (respectively), the latter functions do not converge in the physical limit. Therefore, we omitted these terms from the flow of $p_{_F}(k)$ and $g(k)$. This leads to running functions that converge in the physical limit, but further analysis is necessary to justify this choice.

[17] This expansion would be analogous to the broken-phase expansion in $U(\phi, \phi^\dagger)$. In the interaction terms, ϕ would be replaced by $(\phi - \phi_0)$ and $\phi^\dagger$ would be replaced by $(\phi^\dagger - \phi_0)$. For example, the interaction term $-\frac{v}{2}\left(\phi^\dagger\phi^\dagger\,\psi_1\psi_2\phi + \phi^\dagger\psi_2^\dagger\psi_1^\dagger\,\phi\phi\right)$ would become $-\frac{v}{2}\left((\phi^\dagger - \phi_0)^2\,\psi_1\,\psi_2\,(\phi - \phi_0) + (\phi^\dagger - \phi_0)\,\psi_2^\dagger\,\psi_1^\dagger\,(\phi - \phi_0)^2\right)$.

5.5 Results and physical limit

With the ingredients discussed above, we are able to integrate the flow equations for the running functions in the action. The q^0-integration in the driving terms is performed analytically, using Cauchy's integral theorem. The d^3q-integration in the driving terms is performed numerically.[18] The scale k is also integrated numerically. At every step in the k-integration a d^3q-integral is performed as well.

We calculated the flow of the running action both at the unitary limit, and near it. Two dimensionless ratios specify the flow, $\left(\sqrt{2\,m\,\mu}/K_0\right)$ and $\left(a^{-1}/K_0\right)$. In the results presented here, we use $\left(\sqrt{2\,m\,\mu}/K_0\right) = 10^{-3}$ and $-4\times10^{-5} \leq \left(a^{-1}/K_0\right) \leq +4\times10^{-5}$.

With these parameters, the physical limit of the flow gives finite values for $p_{\scriptscriptstyle F}$, Z_a, Z_d, ϕ_0, g, λ, and v. In contrast, the coupling w diverges as $\propto k^{-\alpha}$, where $\alpha \simeq 1.143$, and u_{dd} converges to zero with a behaviour $\propto k^{\alpha}$, with the same value of α. Since u_{dd} vanishes in the physical limit, the gap-like terms in the dimer propagator vanish as well.[19]

Fig. 5.4 displays the evolution of the radius of the Fermi sphere. It shows both $p_{\scriptscriptstyle F}(k)$ and the effective radius $p_{\scriptscriptstyle F}^{\mathrm{eff}}$ in the broken phase. We see that in the unitary limit,

$$\frac{p_{\scriptscriptstyle F}(k\to 0)}{p_{\scriptscriptstyle F}(K_0)} = 0.53 \qquad \text{and} \qquad \frac{p_{\scriptscriptstyle F}^{\mathrm{eff}}(k\to 0)}{p_{\scriptscriptstyle F}(K_0)} = 0.63. \tag{5.19}$$

For a fixed value of $\left(\sqrt{2\,m\,\mu}/K_0\right)$, the ratios in Eq. (5.19) depend on $\left(a^{-1}/K_0\right)$. However, these ratios do not depend on $\left(\sqrt{2\,m\,\mu}/K_0\right)$ and $\left(a^{-1}/K_0\right)$ separately. Instead they only depend on $a^{-1}/\sqrt{2\,m\,\mu}$.

The atom gap, $\Delta = g\,\phi_0 + v\,\phi_0^3/2$, is finite in the physical limit. In the unitary limit, we find $\Delta/\mu = 1.2$. This is consistent with quantum Monte Carlo and many-body variational approaches [16, 18, 46]. These studies find Δ/μ between 1.2 and 1.3. Fig. 5.5 shows the physical limit of Δ/μ as a function of $\left(a^{-1}/K_0\right)$ with a fixed atom chemical potential $\left(\sqrt{2\,m\,\mu}/K_0\right)$.

5.6 Conclusions

In the unitary limit we find $\Delta/\mu = 1.2$, which is close to results from quantum Monte Carlo simulations [16, 18] and many-body variational methods [46]. Previous FRG approaches [33, 13], which do not include the four-body interaction terms, find values of Δ/μ in the same range, but 15–30% smaller than quantum Monte Carlo results, which are expected to be more accurate. We conclude that the four-body interaction

[18] The d^3q-integration reduces to a one-dimensional integral.

[19] These terms arise from entries in $\left(\Gamma_k^{(2)} - \mathbf{R}\right)_{\mathrm{clss}}$ which correspond to pairs of fields (ϕ,ϕ) and $(\phi^\dagger,\phi^\dagger)$. These terms are discussed at the end of Subsection 5.2.4.

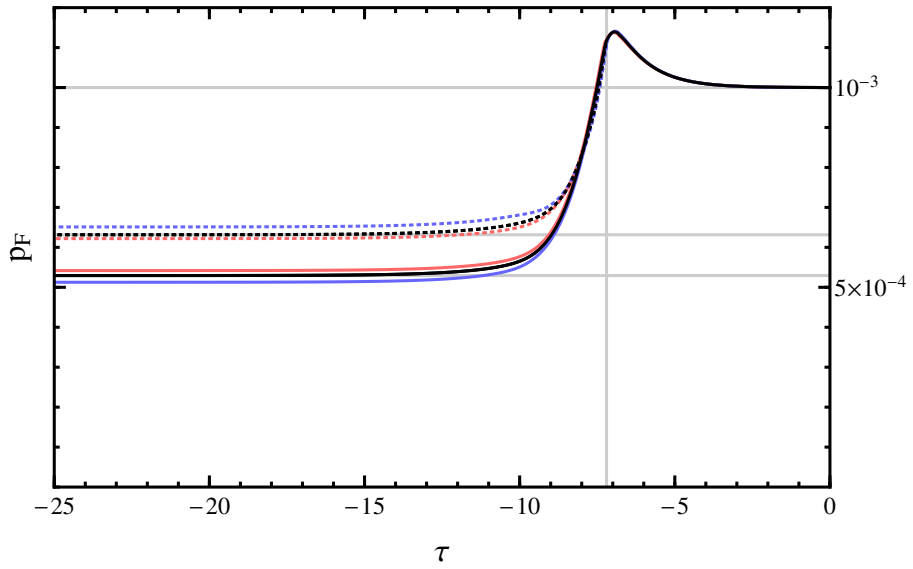

Figure 5.4: Flow of the radius of the Fermi sphere. The solid curves correspond to $p_{_F}(k)$ and the dotted curves correspond to $p_{_F}^{\text{eff}}$. The black curves corresponds to $a^{-1}/K_0 = 0$, the red curves to $a^{-1}/K_0 = -4 \times 10^{-5}$, and the blue curves to $a^{-1}/K_0 = -4 \times 10^{-5}$. The horizontal axis corresponds to $\tau = k/K_0$, and the vertical grey line signals the value of τ where the broken phase begins in the unitary limit.

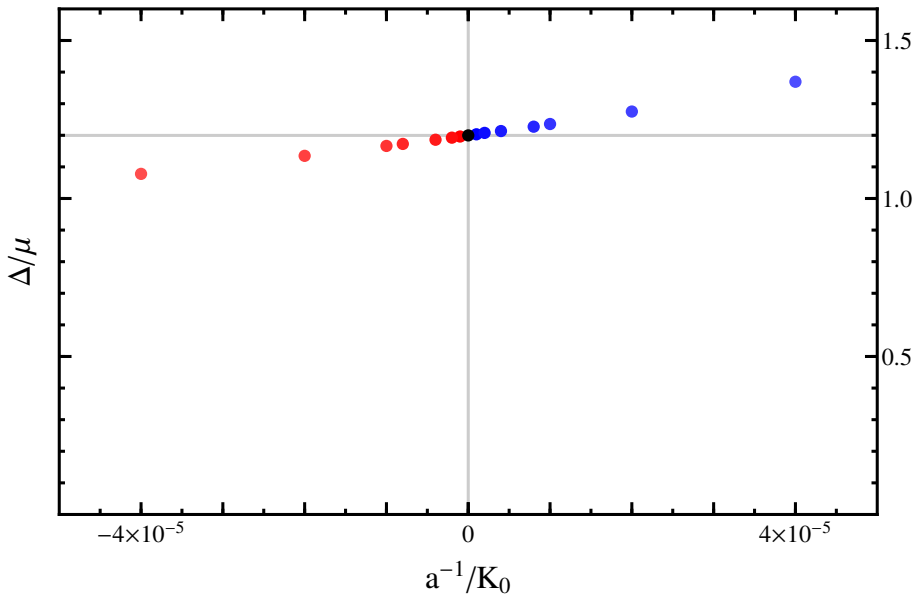

Figure 5.5: Δ/μ as a function of a^{-1}/K_0. The vertical grey line signals the unitary limit, where $a^{-1} = 0$, and the horizontal grey line signals $\Delta/\mu = 1.2$, which is the result in the unitary limit.

terms play a role in this ratio. Furthermore, the inclusion of the four-body terms gives an extra term to the atom gap, through the coupling v.

Despite the good agreement with other results, our analysis is incomplete in the sense that we have not studied the convergence of our results with respect to unphysical changes in the regulators. This analysis is necessary to have an estimate of the error in our truncation. Furthermore, we could also improve the present truncation by including the mean-field evolution of terms $u_n \left(\phi^\dagger \phi - \phi_0\right)^n$, where $n \geq 3$, in the potential.

Finally, it is also necessary to explore the elimination of the contribution $\propto \partial_k v$ in $\partial_k g$, and the contribution $\propto \partial_k \lambda$ in $\partial_k p_{_F}$.[20] We stress that if these terms are included the flow diverges. However, a better understanding of this choice is still necessary. This would likely require a consistent expansion all the interaction terms around ϕ_0.

[20] These terms are displayed in Eq. (5.17), and discussed in Subsection 5.4.3.

Chapter 6

Conclusions

This thesis discusses the FRG flow of three running-action ansätze. These ansätze describe diverse systems formed by particles with low energy. The particle-particle interaction is an essential ingredient to study these systems. We focused on particle-particle interactions that are very close to forming a two-particle bound state. This region is close to (and includes) the unitary limit. Systems in this region may display different forms of universal behaviour. Our framework emphasises universal behaviour because the particle-particle interaction is solely characterised by its scattering length.

This work covers some systems with zero density (systems in vacuum) and it also covers systems with finite density. In systems with finite density, we neglect the effect of thermal fluctuations: we work with zero-temperature systems. This regime is relevant for nuclear matter and for ultracold gases of atoms.

Scalar atoms in vacuum

Chapter 3 introduces a running-action ansatz for zero-density systems. It is devised to describe systems formed by three and four scalar atoms.[1] This running action contains three types of energy-dependent fields, atoms, dimers, and trimers. Dimer and trimer fields track some of the energy-dependence in two- and three-atom subsystems (respectively). Using energy-dependent trimers to study the FRG flow is an original contribution from this project [3]. Furthermore, as we discuss below, the energy dependence from three-atom subsystems has important effects in the flow of the four-atom sector.

[1] The word *atom* refers to the fundamental particles in our framework. This use of the word atom should not be confused with its normal use, which refers to physical atoms.

Scalar atoms in vacuum: three-atom sector

Three-particle systems where the two-particle interaction is close enough to the unitary limit may display Efimov effect [28, 29]. This effect can be studied with the FRG, and our description of the three-body system is consistent with previous works [34, 35, 67].

The FRG flow of the three-body sector shows Efimov-like behaviour when $k \gg 1/|a|$. Describing this flow requires the introduction of a dimensionful parameter which breaks universality. This parameter is associated with the Efimov parameter. However, the Efimov-like behaviour of the flow appears out of the physical limit, before the flow has converged. In the physical limit, when $k \ll 1/|a|$, the flow converges. There, parameters from the three-body sector depend on the Efimov parameter and on powers of a.

Scalar atoms in vacuum: four-atom sector

Near the unitary limit, four-atom systems seem to have two states (tetramers) in each Efimov cycle. Experimental studies on ultracold gases of atoms find evidence of these two tetramers [30, 31]. Quantum-mechanical approaches find two [62, 43, 71, 27, 21] or more [41, 42, 75] tetramers in each Efimov cycle. Furthermore, quantum-mechanical approaches [21, 41] find tetramer energies which are consistent with the tetramer energies extracted from experimental studies [30]. In this work we also find two tetramers with energies in agreement with Ref. [30, 21, 41]. This is discussed below.

Four-body systems may or may not need an extra dimensionful parameter to describe them. This parameter would be fixed by the detailed form of the interactions, and would be independent of the particle-particle scattering length and on the Efimov parameter. Some theoretical studies find independence of any four-body parameter [62, 43, 71, 27, 21], whereas other studies find some dependence on a four-body parameter [41, 42, 75]. The flow studied in this work does not reveal dependence on any four-body parameter.

In the scaling limit, the flow of the four-atom sector inherits the Efimov periodicity of the three-body sector. Each Efimov cycle has one atom-trimer threshold, and before each threshold we find a sequence of peaks in the four-atom couplings. These peaks appear periodically in a double logarithm of k. This is similar to the super Efimov effect found by Nishida *et al.* in two-dimensional systems [56].

In our four-body sector, the super Efimov behaviour arises from the channel structure of the four-atom couplings in the flow. This is discussed in Subsection 3.9.2. This behaviour however, occurs in a region where the flow cannot converge due to its Efimov periodicity.

If we include a finite scattering length, the behaviour of the flow changes, and the four-atom couplings converge. In the last Efimov cycle, only three peaks survive to the physical limit. We regard these three peaks as tetramer states. Two of these three tetramers have energy in agreement with Ref. [30, 21, 41]. Our third tetramer has a very shallow energy, and may be an artifact of our truncation. If it is a physical state, its detection might be difficult due to its shallow energy.

Even though the sequences of super Efimov states do not appear in the physical limit, they might still be relevant to the four-body spectrum. For example, for a large and positive scattering length, there is a sequence of four-body states right below the atom-atom-dimer threshold [22].

Schmidt and Moroz also studied four-body systems with the FRG [67]. However, they did not use energy-dependent trimers. They found one tetramer in each Efimov cycle, but these tetramers where latter found to be a numerical artifact.[2] We conclude that the energy dependence from trimer fields is essential to generate the super Efimov behaviour and the tetramer states in the physical limit.

Scalar atoms in vacuum: finite energy

In Section 3.11, we extended the running-action ansatz for scalar atoms. In the extension, there is a finite energy flowing through the Feynman diagrams. This finite energy allows us to explore the spectrum of three- and four-atom systems. This reveals a spectrum with some truncation defects, but that is in qualitative agreement with experimental [30, 31] and quantum-mechanical [43, 71, 27] studies.

Spin-$\frac{1}{2}$ atoms in vacuum

Chapter 4 introduces an action that describes systems of three and four atoms with spin-$\frac{1}{2}$. Unlike scalar atoms, spin-$\frac{1}{2}$ atoms cannot form Efimov states, and there is no Efimov parameter to break the universality in three-atom systems.

Spin-$\frac{1}{2}$ atoms in vacuum: universality

In the scaling limit, we find one attractive fixed point for each coupling in the three- and four-atom sectors. Away from the scaling limit, the behaviour of the flow changes. There, the couplings from the three- and four-atom sectors converge to powers of k and a. This is a sign of the expected universality in these systems.

[2] This was clarified with Schmidt and Moroz through private communications, and is also stated in Section IV of [10].

Spin-$\frac{1}{2}$ atoms in vacuum: atom-dimer and dimer-dimer scattering

In Section 4.9, we modified the running-action ansatz to include a finite energy flowing through the Feynman diagrams. This allows us to fix the dimer threshold at the correct energy in the dimer propagator.

Using this modified running action, we calculated the atom-dimer and dimer-dimer scattering lengths. For the atom-dimer scattering length, we find $a_{\psi\,\phi} = 1.56\, a_{\psi\,\psi}$, which has a significant deviation, $\sim 30\%$, from the exact value $a_{\psi\,\phi} = 1.2\, a_{\psi\,\psi}$ [69, 58, 61]. Ref. [26] uses the FRG to study atom-dimer scattering and finds significant dependence on the regulators. This dependence can be decreased if the momentum dependence in the regulators is improved. However, it is also necessary to extend the work in Chapter 4 to include parameters that monitor the regulator dependence on the effective action. For the dimer-dimer scattering length we find $a_{\phi\,\phi} = 0.57\, a_{\psi\,\psi}$, which is consistent with other FRG approaches [50, 9] and close to the exact result, $a_{\phi\,\phi} = 0.6\, a_{\psi\,\psi}$ [60]. However, it is also necessary to extend this work to study the dependence on unphysical changes on the regulators to estimate the errors associated with this truncation.

Fermions with finite density

Chapter 5 discusses the FRG flow for a running action that describes dense-matter systems. This running action incorporates all the four-body contact-interaction terms that can appear in the ansatz. This is the first finite-density FRG description of the unitary Fermi gas that incorporates these terms.

We calculated the evolution in the unitary limit, $a^{-1} = 0$, and near it. In the unitary limit, we find a gap to chemical potential ratio of $\Delta/\mu = 1.2$. This is close to results from quantum Monte Carlo simulations [16, 18], which yield $\Delta/\mu = 1.3$ and 1.2 respectively; variational many-body methods [46], which yield $\Delta/\mu = 1.3$.

The four-body terms play a role in this result. A similar FRG analysis which does not include all the four-body terms yields $\Delta/\mu = 0.90$ [33].[3]

Even though our result for Δ/μ is consistent with quantum Monte Carlo (and other) approaches, there are two immediate extensions to our work. **a)** We can include higher order terms for the expansion of the potential. These terms have the form $u_n\,(\phi^\dagger\,\phi - \phi_0^2)^n$, with $n \geq 3$. The running of u_n can be calculated in the mean-field approximation and substituted in the flow. **b)** We should analyse the convergence of our results with respect to unphysical changes in the regulators. This

[3] A simpler truncation of our running-action ansatz produces a similar ratio, $\Delta/\mu = 0.90$. This truncation has the minimum necessary ingredients to find superfluidity: it eliminates the three- and four-body terms, the running of the atom self-energy, and the running of g.

analysis is necessary to estimate the errors in our truncation, and it would give more solid results.

Appendix A

Auxiliary identities for the derivation of the flow equation

This appendix provides the derivation for one auxiliary identity used in the derivation of the FRG flow equation, in Subsection 2.1.3. This identity is associated with second-order field derivatives of $\Gamma_{\text{MOD}}[\mathbf{\Phi}^{\text{clss}}]$. It is

$$\langle \Phi_b(\mathbf{q}_2')\ \Phi_a(\mathbf{q}_1')\rangle = \mathfrak{i}\left(\left(\frac{\delta}{\delta\Phi_b^{\text{clss}}(\mathbf{q}_2')}\left(\Gamma_{\text{MOD}}\right)\right)\frac{\overleftarrow{\delta}}{\delta\Phi_a^{\text{clss}}(\mathbf{q}_1')}\right)^{-1} + \Phi_b^{\text{clss}}(\mathbf{q}_2')\ \Phi_a^{\text{clss}}(\mathbf{q}_1'), \quad \text{(A.1)}$$

where the operator $\frac{\overleftarrow{\delta}}{\delta f}$ denotes a functional derivative acting from the right.[1] Furthermore, $(\ \bullet\ )^{-1}$ is not used in the usual sense of inverse matrix, it is the inverse under a more general operation: sum over field indices and integration over the four-momenta variables.[2]

We use three steps to show that Eq. (A.1) holds. The first step consists of taking two field derivatives in W_{MOD}, one from the left and then one from the right. This yields

$$\left(\left(\frac{\delta}{\delta J_b(-\mathbf{q}_2')}\left(W_{\text{MOD}}\right)\right)\frac{\overleftarrow{\delta}}{\delta J_a(-\mathbf{q}_1')}\right)_{\mathbf{J}=0} = \mathfrak{i}\ \langle \Phi_b(\mathbf{q}_2')\ \Phi_a(\mathbf{q}_1')\rangle - \mathfrak{i}\ \Phi_b^{\text{clss}}(\mathbf{q}_2')\ \Phi_a^{\text{clss}}(\mathbf{q}_1'), \quad \text{(A.2)}$$

where this identity holds for the W-functional in any field theory, but in this case, we use the W_{MOD}.

The second step consists of showing

$$\left(\left(\frac{\delta}{\delta J_b(-\mathbf{q}_2')}\left(W_{\text{MOD}}\right)\right)\frac{\overleftarrow{\delta}}{\delta J_a(-\mathbf{q}_1')}\right) = -\left(\left(\frac{\delta}{\delta\Phi_b^{\text{clss}}(\mathbf{q}_2')}\left(\Gamma_{\text{MOD}}\right)\right)\frac{\overleftarrow{\delta}}{\delta\Phi_a^{\text{clss}}(\mathbf{q}_1')}\right)^{-1}. \quad \text{(A.3)}$$

[1] The distinction between derivatives acting from the left and from the right is necessary only when differentiating with respect to an anticommuting object, for example, a fermion field or the source of a fermion field.

[2] We may consider four-momentum as an extended type of index (a continuous index), and integration over four-momentum as an extended type of matrix multiplication.

To see that this equation is true, we use two more auxiliary identities,

$$\left(\frac{\delta}{\delta J_c(-\mathbf{q}_c)}\left(W_{\text{MOD}}\right)\right)\frac{\overleftarrow{\delta}}{\delta J_d(-\mathbf{q}_d)} = \left(\Phi_c^{\text{clss}}(\mathbf{q}_c)\right)\frac{\overleftarrow{\delta}}{\delta J_d(-\mathbf{q}_d)}, \tag{A.4a}$$

$$-\left(\frac{\delta}{\delta \Phi_d^{\text{clss}}(\mathbf{q}_d)}\left(\Gamma_{\text{MOD}}\right)\right)\frac{\overleftarrow{\delta}}{\delta \Phi_e^{\text{clss}}(\mathbf{q}_e)} = \left(J_d(-\mathbf{q}_d)\right)\frac{\overleftarrow{\delta}}{\delta \Phi_e^{\text{clss}}(\mathbf{q}_e)}. \tag{A.4b}$$

Combining the left-hand sides of these auxiliary identities yields

$$\begin{aligned}
&\sum_d \int_{\mathbf{q}_d} \left\{ \left(\left(\frac{\delta}{\delta J_c(-\mathbf{q}_c)}\left(W_{\text{MOD}}\right)\right)\frac{\overleftarrow{\delta}}{\delta J_d(-\mathbf{q}_d)} \right) \times \left(-\left(\frac{\delta}{\delta \Phi_d^{\text{clss}}(\mathbf{q}_d)}\left(\Gamma_{\text{MOD}}\right)\right)\frac{\overleftarrow{\delta}}{\delta \Phi_e^{\text{clss}}(\mathbf{q}_e)} \right) \right\} \\
&= \sum_d \int_{\mathbf{q}_d} \left\{ \left(\left(\Phi_c^{\text{clss}}(\mathbf{q}_c)\right)\frac{\overleftarrow{\delta}}{\delta J_d(-\mathbf{q}_d)} \right) \times \left(\left(J_d(-\mathbf{q}_d)\right)\frac{\overleftarrow{\delta}}{\delta \Phi_e^{\text{clss}}(\mathbf{q}_e)} \right) \right\} \\
&= \delta_{ce}\ (2\pi)^4\ \delta^4\left(\mathbf{q}_c - \mathbf{q}_e\right),
\end{aligned} \tag{A.5}$$

where the second step uses the auxiliary identities Eq. (A.4a) and (A.4b). This shows that Eq. (A.3) holds, and completes the second step.

The third step is combining Eq. (A.2) and (A.3). Finally, this yields Eq. (A.1), which is the auxiliary identity in question.

Appendix B

Two-atom systems for scalars

This appendix contains a running-action ansatz for systems with two scalar atoms. This action is analogous to the action for spin-$\frac{1}{2}$ atoms in Subsection 2.2.3.

The running action for scalar atoms is

$$\Gamma_k = \int \mathrm{d}^4x \left\{ \psi^\dagger(x) \left(\mathfrak{i}\,\partial_0 + \frac{\nabla^2}{2m} \right) \psi(x) + Z_d\ \phi^\dagger(x) \left(\mathfrak{i}\,\partial_0 + \frac{\nabla^2}{4m} - \frac{u_d}{Z_d} \right) \phi(x) \right. \\ \left. - \frac{g}{2} \left(\phi^\dagger(x)\ \psi(x)\,\psi(x) + \psi^\dagger(x)\,\psi^\dagger(x)\ \phi(x) \right) \right\}, \tag{B.1}$$

where all the fields are evaluated at the same space-time coordinate, x. The first and second terms in this ansatz are the atom and dimer kinetic terms (respectively), and the third term is the $\psi\,\psi \to \phi$ interaction.

The atom-atom scattering amplitude is

$$T_{\psi\psi}(p) = -\frac{4\pi}{\mu_{\psi\psi}} \left(\frac{1}{-\mathfrak{i}p - 1/a_{\psi\psi} + \ldots} \right) \to \frac{8\pi}{m} a_{\psi\psi}. \tag{B.2}$$

There is a difference in the factors of 4 and 8 compared with the case of spin-$\frac{1}{2}$ atoms [see Eq. (2.35)]. This is because for scalar atoms, atom-atom scattering is a process with identical particles, but for spin-$\frac{1}{2}$ atoms, it is not.

The amplitude for atom-atom scattering given by the running action is

$$T_{\psi\psi} = 4 \times \frac{(g/2)^2}{\Pi_\phi(k \to 0)} = \frac{g^2}{-u_d(k \to 0)}. \tag{B.3}$$

Matching Eq. (B.2) and Eq. (B.3) yields a restriction for u_d in the physical limit,

$$u_d(k \to 0) = -\frac{g^2\, m}{8\,\pi\, a_{\psi\psi}}. \tag{B.4}$$

Equations (2.47) and (2.58), give the driving terms for $u_d(k)$ for spin-$\frac{1}{2}$ atoms before and after $\mathbf{q}$-integration (respectively). For scalar atoms these driving terms

become

$$\partial_k u_d(k) = \int_{\mathbf{q}} \left(\frac{\mathrm{i}\, g^2\, \partial_k R_a}{2\, \Pi_{\psi^\dagger}^2\, \Pi_\psi} - \frac{\mathrm{i}\, g^2\, \partial_k R_a}{2\, \Pi_{\psi^\dagger}\, \Pi_\psi^2} \right), \tag{B.5}$$

$$\partial_k u_d(k) = \int \frac{\mathrm{d}^3 q}{(2\pi)^3} \left\{ \frac{g^2\ \partial_k R_a(q,k)}{4\, E_a^R(q,k)^2} \right\}, \tag{B.6}$$

respectively.

Appendix C

Cauchy's integral formula in q^0-integrals

This appendix contains the explicit formulas that are used to integrate $I_{a,b,c,d}$, in Eq. (2.55) in Subsection 2.2.6. This works for running actions where all the classical fields are zero.

The integration is performed in the case where s in Eq. (2.57) is $s = \mathrm{sgn}\big(E_a^R\big)$. The integration for few-atom systems and scalar atom systems, with $s = +1$, matches the integration with $\mathrm{sgn}\big(E_a^R\big) = +1$.

Integration on $\mathcal{C}_u$ and $\mathcal{C}_l$ should yield the same results (if the integrand is the same), therefore Eq. (C.1) is equal to Eq. (C.3), and Eq. (C.2) is equal to Eq. (C.4).

These expressions use the symbol θ_i, where $\theta_i = 0$ if $i = 0$, and $\theta_i = 1$ if $i = 1, 2, 3, \ldots$

Upper contour: above the Fermi surface

The integral in the upper contour, for $\mathrm{sgn}\big(E_a^R\big) > 0$,

$$
\begin{aligned}
I_{a,b,c,d} = \oint_{\mathcal{C}_u} \mathrm{d}q^0 \, \Bigg\{ & \frac{1}{\left(q^0 - \left(E_a^R - \mathfrak{i}\,\epsilon\right)\right)^a \left(q^0 - \left(-E_a^R + \mathfrak{i}\,\epsilon\right)\right)^b} \times \\
& \times \frac{1}{\left(q^0 - \left(E_d^R - \mathfrak{i}\,\epsilon\right)\right)^c \left(q^0 - \left(-E_d^R + \mathfrak{i}\,\epsilon\right)\right)^d} \Bigg\} \\
= \; & \frac{2\pi\mathfrak{i}\,\theta_b}{(b-1)!} \frac{\mathrm{d}^{b-1}}{(\mathrm{d}q^0)^{b-1}} \left(\frac{1}{\left(q^0 - E_a^R\right)^a \left(q^0 - E_d^R\right)^c \left(q^0 + E_d^R\right)^d} \right)_{q^0 = -E_a^R} \\
& + \frac{2\pi\mathfrak{i}\,\theta_d}{(d-1)!} \frac{\mathrm{d}^{d-1}}{(\mathrm{d}q^0)^{d-1}} \left(\frac{1}{\left(q^0 - E_a^R\right)^a \left(q^0 + E_a^R\right)^b \left(q^0 - E_d^R\right)^c} \right)_{q^0 = -E_d^R} . \qquad \text{(C.1)}
\end{aligned}
$$

Upper contour: below the Fermi surface

The integral on the upper contour, for $\mathrm{sgn}\big(E_a^R\big) < 0$,

$$\begin{aligned} I_{a,b,c,d} &= \oint_{\mathcal{C}_u} \mathrm{d}q^0 \left\{ \frac{1}{\left(q^0 - (E_a^R + \mathfrak{i}\,\epsilon)\right)^a \left(q^0 - (-E_a^R - \mathfrak{i}\,\epsilon)\right)^b} \times \right. \\ &\qquad \left. \times \frac{1}{\left(q^0 - (E_d^R - \mathfrak{i}\,\epsilon)\right)^c \left(q^0 - (-E_d^R + \mathfrak{i}\,\epsilon)\right)^d} \right\} \\ &= \frac{2\pi\mathfrak{i}\,\theta_a}{(a-1)!} \frac{\mathrm{d}^{a-1}}{(\mathrm{d}q^0)^{a-1}} \left(\frac{1}{\left(q^0 + E_a^R\right)^b \left(q^0 - E_d^R\right)^c \left(q^0 + E_d^R\right)^d} \right)_{q^0 = E_a^R} \\ &\quad + \frac{2\pi\mathfrak{i}\,\theta_d}{(d-1)!} \frac{\mathrm{d}^{d-1}}{(\mathrm{d}q^0)^{d-1}} \left(\frac{1}{\left(q^0 - E_a^R\right)^a \left(q^0 + E_a^R\right)^b \left(q^0 - E_d^R\right)^c} \right)_{q^0 = -E_d^R} . \end{aligned} \tag{C.2}$$

Lower contour: above the Fermi surface

The integral in the lower contour, for $\mathrm{sgn}\big(E_a^R\big) > 0$,

$$\begin{aligned} I_{a,b,c,d} &= -\oint_{\mathcal{C}_l} \mathrm{d}q^0 \left\{ \frac{1}{\left(q^0 - (E_a^R - \mathfrak{i}\,\epsilon)\right)^a \left(q^0 - (-E_a^R + \mathfrak{i}\,\epsilon)\right)^b} \times \right. \\ &\qquad \left. \times \frac{1}{\left(q^0 - (E_d^R - \mathfrak{i}\,\epsilon)\right)^c \left(q^0 - (-E_d^R + \mathfrak{i}\,\epsilon)\right)^d} \right\} \\ &= -\frac{2\pi\mathfrak{i}\,\theta_a}{(a-1)!} \frac{\mathrm{d}^{a-1}}{(\mathrm{d}q^0)^{a-1}} \left(\frac{1}{\left(q^0 + E_a^R\right)^b \left(q^0 - E_d^R\right)^c \left(q^0 + E_d^R\right)^d} \right)_{q^0 = E_a^R} \\ &\quad - \frac{2\pi\mathfrak{i}\,\theta_c}{(c-1)!} \frac{\mathrm{d}^{c-1}}{(\mathrm{d}q^0)^{c-1}} \left(\frac{1}{\left(q^0 - E_a^R\right)^a \left(q^0 + E_a^R\right)^b \left(q^0 + E_d^R\right)^d} \right)_{q^0 = E_d^R} . \end{aligned} \tag{C.3}$$

Lower contour: below the Fermi surface

The integral in the lower contour, for $\mathrm{sgn}\big(E_a^R\big) < 0$,

$$\begin{aligned} I_{a,b,c,d} &= -\oint_{\mathcal{C}_l} \mathrm{d}q^0 \left\{ \frac{1}{\left(q^0 - (E_a^R + \mathfrak{i}\,\epsilon)\right)^a \left(q^0 - (-E_a^R - \mathfrak{i}\,\epsilon)\right)^b} \times \right. \\ &\qquad \left. \times \frac{1}{\left(q^0 - (E_d^R - \mathfrak{i}\,\epsilon)\right)^c \left(q^0 - (-E_d^R + \mathfrak{i}\,\epsilon)\right)^d} \right\} \\ &= -\frac{2\pi\mathfrak{i}\,\theta_b}{(b-1)!} \frac{\mathrm{d}^{b-1}}{(\mathrm{d}q^0)^{b-1}} \left(\frac{1}{\left(q^0 - E_a^R\right)^a \left(q^0 - E_d^R\right)^c \left(q^0 + E_d^R\right)^d} \right)_{q^0 = -E_a^R} \\ &\quad - \frac{2\pi\mathfrak{i}\,\theta_c}{(c-1)!} \frac{\mathrm{d}^{c-1}}{(\mathrm{d}q^0)^{c-1}} \left(\frac{1}{\left(q^0 - E_a^R\right)^a \left(q^0 + E_a^R\right)^b \left(q^0 + E_d^R\right)^d} \right)_{q^0 = E_d^R} . \end{aligned} \tag{C.4}$$

Appendix D

Four-body flow equations for scalar atoms

The four-body sector in the running action discussed in Chapter 3 comprises three running couplings: $u_{dd}(k)$, $u_{dt}(k)$, and $u_{tt}dd(k)$. To write their flow equations we use the auxiliary object

$$T^{X}_{\alpha,\beta,\gamma,\delta} = \frac{\partial_k R_X \ (Z_d)^{-\beta-\gamma} \, (Z_t)^{-\delta}}{(E_a)^{\alpha} \, (E_d)^{\beta} \, (E_a + E_d)^{\gamma} \, (E_a + E_t)^{\delta}}, \tag{D.1}$$

where X can be a, d, or t which corresponds to atom, dimer or trimer regulators. The exponents α, β, γ, and δ are integer numbers.

The flow equations after the pole integration on q^0 are

$$\begin{aligned} \mathrm{d}_k u_{dd} = \int \frac{d^3q}{(2\,\pi)^3} \Big[& \frac{3\,g^4}{8} T^{a}_{4,0,0,0} + \frac{g^2 h^2}{2} \left(2\, T^{a}_{3,0,0,1} + T^{a}_{2,0,0,2} Z_t + T^{t}_{2,0,0,2} \right) + \frac{(u_{dd})^2}{2} \, \frac{T^{d}_{0,2,0,0}}{Z_d} \\ & - 2\, g\, h\, u_{dt} \left(T^{a}_{2,0,0,1} + T^{a}_{1,0,0,2} Z_t + T^{t}_{1,0,0,2} \right) \\ & + 2\, (u_{dt})^2 \left(T^{a}_{0,0,0,2} Z_t + T^{t}_{0,0,0,2} \right) \Big], \end{aligned} \tag{D.2a}$$

$$
\begin{aligned}
\mathrm{d}_k u_{dt} = \int \frac{d^3q}{(2\,\pi)^3}\Bigg[& -\frac{g^2 u_t\, u_{dt}}{2}\left(T^a_{2,0,1,1} + T^a_{1,0,2,1}Z_d + T^a_{1,0,1,2}Z_t + T^d_{1,0,2,1} + T^t_{1,0,1,2}\right) \\
& + \frac{g^3 h\, u_t}{4}\left(2\,T^a_{3,0,1,1} + T^a_{2,0,2,1}Z_d + T^a_{2,0,1,2}Z_t + T^d_{2,0,2,1} + T^t_{2,0,1,2}\right) \\
& + \frac{g\,h^3}{2}\left(T^a_{2,0,1,1} + T^a_{1,0,2,1}Z_d + T^a_{1,0,1,2}Z_t + T^d_{1,0,2,1} + T^t_{1,0,1,2}\right) \\
& - h^2 u_{dt}\left(T^a_{0,0,2,1}Z_d + T^a_{0,0,1,2}Z_t + T^d_{0,0,2,1} + T^t_{0,0,1,2}\right) \\
& - \frac{g^3 u_t\, u_{dd}}{4\,h}\left(T^a_{2,1,1,0} + T^a_{1,1,2,0}Z_d + T^d_{1,2,1,0} + T^d_{1,1,2,0}\right) + \frac{u_{dd}\, u_{dt}}{2}\,\frac{T^d_{0,2,0,0}}{Z_d} \\
& + u_{dt}\, u_{tt}\left(T^a_{0,0,0,2}Z_t + T^t_{0,0,0,2}\right) - \frac{g\,h\,u_{tt}}{2}\left(T^a_{2,0,0,1} + T^a_{1,0,0,2}Z_t + T^t_{1,0,0,2}\right) \\
& - \frac{g\,h\,u_{dd}}{2}\left(T^a_{0,1,2,0}Z_d + T^d_{0,2,1,0} + T^d_{0,1,2,0}\right) \\
& + \frac{g^4 u_t\, u_{dt}}{8\,h^2}\left(2\,T^a_{3,0,1,0} + T^a_{2,0,2,0}Z_d + T^d_{2,0,2,0}\right)\Bigg],
\end{aligned}
\tag{D.2b}
$$

$$
\begin{aligned}
\mathrm{d}_k u_{tt} = \int \frac{d^3q}{(2\,\pi)^3}\Bigg[& g^2h^2\left(T^a_{2,1,1,0} + T^a_{1,1,2,0}Z_d + T^d_{1,2,1,0} + T^d_{1,1,2,0}\right) \\
& + \frac{g^4\,(u_t)^2}{4}\left(2\,T^a_{3,0,2,1} + 2\,T^a_{2,0,3,1}Z_d + T^a_{2,0,2,2}Z_t + 2\,T^d_{2,0,3,1} + T^t_{2,0,2,2}\right) \\
& + g^2h^2u_t\left(T^a_{2,0,2,1} + 2\,T^a_{1,0,3,1}Z_d + T^a_{1,0,2,2}Z_t + 2\,T^d_{1,0,3,1} + T^t_{1,0,2,2}\right) \\
& - g^2 u_t\, u_{tt}\left(T^a_{1,0,1,2}Z_t + T^d_{1,0,2,1} + T^t_{1,0,1,2} + T^a_{2,0,1,1} + T^a_{1,0,2,1}Z_d\right) \\
& + (u_{dt})^2\,T^d_{0,2,0,0}\,(Z_d)^{-1} + (u_{tt})^2\left(T^a_{0,0,0,2}Z_t + T^t_{0,0,0,2}\right) \\
& - 2\,h^2u_{tt}\left(T^a_{0,0,2,1}Z_d + T^a_{0,0,1,2}Z_t + T^d_{0,0,2,1} + T^t_{0,0,1,2}\right) \\
& + \frac{g^6\,(u_t)^2}{4\,h^2}\left(3\,T^a_{4,1,1,0} + T^a_{3,1,2,0}Z_d + T^d_{3,2,1,0} + T^d_{3,1,2,0}\right) \\
& - \frac{g^3 u_t\, u_{dt}}{h}\left(T^a_{2,1,1,0} + T^a_{1,1,2,0}Z_d + T^d_{1,2,1,0} + T^d_{1,1,2,0}\right) \\
& + h^4\left(2\,T^a_{0,0,3,1}Z_d + T^a_{0,0,2,2}Z_t + 2\,T^d_{0,0,3,1} + T^t_{0,0,2,2}\right) \\
& + g^4\,u_t\left(2\,T^a_{3,1,1,0} + T^a_{2,1,2,0}Z_d + T^d_{2,2,1,0} + T^d_{2,1,2,0}\right) \\
& + \frac{g^4 u_t\, u_{tt}}{4\,h^2}\left(2\,T^a_{3,0,1,0} + T^a_{2,0,2,0}Z_d + T^d_{2,0,2,0}\right) \\
& - 2\,g\,h\,u_{dt}\left(T^a_{0,1,2,0}Z_d + T^d_{0,2,1,0} + T^d_{0,1,2,0}\right)\Bigg].
\end{aligned}
\tag{D.2c}
$$

D.1 Flow equations in the scaling limit

In the scaling limit, the four-body flow equations are

$$\begin{aligned}\partial_\tau \hat{u}_{dd} =& \frac{1}{\pi^2} + 3\,\hat{u}_{dd} + \frac{8\pi^2\,\hat{u}_{dd}^2}{15} + \frac{\hat{H}\,\partial_t\hat{Z}_t}{45\pi^2\,\hat{E}_{at}^2\,\hat{Z}_t^2} + \frac{2\,\hat{H}\,\hat{u}_t}{3\pi^2\,\hat{E}_{at}^2\hat{Z}_t^2} + \frac{1573\,\hat{H}}{1875\pi^2\,\hat{E}_{at}^2\,\hat{Z}_t} \\ &+ \frac{2\,\hat{H}}{3\pi^2\,\hat{E}_{at}\hat{Z}_t} - \frac{2\,\hat{U}_{dt}\,\partial_t\hat{Z}_t}{45\pi^2\,\hat{E}_{at}^2\,\hat{Z}_t^2} - \frac{2\,\hat{u}_t\,\hat{U}_{dt}}{3\pi^2\,\hat{E}_{at}^2\,\hat{Z}_t^2} - \frac{6938\,\hat{U}_{dt}}{5625\pi^2\,\hat{E}_{at}^2\,\hat{Z}_t} - \frac{2\,\hat{U}_{dt}}{3\pi^2\,\hat{E}_{at}\,\hat{Z}_t} \\ &+ \frac{\hat{U}_{dt}^2\,\partial_t\hat{Z}_t}{45\pi^2\,\hat{H}\,\hat{E}_{at}^2\,\hat{Z}_t^2} + \frac{2219\,\hat{U}_{dt}^2}{5625\pi^2\,\hat{H}\,\hat{E}_{at}^2\,\hat{Z}_t}, \end{aligned} \tag{D.3a}$$

$$\begin{aligned}\partial_\tau \hat{U}_{dt} =& -\frac{496\pi^2\,\hat{H}\,\hat{u}_{dd}}{375} - \frac{1096\pi^2\,\hat{u}_{dd}\,\hat{u}_t}{375} + \frac{2\,\hat{H}^2\,\partial_t\hat{Z}_t}{75\,\hat{E}_{at}^2\,\hat{Z}_t^2} + \frac{2\,\hat{H}\,\hat{u}_t\,\partial_t\hat{Z}_t}{75\,\hat{E}_{at}^2\,\hat{Z}_t^2} + \frac{18\,\hat{H}^2\,\hat{u}_t}{25\,\hat{E}_{at}^2\hat{Z}_t^2} \\ &+ \frac{28\,\hat{H}\,\hat{u}_t^2}{25\,\hat{E}_{at}^2\,\hat{Z}_t^2} + \frac{8938\,\hat{H}^2}{9375\,\hat{E}_{at}^2\,\hat{Z}_t} + \frac{11438\,\hat{H}\,\hat{u}_t}{9375\,\hat{E}_{at}^2\,\hat{Z}_t} + \frac{66\,\hat{H}^2}{125\,\hat{E}_{at}\,\hat{Z}_t} + \frac{116\,\hat{H}\,\hat{u}_t}{125\,\hat{E}_{at}\,\hat{Z}_t} \\ &- \frac{\hat{H}\,\hat{u}_{tt}\,\partial_t\hat{Z}_t}{90\pi^2\,\hat{E}_{at}^2\,\hat{Z}_t^2} - \frac{\hat{H}\,\hat{u}_t\,\hat{u}_{tt}}{6\pi^2\,\hat{E}_{at}^2\,\hat{Z}_t^2} - \frac{3469\,\hat{H}\,\hat{u}_{tt}}{11250\pi^2\,\hat{E}_{at}^2\,\hat{Z}_t} - \frac{\hat{H}\,\hat{u}_{tt}}{6\pi^2\,\hat{E}_{at}\,\hat{Z}_t} + 3\,\hat{U}_{dt} \\ &+ \frac{8\pi^2\,\hat{u}_{dd}\,\hat{U}_{dt}}{15} - \frac{2\,\hat{H}\,\hat{U}_{dt}\,\partial_t\hat{Z}_t}{75\,\hat{E}_{at}^2\,\hat{Z}_t^2} - \frac{2\,\hat{u}_t\,\hat{U}_{dt}\,\partial_t\hat{Z}_t}{75\,\hat{E}_{at}^2\,\hat{Z}_t^2} - \frac{8\,\hat{H}\,\hat{u}_t\,\hat{U}_{dt}}{25\,\hat{E}_{at}^2\,\hat{Z}_t^2} - \frac{18\,\hat{u}_t^2\,\hat{U}_{dt}}{25\,\hat{E}_{at}^2\,\hat{Z}_t^2} \\ &- \frac{2146\,\hat{H}\,\hat{U}_{dt}}{3125\,\hat{E}_{at}^2\,\hat{Z}_t} - \frac{8938\,\hat{u}_t\,\hat{U}_{dt}}{9375\,\hat{E}_{at}^2\,\hat{Z}_t} - \frac{16\,\hat{H}\,\hat{U}_{dt}}{125\,\hat{E}_{at}\,\hat{Z}_t} - \frac{66\,\hat{u}_t\,\hat{U}_{dt}}{125\,\hat{E}_{at}\,\hat{Z}_t} + \frac{\hat{u}_{tt}\,\hat{U}_{dt}\,\partial_t\hat{Z}_t}{90\pi^2\,\hat{E}_{at}^2\,\hat{Z}_t^2} \\ &+ \frac{2219\,\hat{u}_{tt}\,\hat{U}_{dt}}{11250\pi^2\,\hat{E}_{at}^2\,\hat{Z}_t}, \end{aligned} \tag{D.3b}$$

$$\begin{aligned}\partial_\tau \hat{u}_{tt} =& \frac{4384\pi^2\,\hat{H}}{375} + \frac{13568\pi^2\,\hat{u}_t}{375} + \frac{9184\pi^2\,\hat{u}_t^2}{375\,\hat{H}} + \frac{8\pi^2\,\hat{H}^2\,\partial_t\hat{Z}_t}{125\,\hat{E}_{at}^2\,\hat{Z}_t^2} + \frac{16\pi^2\,\hat{H}\,\hat{u}_t\,\partial_t\hat{Z}_t}{125\,\hat{E}_{at}^2\,\hat{Z}_t^2} \\ &+ \frac{192\pi^2\,\hat{H}^2\,\hat{u}_t}{125\,\hat{E}_{at}^2\,\hat{Z}_t^2} + \frac{8\pi^2\,\hat{u}_t^2\,\partial_t\hat{Z}_t}{125\,\hat{E}_{at}^2\hat{Z}_t^2} + \frac{624\pi^2\,\hat{H}\,\hat{u}_t^2}{125\,\hat{E}_{at}^2\,\hat{Z}_t^2} + \frac{432\pi^2\,\hat{u}_t^3}{125\,\hat{E}_{at}^2\,\hat{Z}_t^2} + \frac{33752\pi^2\,\hat{H}^2}{15625\,\hat{E}_{at}^2\,\hat{Z}_t} \\ &+ \frac{87504\pi^2\,\hat{H}\,\hat{u}_t}{15625\,\hat{E}_{at}^2\,\hat{Z}_t} + \frac{53752\pi^2\,\hat{u}_t^2}{15625\,\hat{E}_{at}^2\,\hat{Z}_t} + \frac{384\pi^2\,\hat{H}^2}{625\,\hat{E}_{at}\,\hat{Z}_t} + \frac{1968\pi^2\,\hat{H}\,\hat{u}_t}{625\,\hat{E}_{at}\,\hat{Z}_t} + \frac{1584\pi^2\,\hat{u}_t^2}{625\,\hat{E}_{at}\,\hat{Z}_t} \\ &+ \frac{406\,\hat{u}_{tt}}{125} + \frac{256\,\hat{u}_t\,\hat{u}_{tt}}{125\,\hat{H}} - \frac{4\,\hat{H}\,\hat{u}_{tt}\,\partial_t\hat{Z}_t}{75\,\hat{E}_{at}^2\,\hat{Z}_t^2} - \frac{4\,\hat{u}_t\,\hat{u}_{tt}\,\partial_t\hat{Z}_t}{75\,\hat{E}_{at}^2\,\hat{Z}_t^2} - \frac{16\,\hat{H}\,\hat{u}_t\,\hat{u}_{tt}}{25\,\hat{E}_{at}^2\,\hat{Z}_t^2} - \frac{36\,\hat{u}_t^2\,\hat{u}_{tt}}{25\,\hat{E}_{at}^2\,\hat{Z}_t^2} \\ &- \frac{4292\,\hat{H}\,\hat{u}_{tt}}{3125\,\hat{E}_{at}^2\,\hat{Z}_t} - \frac{17876\,\hat{u}_t\,\hat{u}_{tt}}{9375\,\hat{E}_{at}^2\,\hat{Z}_t} - \frac{32\,\hat{H}\,\hat{u}_{tt}}{125\,\hat{E}_{at}\,\hat{Z}_t} - \frac{132\,\hat{u}_t\,\hat{u}_{tt}}{125\,\hat{E}_{at}\,\hat{Z}_t} + \frac{\hat{u}_{tt}^2\,\partial_t\hat{Z}_t}{90\pi^2\,\hat{E}_{at}^2\,\hat{Z}_t^2} \\ &+ \frac{2219\,\hat{u}_{tt}^2}{11250\pi^2\hat{E}_{at}^2\,\hat{Z}_t} - \frac{1984\pi^2\,\hat{U}_{dt}}{375} - \frac{4384\pi^2\,\hat{u}_t\,\hat{U}_{dt}}{375\,\hat{H}} + \frac{16\pi^2\,\hat{U}_{dt}^2}{15\,\hat{H}}, \end{aligned} \tag{D.3c}$$

where $\hat{E}_{at}(k) = \frac{2}{3} + \frac{\hat{u}_t(k)}{\hat{Z}_t(k)}$ is the rescaled atom-trimer energy, defined in Eq. (3.30).

Appendix E

Four-body flow equations for fermionic atoms

The four-body sector in the running action discussed in Chapter 4 comprises the running couplings $w(k)$, $v(k)$, and $u_{dd}(k)$. After the pole integration on q^0, the flow equations for these couplings are

$$\begin{aligned}
\mathrm{d}_k w = \int \frac{\mathrm{d}^3 q}{(2\pi)^3} \Big\{ & g^3\, v \left(- F^{(d)}_{(0,2,2,3)} - 2\, F^{(d)}_{(1,1,2,3)} - F^{(a)}_{(2,0,2,2)} - 2\, F^{(a)}_{(1,1,2,2)} \right) + \frac{1}{4}\, v^2\, F^{(d)}_{(0,2,0,3)} \\
& + g^6 \left(\frac{1}{2}\, F^{(d)}_{(3,0,3,3)} + 3\, F^{(d)}_{(2,1,3,3)} + F^{(d)}_{(1,2,3,3)} + \frac{3}{4}\, F^{(a)}_{(4,-1,3,2)} + \frac{13}{4}\, F^{(a)}_{(3,0,3,2)} \right. \\
& \qquad \left. + 4\, F^{(a)}_{(2,1,3,2)} \right) + g^2\, w \left(2\, F^{(d)}_{(1,0,2,2)} + 2\, F^{(a)}_{(2,-1,2,1)} + 4\, F^{(a)}_{(1,0,2,1)} \right) \\
& + g^4\, \lambda \left(4\, F^{(d)}_{(0,2,3,3)} + F^{(d)}_{(2,0,3,3)} + 12\, F^{(d)}_{(1,1,3,3)} + F^{(a)}_{(3,-1,3,2)} + 6\, F^{(a)}_{(2,0,3,2)} \right. \\
& \qquad \left. + 12\, F^{(a)}_{(1,1,3,2)} \right) + \lambda^3 \left(- 4\, F^{(d)}_{(0,0,3,3)} - 4\, F^{(a)}_{0,0,3,2} \right) \\
& + g^2\, \lambda^2 \Big(12\, F^{(d)}_{(0,1,3,3)} - 2\, F^{(d)}_{(1,0,3,3)} + 4\, F^{(d)}_{(-1,2,3,3)} + 8\, F^{(a)}_{(0,1,3,2)} - F^{(a)}_{(2,-1,3,2)} \\
& \qquad - 3\, F^{(a)}_{(1,0,3,2)} \Big) + w\, \lambda \left(4\, F^{(d)}_{(0,0,2,2)} + 4\, F^{(a)}_{(0,0,2,1)} \right) \\
& + g\, v\, \lambda \left(- 4\, F^{(d)}_{(0,1,2,3)} - 2\, F^{(d)}_{(-1,2,2,3)} - 2\, F^{(a)}_{(0,1,2,2)} \right) \Big\}, \qquad \text{(E.1a)}
\end{aligned}$$

$$\begin{aligned}
\mathrm{d}_k v = \int \frac{\mathrm{d}^3 q}{(2\pi)^3} \Big\{ & g^2\, v \left(F^{(d)}_{(1,0,2,2)} + F^{(a)}_{(2,-1,2,1)} + 2\, F^{(a)}_{(1,0,2,1)} \right) + \frac{u_{dd}\, v}{2}\, F^{(d)}_{(0,2,0,3)} + g\, w\, F^{(a)}_{(2,0,0,0)} \\
& + g^3\, u_{dd} \left(- F^{(d)}_{(0,2,2,3)} - 2\, F^{(d)}_{(1,1,2,3)} - F^{(a)}_{2,0,2,2} - 2\, F^{(a)}_{(1,1,2,2)} \right) \\
& + g\, u_{dd}\, \lambda \left(- 4\, F^{(d)}_{(0,1,2,3)} - 2\, F^{(d)}_{-1,2,2,3} - 2\, F^{(a)}_{(0,1,2,2)} \right) + 2\, v\, \lambda\, F^{(d)}_{(0,0,2,2)} \\
& + g\, \lambda^2 \left(- 2\, F^{(d)}_{(1,0,2,2)} - 2\, F^{(a)}_{(2,-1,2,1)} - 4\, F^{(a)}_{(1,0,2,1)} \right) + 2\, v\, \lambda\, F^{(a)}_{0,0,2,1} \\
& + g^3\, \lambda \left(- F^{(d)}_{(2,0,2,2)} - 2\, F^{(a)}_{(3,-1,2,1)} - 3\, F^{(a)}_{(2,0,2,1)} \right) \Big\}, \qquad \text{(E.1b)}
\end{aligned}$$

$$\mathrm{d}_k u_{dd} = \int \frac{\mathrm{d}^3 q}{(2\pi)^3} \Big\{ -\frac{3}{4}\, g^4\, F^{(a)}_{(4,0,0,0)} + g\, v\, F^{(a)}_{(2,0,0,0)} + \frac{1}{2}\, (u_{dd})^2\, F^{(d)}_{(0,2,0,3)} - 2\, g^2\, \lambda\, F^{(a)}_{(3,0,0,0)} \Big\}. \tag{E.1c}$$

These flow equations use the auxiliary definition

$$F^{(X)}_{(\alpha,\beta,\gamma,\delta)} = \frac{\partial_k R_X}{E_a^\alpha\; E_d^\beta\; (E_{a+d})^\gamma\; Z_d^\delta}, \tag{E.2}$$

where symbol $X = a,\, d$ refers to atom or dimer fields.

Appendix F

Inverse interaction matrix in broken phase

F.1 Propagator matrix

Chapter 5 discusses the flow of a running action that describes finite-density systems of spin-$\frac{1}{2}$ atoms. In the broken phase, the matrix $\left(\Gamma_k^{(2)} - \mathbf{R}\right)_{\text{clss}}$ has the form

$$\left(\Gamma_k^{(2)} - \mathbf{R}\right)_{\text{clss}} = \begin{pmatrix} 0 & c_1 & \Pi_{\psi}^{(\text{br})} & 0 & 0 & 0 \\ -c_1 & 0 & 0 & \Pi_{\psi^\dagger}^{(\text{br})} & 0 & 0 \\ \Pi_{\psi^\dagger}^{(\text{br})} & 0 & 0 & -c_1 & 0 & 0 \\ 0 & \Pi_{\psi^\dagger}^{(\text{br})} & c_1 & 0 & 0 & 0 \\ 0 & 0 & 0 & 0 & c_2 & \Pi_{\phi}^{(\text{br})} \\ 0 & 0 & 0 & 0 & \Pi_{\phi^\dagger}^{(\text{br})} & c_2 \end{pmatrix}, \tag{F.1}$$

where the symbols $c_{1,2,3}$ are defined as

$$c_1 = g\,\phi_0 + \frac{1}{2} v\,\phi_0^3 \tag{F.2a}$$

$$c_2 = -u_{dd}\,\phi_0^2 \tag{F.2b}$$

$$c_3 = \lambda\,\phi_0^2, \tag{F.2c}$$

and the inverse propagators $\Pi_X^{(\text{br})}$ have the form

$$\Pi_{\psi}^{(\text{br})} = Z_a\ \left(q^0 - E_{a,1}\right) \tag{F.3a}$$

$$\Pi_{\psi^\dagger}^{(\text{br})} = Z_a\ \left(q^0 + E_{a,1}\right) \tag{F.3b}$$

$$\Pi_{\phi}^{(\text{br})} = Z_d\ \left(q^0 - E_{d,1}\right) \tag{F.3c}$$

$$\Pi_{\phi^\dagger}^{(\text{br})} = -Z_d\ \left(q^0 + E_{d,1}\right). \tag{F.3d}$$

The regulated energies in the inverse propagators, $\Pi_X^{(\mathrm{br})}$, are

$$E_{a,1} = \frac{q^2}{2\,m} - \frac{p_F^2}{2\,m} + \frac{\lambda\,\phi_0^2}{Z_a} + \frac{R_\psi(q,k)}{Z_a} \tag{F.4a}$$

$$E_{d,1} = \frac{q^2}{4\,m} + \frac{R_\phi(q,k)}{Z_d} + \frac{u_{dd}\,\phi_0^2}{Z_d}. \tag{F.4b}$$

The inverse matrix of $\left(\Gamma_k^{(2)} - \mathbf{R}\right)_{\mathrm{clss}}$ has the form

$$\left(\Gamma_k^{(2)} - \mathbf{R}\right)^{-1}_{\mathrm{clss}} = \begin{pmatrix} 0 & -i_A[c_1] & i_A[\psi^\dagger] & 0 & 0 & 0 \\ i_A[c_1] & 0 & 0 & i_A[\psi^\dagger] & 0 & 0 \\ i_A[\psi] & 0 & 0 & i_A[c_1] & 0 & 0 \\ 0 & i_A[\psi] & -i_A[c_1] & 0 & 0 & 0 \\ 0 & 0 & 0 & 0 & i_A[c_2] & i_A[\phi^\dagger] \\ 0 & 0 & 0 & 0 & i_A[\phi] & i_A[c_2] \end{pmatrix} \tag{F.5}$$

where the symbols i_A are

$$i_A[\psi] = \frac{\Pi_{\psi^\dagger}^{(\mathrm{br})}}{-c_1^2 + \Pi_{\psi^\dagger}^{(\mathrm{br})}\,\Pi_{\psi}^{(\mathrm{br})}} \tag{F.6a}$$

$$i_A[\psi^\dagger] = \frac{\Pi_{\psi}^{(\mathrm{br})}}{-c_1^2 + \Pi_{\psi^\dagger}^{(\mathrm{br})}\,\Pi_{\psi}^{(\mathrm{br})}} \tag{F.6b}$$

$$i_A[\phi] = \frac{\Pi_{\phi^\dagger}^{(\mathrm{br})}}{-c_2^2 + \Pi_{\phi^\dagger}^{(\mathrm{br})}\,\Pi_{\phi}^{(\mathrm{br})}} \tag{F.6c}$$

$$i_A[\phi^\dagger] = \frac{\Pi_{\phi}^{(\mathrm{br})}}{-c_2^2 + \Pi_{\phi^\dagger}^{(\mathrm{br})}\,\Pi_{\phi}^{(\mathrm{br})}} \tag{F.6d}$$

$$i_A[c_1] = \frac{c_1}{c_1^2 - \Pi_{\psi^\dagger}^{(\mathrm{br})}\,\Pi_{\psi}^{(\mathrm{br})}} \tag{F.6e}$$

$$i_A[c_2] = \frac{c_2}{c_2^2 - \Pi_{\phi^\dagger}^{(\mathrm{br})}\,\Pi_{\phi}^{(\mathrm{br})}}. \tag{F.6f}$$

In the broken phase, the objects i_A are the nonzero entries in the matrix $\left(\Gamma_k^{(2)} - \mathbf{R}\right)^{-1}_{\mathrm{clss}}$. In consequence, these objects appear in the driving terms for the running functions in Chapter 5. These driving terms are integrated over q^0 using Cauchy's integral theorem. This requires to look at the poles in i_A. To do so, we rewrite these objects

as

$$i_A[\psi] = \frac{\big(q^0 + E_{a,1}\big)}{Z_a\,\big(q^0 + E_{a,2}\big)\big(q^0 - E_{a,2}\big)} \tag{F.7a}$$

$$i_A[\psi^\dagger] = \frac{\big(q^0 - E_{a,1}\big)}{Z_a\,\big(q^0 + E_{a,2}\big)\big(q^0 - E_{a,2}\big)} \tag{F.7b}$$

$$i_A[\phi] = \frac{\big(q^0 + E_{d,1}\big)}{Z_d\,\big(q^0 + E_{d,2}\big)\big(q^0 - E_{d,2}\big)} \tag{F.7c}$$

$$i_A[\phi^\dagger] = \frac{-\big(q^0 - E_{d,1}\big)}{Z_d\,\big(q^0 + E_{d,2}\big)\big(q^0 - E_{d,2}\big)} \tag{F.7d}$$

$$i_A[c_1] = \frac{-c_1}{(Z_a)^2\,\big(q^0 + E_{a,2}\big)\big(q^0 - E_{a,2}\big)} \tag{F.7e}$$

$$i_A[c_2] = \frac{c_2}{(Z_d)^2\,\big(q^0 + E_{d,2}\big)\big(q^0 - E_{d,2}\big)}, \tag{F.7f}$$

where

$$E_{a,2} = \sqrt{(E_{a,1})^2 + (c_1/Z_a)^2} \tag{F.8a}$$

$$E_{d,2} = \sqrt{(E_{d,1})^2 - (c_2/Z_d)^2}. \tag{F.8b}$$

F.2 Driving terms

Throughout this work we use the method in Subsection 2.2.5 to find the driving terms for the running functions. In the broken phase, this method yields driving terms that contain the objects i_A. For any running function, say $c(k)$, the driving terms have the form

$$\frac{\mathrm{d}c}{\mathrm{d}k}(k) = \sum_i \int_{\mathbf{q}} \Big\{ f_i(k)\ \big(i_A[\psi]\big)^{\alpha_i}\ \big(i_A[\psi^\dagger]\big)^{\beta_i}\ \big(i_A[\phi]\big)^{\gamma_i}\ \big(i_A[\phi^\dagger]\big)^{\delta_i}\ \big(i_A[c_1]\big)^{\epsilon_i}\ \big(i_A[c_2]\big)^{\zeta_i} \Big\}, \tag{F.9}$$

where the exponents α_i, β_i, γ_i, δ_i, ϵ_i, ζ_i are positive integers, and the function $f_i(k)$ is independent of q^0. The latter is the product of powers of the running functions times $\partial_k R$. The symbols i_A are defined above.

We use Cauchy's integral theorem to integrate the q^0 component in the driving terms, Eq. (F.9). This requires shifting the poles in q^0-complex plane according to the prescription

$$E_{a,1} \to E_{a,1} - \mathrm{i}\,\varepsilon \times \mathrm{sign}\big(q - p_F^{\mathrm{eff}}\big) \tag{F.10a}$$

$$E_{d,1} \to E_{d,1} - \mathrm{i}\,\varepsilon, \tag{F.10b}$$

where $\mathrm{sign}\big(q - p_F^{\mathrm{eff}}\big)$ chooses whether we are below or above the Fermi sphere, and p_F^{eff} is the effective radius of the Fermi sphere [defined in Eq. (5.8)]. Furthermore, ε is a small and positive number. After the q^0-integration we take the limit $\varepsilon \to 0^+$ in the driving terms.

The shift in $E_{a,1}$ and $E_{d,1}$, in Eq. (F.10), produces a shift

$$E_{a,2} \to E_{a,2} - \mathrm{i}\,\varepsilon' \tag{F.11a}$$

$$E_{a,2} \to E_{a,2} - \mathrm{i}\,\varepsilon' \times \mathrm{sign}\big(E_{d,1}\big), \tag{F.11b}$$

where ε' is another small and positive number, and we take the limit $\varepsilon' \to 0^+$ after the q^0-integration is performed. The function $\mathrm{sign}\big(E_{d,1}\big)$, remains positive throughout the flow. This function would become negative if $u_{dd}(k) < 0$, but this would mean that the potential is unbound from below, and the classic dimer field would diverge.

The q^0-integral in the driving terms in Eq. (F.9) can be performed by substituting i_A in Eq. (F.7) and using the shifts it Eq. (F.11). With these substitutions we can identify the poles in the driving terms and use Cauchy's integral theorem.

Appendix G

Smooth regulators

The regulators of dense-matter systems used in Chapter 5 are

$$R_a(q,k,p_F^{\text{eff}}) = \begin{cases} Z_a(k)\,\frac{k^2}{2\,m}\,\theta^{(a,-)}(q,k,p_F^{\text{eff}}) & \text{for } 0 < q < p_F^{\text{eff}} \\ Z_a(k)\,\frac{k^2}{2\,m}\,\theta^{(a,+)}(q,k,p_F^{\text{eff}}) & \text{for } p_F^{\text{eff}} < q \end{cases}, \tag{G.1a}$$

and

$$R_d(q,k) = Z_d(k)\,\frac{k^2}{4\,m}\,\theta^{(d)}(q,k), \tag{G.1b}$$

where the functions $\theta^{(a,+)}(q,k,p_F^{\text{eff}})$, $\theta^{(a,-)}(q,k,p_F^{\text{eff}})$, and $\theta^{(d)}(q,k)$ are smoothed step functions. Their explicit form is

$$\theta^{(a,+,\sigma)}(q,k,p_F^{\text{eff}}) = \frac{1}{2\,\text{Erf}\,(1/\sigma)}\left(\text{Erf}\left(\frac{\left(k+p_F^{\text{eff}}\right)+q}{\left(k+p_F^{\text{eff}}\right)\,\sigma}\right)+\text{Erf}\left(\frac{\left(k+p_F^{\text{eff}}\right)-q}{\left(k+p_F^{\text{eff}}\right)\,\sigma}\right)\right), \tag{G.2a}$$

$$\theta^{(a,-,\sigma)}(q,k,p_F^{\text{eff}}) = -\frac{1}{2\,\text{Erf}\,(1/\sigma)}\left(\text{Erf}\left(\frac{\left(k+p_F^{\text{eff}}\right)+\left(2p_F^{\text{eff}}-q\right)}{\left(k+p_F^{\text{eff}}\right)\,\sigma}\right) + \text{Erf}\left(\frac{\left(k+p_F^{\text{eff}}\right)-\left(2p_F^{\text{eff}}-q\right)}{\left(k+p_F^{\text{eff}}\right)\,\sigma}\right)\right), \tag{G.2b}$$

and

$$\theta_{(d,\sigma)}(q,k) = \frac{1}{2\,\text{Erf}\,(1/\sigma)}\left(\text{Erf}\left(\frac{k+q}{k\,\sigma}\right)+\text{Erf}\left(\frac{k-q}{k\,\sigma}\right)\right). \tag{G.3}$$

The step functions depend on the error function, $\text{Erf}(z)$, defined as

$$\text{Erf}(z) = \frac{2}{\sqrt{\pi}}\int_0^z \text{e}^{-t^2}\,\text{d}t. \tag{G.4}$$

Bibliography

[1] F. Alzetto, R. Combescot, and X. Leyronas. Atom-dimer scattering length for fermions with different masses: Analytical study of limiting cases. *Phys. Rev.*, A 82:062706, 2010. DOI: 10.1103/PhysRevA.82.062706.

[2] R. D. Amado and F. C. Greenwood. There is no Efimov effect for four or more particles. *Phys. Rev.*, D 7:2517, 1973. DOI: 10.1103/PhysRevD.7.2517.

[3] B. Jaramillo Ávila and M. C. Birse. Universal behavior of four-boson systems from a functional-renormalization-group analysis. *Phys. Rev.*, A 88:043613, 2013. DOI: 10.1103/PhysRevA.88.043613.

[4] C. Bagnuls and C. Bervillier. Exact renormalization group equations: an introductory review. *Phys. Rept.*, 348:91, 2001. DOI: 10.1016/S0370-1573(00)00137-X.

[5] L. Bartosch, P. Kopietz, and A. Ferraz. Renormalization of the BCS-BEC crossover by order-parameter fluctuations. *Phys. Rev.*, B 80:104514, 2009. DOI: 10.1103/PhysRevB.80.104514 e-print arXiv:0907.2687 [cond-mat.quant-gas].

[6] P. F. Bedaque and U. van Kolck. Effective field theory for few-nucleon systems. *Annu. Rev. Nucl. Part. Sci.*, 52:339, 2002. DOI: 10.1146/annurev.nucl.52.050102.090637.

[7] J. Berges, N. Tetradis, and C. Wetterich. Non-perturbative renormalization flow in quantum field theory and statistical physics. *Phys. Rept.*, 363:223, 2002. DOI: 10.1016/S0370-1573(01)00098-9.

[8] M. C. Birse, B. Krippa, J. A. McGovern, and N. R. Walet. Pairing in many-fermion systems: an exact renormalisation group treatment. *Phys. Lett.*, B 605:287, 2005. DOI: 10.1016/j.physletb.2004.11.044.

[9] M. C. Birse, B. Krippa, and N. R. Walet. Convergence of a renormalization-group approach to dimer-dimer scatterings. *Phys. Rev.*, A 83:023621, 2011. DOI: 10.1103/PhysRevA.83.023621.

[10] M. C. Birse, B. Krippa, and N. R. Walet. Functional renormalisation group for few-nucleon sytems: $SU(4)$ symmetry and its breaking. *Phys. Rev.*, C 87:054001, 2013. DOI: 10.1103/PhysRevC.87.054001.

[11] M. C. Birse, J. A. McGovern, and K. G. Richardson. A renormalisation-group treatment of two-body scattering. *Phys. Lett.*, B 464:169, 1999. DOI: 10.1016/S0370-2693(99)00991-0.

[12] I. Boettcher, S. Diehl, J. M. Pawlowski, and C. Wetterich. Tan contact and universal high momentum behavior of the fermion propagator in the BCS-BEC crossover. *Phys. Rev.*, A 87:023606, 2013. DOI: 10.1103/PhysRevA.87.023606.

[13] I. Boettcher, J. M. Pawlowski, and C. Wetterich. Critical temperature and superfluid gap of the unitary Fermi gas from functional renormalization. *Phys. Rev.*, A 89:053630, 2014. DOI: 10.1103/PhysRevA.89.053630.

[14] E. Braaten and H. W. Hammer. Universality in few-body systems with large scattering length. *Phys. Rept.*, 428:259, 2006. DOI: 10.1016/j.physrep.2006.03.001.

[15] A. Bulgac, J. E. Drut, and P. Magierski. Quantum Monte Carlo simulations of the BCS-BEC crossover at finite temperature. *Phys. Rev.*, A 78:023625, 2008. DOI: 10.1103/PhysRevA.78.023625 e-print arXiv:0803.3238 [cond-mat.stat-mech].

[16] J. Carlson, S.-Y. Chang, V. R. Pandharipande, and K. E. Schmidt. Superfluid Fermi gases with large scattering length. *Phys. Rev. Lett.*, 91:050401, 2003. DOI: 10.1103/PhysRevLett.91.050401 e-print arXiv:physics/0303094 [physics.atom-ph].

[17] J. Carlson, S. Gandolfi, K. E. Schmidt, and S. Zhang. Auxiliary-field quantum Monte Carlo method for strongly paired fermions. *Phys. Rev.*, A 84:061602, 2011. DOI: 10.1103/PhysRevA.84.061602 e-print arXiv:1107.5848 [cond-mat.quant-gas].

[18] J. Carlson and S. Reddy. Asymmetric two-component fermion systems in strong coupling. *Phys. Rev. Lett.*, 95:060401, 2005. DOI: 10.1103/PhysRevLett.95.060401 e-print arXiv:cond-mat/0503256 [cond-mat.other].

[19] J. Carlson and S. Reddy. Superfluid pairing gap in strong coupling. *Phys. Rev. Lett.*, 100:150403, 2008. DOI: 10.1103/PhysRevLett.100.150403 e-print arXiv:0711.0414 [cond-mat.str-el].

[20] C. Chin, R. Grimm, P. Julienne, and E. Tiesinga. Feshbach resonances in ultracold gases. *Rev. Mod. Phys.*, 82:1225, 2010. DOI: 10.1103/RevModPhys.82.1225.

[21] A. Deltuva. Efimov physics in bosonic atom-trimer scattering. *Phys. Rev.*, A 82:040701, 2010. DOI: 10.1103/PhysRevA.82.040701.

[22] A. Deltuva. Momentum-space calculation of four-boson recombination. *Phys. Rev.*, A 85:012708, 2012. DOI: 10.1103/PhysRevA.85.012708.

[23] S. Diehl, S. Floerchinger, H. Gies, J. M. Pawlowski, and C. Wetterich. Functional renormalization group approach to the BCS-BEC crossover. *Ann. Phys.*, 522:615, 2010. DOI: 10.1002/andp.201010458.

[24] S. Diehl, H. Gies, J. M. Pawlowski, and C. Wetterich. Flow equations for the BCS-BEC crossover. *Phys. Rev.*, A 76:021602(R), 2007. DOI: 10.1103/PhysRevA.76.021602.

[25] S. Diehl, H. Gies, J. M. Pawlowski, and C. Wetterich. Renormalization flow and universality for ultracold fermionic atoms. *Phys. Rev.*, A 76:053627, 2007. DOI: 10.1103/PhysRevA.76.053627.

[26] S. Diehl, H. C. Krahl, and M. Scherer. Three-body scattering from nonperturbative flow equations. *Phys. Rev.*, C 78:034001, 2008. DOI: 10.1103/PhysRevC.78.034001.

[27] J. P. D'Incao, J. von Stecher, and C. H. Greene. Universal four-boson states in ultracold molecular gases: resonant effects in dimer-dimer collisions. *Rev. Phys. Lett.*, 103:033004, 2009. DOI: 10.1103/PhysRevLett.103.033004.

[28] V. Efimov. Energy levels arising form the resonant two-body forces in a three-body system. *Phys. Lett.*, B 33:563, 1970. DOI: 10.1016/0370-2693(70)90349-7.

[29] V. Efimov. Weakly-bound states of three resonantly-interacting particles. *Sov. J. Nucl. Phys.*, 12:589, 1971.

[30] F. Ferlaino, S. Knoop, M. Berninger, W. Harm, H. C. Nägerl J. P. D'Incao, and R. Grimm. Evidence for universal four-body states tied to an Efimov trimer. *Phys. Rev. Lett.*, 102:140401, 2009. DOI: 10.1103/PhysRevLett.102.140401.

[31] F. Ferlaino, A. Zenesini, M. Berninger, B. Huang, H. C. Nägerl, and R. Grimm. Efimov resonances in ultracold quantum gases. *Few-Body Syst.*, 51:113, 2011. DOI: 10.1007/s00601-011-0260-7.

[32] S. Floerchinger, M. Scherer, S. Diehl, and C. Wetterich. Particle-hole fluctuations in BCS-BEC crossover. *Phys. Rev.*, B 78:174528, 2008. DOI: 10.1103/PhysRevB.78.174528.

[33] S. Floerchinger, M. M. Scherer, and C. Wetterich. Modified fermi sphere, pairing gap, and critical temperature for the BCS-BEC crossover. *Phys. Rev.*, A 81:063619, 2010. DOI: 10.1103/PhysRevA.81.063619.

[34] S. Floerchinger, R. Schmidt, S. Moroz, and C. Wetterich. Functional renormalization for trion formation in ultracold fermion gases. *Phys. Rev.*, A 79:013603, 2009. DOI: 10.1103/PhysRevA.79.013603.

[35] S. Floerchinger, R. Schmidt, and C. Wetterich. Three-body loss in lithium from functional renormalization. *Phys. Rev.*, A 79:053633, 2009. DOI: 10.1103/PhysRevA.79.053633.

[36] S. Floerchinger and C. Wetterich. Exact flow equation for composite operators. *Phys. Lett.*, B 680:371, 2009. DOI: 10.1016/j.physletb.2009.09.014 e-print arXiv:0905.0915v2 [hep-th].

[37] A. C. Fonseca and P. E. Shanley. Soluble model involving four identical particles. *Phys. Rev.*, C 14:1343, 1976. DOI: 10.1103/PhysRevC.14.1343.

[38] H. Gies and C. Wetterich. Renormalization flow of bound states. *Phys. Rev.*, D 65:065001, 2002. DOI: 10.1103/PhysRevD.65.065001 e-print arXiv:hep-th/0107221v2.

[39] W. Glöckle, H. Witała, D. Hüber, H. Kamada, and J. Golak. The three-nucleon continuum: achievements, challenges and applications. *Phys. Rept.*, 274:107, 1996. DOI: 10.1016/0370-1573(95)00085-2.

[40] R. E. Grisenti, W. Schöllkopf, J. P. Toennies, G.C. Hegerfeldt, T. Köhler, and M. Stoll. Determination of the bond length and binding energy of the helium dimer by diffraction from a transmission grating. *Phys. Rev. Lett.*, 85:2284, 2000. DOI: 10.1103/PhysRevLett.85.2284.

[41] M. R. Hadizadeh, M. T. Yamashita, Lauro Tomio, A. Delfino, and T. Frederico. Scaling properties of universal tetramers. *Phys. Rev. Lett.*, 107:135304, 2011. DOI: 10.1103/PhysRevLett.107.135304.

[42] M. R. Hadizadeh, M. T. Yamashita, Lauro Tomio, A. Delfino, and T. Frederico. Binding and structure of tetramers in the scaling limit. *Phys. Rev.*, A 85:023610, 2012. DOI: 10.1103/PhysRevA.85.023610.

[43] H. W. Hammer and L. Platter. Universal properties of the four-body system with large scattering length. *Eur. Phys. J.*, A 32:113, 2007. DOI: 10.1140/epja/i2006-10301-8.

[44] H. W. Hammer and L. Platter. Efimov states in nuclear and particle physics. *Ann. Rev. Nucl. Part. Sci.*, 60:207, 2010. DOI: 10.1146/annurev.nucl.012809.104439.

[45] H. W. Hammer and L. Platter. Efimov physics from a renormalization group perspective. *Phil. Trans. Roy. Soc.*, 369:2679, 2011. DOI: 10.1098/rsta.2011.0001.

[46] R. Haussmann, W. Rantner, S. Cerrito, and W. Zwerger. Thermodynamics of the BCS-BEC crossover. *Phys. Rev.*, A 75:023610, 2007. DOI: 10.1103/PhysRevA.75.023610 e-print arXiv:cond-mat/0608282 [cond-mat.stat-mech].

[47] M. Horikoshi, S. Nakajima, M. Ueda, and T. Mukaiyama. Measurement of universal thermodynamic functions for a unitary fermi gas. *Science*, 327:442, 2010. DOI: 10.1126/science.1183012.

[48] J. Hubbard. Calculation of partition functions. *Phys. Rev. Lett.*, 2:77, 1959. DOI: 10.1103/PhysRevLett.3.77.

[49] T. Kraemer, M. Mark, P. Waldburger, J. G. Danzl, C. Chin, B. Engeser, A. D. Lange, K. Pilch, A. Jaakkola, H. C. Nägerl, and R. Grimm. Evidence for Efimov quantum states in an ultracold gas of caesium atoms. *Nature*, 440:315, 2006. DOI: 10.1038/nature04626.

[50] B. Krippa, N. R. Walet, and M. C. Birse. Renormalization group, dimer-dimer scattering, and three-body forces. *Phys. Rev.*, A 81:043628, 2010. DOI: 10.1103/PhysRevA.81.043628.

[51] M. J. H. Ku, A. T. Sommer, L. W. Cheuk, and M. W. Zwierlein. Revealing the superfluid lambda transition in the universal thermodynamics of a unitary fermi gas. *Science*, 335:563, 2012. DOI: 10.1126/science.1214987.

[52] D. Litim. Optimized renormalization group flows. *Phys. Rev.*, D 64:105007, 2001. DOI: 10.1103/PhysRevD.64.105007.

[53] C. Mora, R. Egger, A. O. Gogolin, and A. Komnik. Atom-dimer scattering for confined ultracold fermion gases. *Phys. Rev. Lett.*, 93:170403, 2004. DOI: 10.1103/PhysRevLett.93.170403.

[54] Nascimbène, N. Navon, K. J. Jiang, F. Chevy, and C. Salomon. Exploring the thermodynamics of a universal fermi gas. *Nature (London)*, 463:1057, 2010. DOI: 10.1038/nature08814.

[55] N. Navon, S. Nascimbène, F. Chevy, and C. Salomon. The equation of state of a low-temperature fermi gas with tunable interactions. *Science*, 328:729, 2010. DOI: 10.1126/science.1187582.

[56] Y. Nishida, S. Moroz, and D. T. Son. Super Efimov effect of resonantly interacting fermions in two dimensions. *Phs. Rev. Lett.*, 110:235301, 2013. 10.1103/PhysRevLett.110.235301 e-print arXiv:1301.4473v2 [cond-mat.quant-gas].

[57] J. M. Pawlowski. Aspects of the functional renormalisation group. *Ann. Phys.*, 322:2831, 2007. DOI: 10.1016/j.aop.2007.01.007.

[58] D. S. Petrov. Three-body problem in fermi gases with short-range interparticle interaction. *Phys. Rev.*, A 67:010703(R), 2003. DOI: 10.1103/PhysRevA.67.010703.

[59] D. S. Petrov. The few-atom problem. 2012. eprint arXiv:1206.5752v2 [cond-mat.quant-gas].

[60] D. S. Petrov, C. Salomon, and G. V. Shlyapnikov. Weakly bound dimers of fermionic atoms. *Phys. Rev. Lett.*, 93:090404, 2004. DOI: 10.1103/PhysRevLett.93.090404.

[61] D. S. Petrov, C. Salomon, and G. V. Shlyapnikov. Resonant dimer relaxation in cold atoms with a large scattering length. *Phys. Rev.*, A 71:012708, 2005. DOI: 10.1103/PhysRevA.71.012708.

[62] L. Platter, H. W. Hammer, and U. G. Meißner. Four-boson system with short-range interactions. *Phys. Rev.*, A 70:052101, 2004. DOI: 10.1103/PhysRevA.70.052101.

[63] J. Polonyi. Lectures on the functional renormalization group method. *Central Eur. J. Phys.*, 1:1, 2003. DOI: 10.2478/BF02475552.

[64] R. Rajaraman and H. Bethe. Three-body problem in nuclear matter. *Rev. Mod. Phys.*, 39:745, 1967. DOI: 10.1103/RevModPhys.39.745.

[65] C. A. Regal, M. Greiner, and D. S. Jin. Observation of resonance condensation of fermionic atom pairs. *Phys. Rev. Lett.*, 92:040403, 2004. DOI: 10.1103/PhysRevLett.92.040403 e-print arXiv:cond-mat/0401554 [cond-mat.stat-mech].

[66] M. Salmhofer and C. Honerkamp. Fermionic renormalization group flows technique and theory. *Prog. Theor. Phys.*, 105:1, 2001. DOI: 10.1143/PTP.105.1.

[67] R. Schmidt and S. Moroz. Renormalization group study of the four-body problem. *Phys. Rev.*, A 81:052709, 2010. DOI: 10.1103/PhysRevA.81.052709.

[68] A. Schwenk and J. Polonyi (editors). *Renormalization Group and Effective Field Theory Approaches to Many-Body Systems.* Springer, 2012. ISBN: 978-3642273193.

[69] G. V. Skorniakov and K. A. Ter-Martirosian. Theory of three-body systems. *Zh. Eksp. Teor. Fiz.*, 31:775, 1956.

[70] R. L. Stratonovich. On a method of calculating quantum distribution functions. *Doklady Acad. Nauk S.S.S.R.*, 115:1097, 1957.

[71] J. von Stecher, J. P. D'Incao, and C. H. Greene. Signatures of universal four-body phenomena and their relation to the Efimov effect. *Nature Phys.*, 5:417, 2009. DOI: 10.1038/nphys1253.

[72] C. Wetterich. Average action and the renormalization group equations. *Nucl. Phys.*, B 352:529, 1991. DOI: 10.1016/0550-3213(91)90099-J.

[73] C. Wetterich. Exact evolution equation for the effective potential. *Phys. Lett.*, B 301:90, 1993. DOI: 10.1016/0370-2693(93)90726-X.

[74] O. A. Yakubovsky. On the integral equations in the theory of N particle scattering. *Yad. Fiz.*, 5:1312, 1967.

[75] M. T. Yamashita, Lauro Tomio, A. Delfino, and T. Frederico. Four-boson scale near a Feshbach resonance. *Europhys. Lett.*, 75:555, 2006. DOI: 10.1209/epl/i2006-10141-6.

[76] M. W. Zwierlein, C. A. Stan, C. H. Schunck, S. M. F. Raupach, A. J. Kerman, and W. Ketterle. Condensation of pairs of fermionic atoms near a Feshbach resonance. *Phys. Rev. Lett.*, 92:120403, 2004. DOI: 10.1103/PhysRevLett.92.120403 e-print arXiv:cond-mat/0311617v2.